Some ab initio tudies of the physical properties of materials

Nathalie Madeleine Marguerite Vast

▶ **To cite this version:**

Nathalie Madeleine Marguerite Vast. Some ab initio tudies of the physical properties of materials. Condensed Matter [cond-mat]. Université Pierre et Marie Curie - Paris VI, 2009. tel-00440923

HAL Id: tel-00440923
https://theses.hal.science/tel-00440923

Submitted on 13 Dec 2009

HAL is a multi-disciplinary open access archive for the deposit and dissemination of scientific research documents, whether they are published or not. The documents may come from teaching and research institutions in France or abroad, or from public or private research centers.

L'archive ouverte pluridisciplinaire **HAL**, est destinée au dépôt et à la diffusion de documents scientifiques de niveau recherche, publiés ou non, émanant des établissements d'enseignement et de recherche français ou étrangers, des laboratoires publics ou privés.

Manuscrit présenté pour obtenir le diplôme

HABILITATION À DIRIGER DES RECHERCHES

Spécialité : **Physique - Sciences des Matériaux**

Etude *ab initio* des propriétés physiques des matériaux

par

Nathalie VAST

Soutenue le 13 juillet 2009 devant le jury composé de

Prof. Maria Chamarro	Présidente
Prof. Ulf von Barth	Rapporteur
Dr. Christophe Delerue	Rapporteur
Prof. Giulia Galli	Rapporteure
Dr. Christian Colliex	Examinateur
Dr. Guillaume Petite	Examinateur

Manuscript proposed to acquire the French diploma

HABILITATION À DIRIGER DES RECHERCHES

Topics: **Physics - Science of Materials**

Some *ab initio* studies of the physical properties of materials

by

Nathalie VAST

Defended on July, 13^{th} 2009 in front of the jury composed of

Prof. Maria Chamarro	Chairwoman
Prof. Ulf von Barth	Referee
Prof. Giulia Galli	Referee
Dr. Christophe Delerue	Referee
Dr. Christian Colliex	Member
Dr. Guillaume Petite	Member

Contents

0.1 Résumé (Fr)

Mon activité de recherche fondamentale dans le groupe de théorie du Laboratoire des Solides Irradiés concerne l'étude des propriétés des matériaux d'intérêt pour le CEA, dans les domaines du nucléaire ou de la nanoélectronique. Elle a pour objectif d'atteindre une description théorique -sans paramètre ajustable- des processus contrôlant l'excitation électronique, ainsi que la relaxation -ou désexcitation- électronique, et couvre:

- Les propriétés de la matière hors excitation - l'état fondamental;
- Les propriétés de l'état excité, abordées sous l'angle de la spectroscopie pour les électrons de valence;
- Les vibrations collectives des atomes, leur couplage avec les électrons, et leurs effets sur le transport électronique ou la relaxation électronique.

Ces études requièrent un environnement de calcul intensif et l'accès aux ordinateurs du Grand Equipement National de Calcul Intensif GENCI.

Dans ce manuscrit, est d'abord rappelé comment calculer la fonction diélectrique inverse en théorie de la fonctionnelle de la densité dépendante du temps, et quel est le lien avec la fonction de perte électronique observée. Des résultats théoriques sur la fonction diélectrique inverse dans des oxydes non corrélés représentés par le dioxyde de titane TiO_2 et la zircone ZrO_2 sont décrits. Ensuite sont donnés les principaux résultats théoriques pour les calculs de spectres d'absorption optique pour l'oxyde de cuivre Cu_2O et la zircone ZrO_2. J'y présente une nouvelle interprétation de travail sur le noyau permettant de modéliser les effets excitoniques en théorie de la fonctionnelle de la densité dépendante du temps. Enfin, les derniers calculs menés sur les carbures de bore sont rappelés.

0.2 Abstract

My activities are in fundamental research in the group of theory of the Laboratoire des Solides Irradiés. It includes the study of the physical properties of some of those materials which are of interest to the CEA, to nuclear research and to nanoelectronics. The objective is to achieve a parameter-free description of processes which control electronic excitations or electronic relaxations. This covers :

- The study of the ground state of materials;
- The investigation of the properties of the excited state, from the viewpoint of the spectroscopy of valence electrons;
- The lattice dynamics, its coupling with phonons, and the effect of electron-phonon coupling on electronic transport and electronic relaxation.

These studies involves high performance computing and require computer time from big facilities like the GENCI in France.

In the manuscript, I recall first how the inverse dielectric function is calculated within time dependent, density functional theory, and the link with the measurement of the electronic loss function. Theoretical results are presented for titania TiO_2 and zirconia ZrO_2 which are uncorrelated oxides. Then main theoretical results on optical absorption of cuprous oxide Cu_2O and on zirconia ZrO_2 are presented. A new interpretation on the kernel which allows to model excitonic effects in time dependent density functional theory is presented. Finally, recent calculations on boron carbides, and in particular B_4C are reviewed.

Chapter 1

Introduction et contexte (Fr)

1.1 But général

Mon activité de recherche fondamentale dans le groupe de théorie du LSI concerne l'étude des propriétés des matériaux d'intérêt pour le CEA, dans les domaines du nucléaire ou de la nanoélectronique. Elle a pour objectif d'atteindre une description théorique -sans paramètre ajustable- des processus contrôlant l'excitation électronique, ainsi que la relaxation -ou désexcitation- électronique, et couvre:

- Les propriétés de la matière hors excitation - l'état fondamental;
- Les propriétés de l'état excité, abordées sous l'angle de la spectroscopie pour les électrons de valence;
- Les vibrations collectives des atomes, leurs couplage avec les électrons, et leurs effets sur le transport électronique ou la relaxation électronique.

Ces études requièrent un environnement de calcul intensif et l'accès aux ordinateurs du Grand Equipement National de Calcul Intensif GENCI.

1.2 Cadre théorique

L'objectif général mentionné ci-dessus implique le développement de méthodes théoriques et leur implantation dans des programmes informatiques. Les méthodes numériques que je développe sont essentiellement basées sur la théorie de la fonctionnelle de la densité ou DFT [1]. J'utilise aussi des méthodes à N-corps pour étudier les excitations électroniques.

Les propriétés des matériaux nécessitent différents niveaux de description théorique. Les propriétés de volume [2] -paramètre de maille, constantes élastiques- nécessitent le calcul de l'état fondamental électronique, décrit par la DFT. Les perturbations statiques telles les vibrations du réseau cristallin -les phonons [3]-, et leurs conséquences tel le couplage électron-phonon [4, 5] qui entre en jeu entre autres pour la supraconductivité conventionnelle [4, 6]- requièrent la perturbation de la fonctionnelle de la densité (DFPT) [3]. Enfin, les excitations électroniques -ou perturbations dynamiques- nécessitent la théorie de la fonctionnelle de la densité dépendant du temps (TDDFT) [7, 8].

Ces théories sont exactes, et basées sur la connaissance de la seule densité électronique ou de la matrice densité. Les effets à N-corps sont rassemblés dans un potentiel électronique effectif d'échange et corrélation ou dans la dérivée de ce potentiel par rapport à la densité électronique -le noyau d'échange et corrélation. En pratique on ne dispose que d'approximations pour ce potentiel ou ce noyau. Un des objectifs de la communauté scientifique, auquel j'ai participé [9], est d'améliorer le noyau d'échange et de

corrélation en comparant la réponse électronique obtenue en TDDFT avec celle obtenue par les méthodes à N-corps au-delà de la DFT.

Aller au-delà de la DFT est nécessaire pour décrire l'excitation électronique [10]:

i Les bandes interdites (différence entre la plus haute énergie des états occupés par les électrons et la plus basse énergie des états vides) calculées en DFT dans les semiconducteurs et les isolants sont très fortement sous-estimées. Cela vient du fait que le potentiel d'échange et de corrélation exact -et inconnu- a une discontinuité quand le système passe de N à N$\pm$1 particules [11, 12]. Autrement dit, pour calculer E(N)-E(N$\pm$1), où E est l'énergie totale du système, la DFT n'a pas l'équivalent du théorème de Koopman de la méthode Hartree-Fock [13]. Cette discontinuité est présente quelle que soit la fonctionnelle d'échange et de corrélation considérée, dans l'approximation de densité locale (LDA) ou dans l'approximation de gradient généralisé (GGA). Les fonctionnelles hybrides, basées en partie sur un potentiel d'échange exact de type Hartree-Fock, présentent également cette discontinuité. Un calcul de quasiparticule au-delà de la DFT -par exemple dans l'approximation GW [13, 14]- est rigoureusement nécessaire. Dans la pratique, les bandes interdites calculées avec les fonctionnelles hybrides (B3LYP, PBE0) sont plus proches de l'expérience que celles calculées à l'aide de la GGA ou de la LDA.

ii Pour une excitation électronique neutre, en plus de la correction de quasi-particule précédente, on doit prendre en compte l'interaction de l'électron excité avec le trou qu'il laisse derrière lui -les effets excitoniques [10]. Cette interaction mélange les transitions indépendantes, et ses effets peuvent être décrits par un Hamiltonien effectif [15–18].

Finalement, les vecteurs et valeurs propres de la DFT sont importants

- Pour calculer les propriétés de l'état électronique fondamental;
- Pour calculer la fonction d'écrantage ϵ^{-1}, ou fonction diélectrique inverse, "ingrédient" essentiel des méthodes à N-corps (cf. Chapitre 2).
- Pour calculer la probabilité de transition sous l'effet d'une perturbation -règle d'or de Fermi (cf. Chapitre B).

1.3 Description des travaux de recherche

D'une façon générale, les céramiques et particulièrement la zircone (cf. Annexe A) sont des matériaux dont l'utilisation va se renforcer dans les technologies nucléaires : céramiques pour les réacteurs nucléaires de génération

IV, alliages renforcés par dispersion d'oxydes, matériaux de structure pour la fusion. Pour l'étude de ces matériaux, la simulation numérique joue un rôle capital. Elle ne dispense pas des expériences, car les matériaux utiles pour les applications au CEA sont complexes par le nombre d'atomes de leur maille élémentaire ou par leur structure électronique, incluant par exemple des électrons $3d$. Sur ces matériaux, j'ai travaillÃ© selon trois directions, que je passe maintenant en revue.

Avec les études sur les excitations électroniques, j'ai abordé un champ d'investigation totalement nouveau, sous la direction de Lucia Reining. Puis, sur les conseils de Guillaume Petite, j'ai combiné des nouvelles connaissances avec celles acquises sur les phonons pendant ma thèse, et j'ai ainsi avancé dans la compréhension du rôle du couplage électron-phonon dans la relaxation électronique. Enfin, j'ai toujours mené en parallèle un travail de veille sur les carbures de bore, matériaux qui connaissent aujourd'hui un regain d'intérêt de la part de la communauté scientifique. Cette connaissance ancienne apporte aujourd'hui une reconnaissance internationale à l'équipe que j'anime, comme l'indiquent les citations récentes (cf. annexe D) des travaux menés pendant ma thèse.

1.3.1 Excitations électroniques dans les oxydes.

Le cadre théorique relatif à cette partie est explicité dans les chapitres 2 et 4. Les principaux résultats sont expliqués dans les chapitres 3 et 4. Je donne ici un aperçu de mes travaux de recherche, en expliquant le fil conducteur.

A mon arrivée en 2000, le LSI était un laboratoire de réputation internationale pour les développements théoriques sur la spectroscopie des électrons de valence, impulsés par L. Reining (CNRS), responsable du groupe de théorie. J'y ai abordé l'étude des excitations électroniques de valence sur des matériaux d'intérêt pour le CEA en menant les premières applications à des oxydes de métaux de transition faiblement corrélés, TiO_2 et ZrO_2. Les méthodes théoriques, jusque-là appliquées à des semiconducteurs tel le silicium, ont nécessité des améliorations en raison de la localisation plus grande des électrons dans ces oxydes.

La fonction de perte d'énergie $-\Im(\epsilon^{-1})$ permet de mettre en évidence les excitations électroniques collectives -les plasmons. En TDDFT, elle s'écrit :

$$-\Im(\epsilon^{-1}) = -\Im(1 + v\chi), \chi = \chi_0 + \chi_0(v + f_{xc}), \tag{1.1}$$

où v est le potentiel coulombien, χ_0 est la fonction de réponse d'électrons indépendants, et f_{xc} est le noyau d'échange et corrélation. Le calcul a été comparé à des mesures très précises de perte d'énergie électronique de TiO2 [19] par P. Schattschneider, de l'Université Technique de Vienne en Autriche. J'ai montré la grande importance des effets de champs locaux

$\chi_0 v$ dans la réponse à l'excitation des électrons localisés $3p$. Puis j'ai collaboré à différentes études sur le rôle des champs locaux dans la réponse de nanotubes de carbone [20], ou dans la biréfringence de nanostructures semiconductrices, en coencadrant la thèse de S. Botti [21–23].

J'ai ensuite travaillé sur l'oxyde de zirconium avec L. Dash et Ph. Baranek. La comparaison des données expérimentales obtenues par une collaboration avec M. Cheynet de l'Ecole Nationale Supérieure d'Electrochimie et d'Electrométallurgie de Grenoble sur les différentes phases cristallines de ZrO_2 [24] nous a permis de déterminer quel niveau de théorie est nécessaire pour traiter de façon appropriée les spectres d'excitation électronique dans ces oxydes [25, 26]. J'en ai conclu la validité de la TDDFT pour la spectroscopie de perte d'énergie, et dégagé les perspectives décrites dans la section 1.4.

J'ai collaboré avec M. Izquierdo, F. Sirotti (Synchrotron SOLEIL) et N. Barrett (CEA-DRECAM-SPCSI) dans le cadre de la thèse théorique de F. Bruneval sur l'oxyde de cuivre, coencadrée avec L. Reining. Les mesures de photoémission résolue en angle ou ARPES ont permis de montrer, de façon inattendue, l'insuffisance des valeurs propres obtenues en DFT comme point de départ au calcul de quasi-particule. J'ai orienté le travail de F. Bruneval vers un traitement amélioré [27] de la fonction d'écrantage ϵ^{-1}. Les développements de F. Bruneval [28] ont permis en particulier le calcul de la structure électronique de Cu_2O et du spectre d'absorption optique [29].

Ces travaux ont en outre permis de montrer que la fonction d'onde électronique de quasi-particule diffère peu du vecteur propre de la DFT, dans les matériaux Si, Al, Ar [30] ou Cu_2O [29]. Ce point fondamental a rendu envisageable l'étude, basée sur la DFT, de la relaxation électronique dans la bande de conduction.

1.3.2 Relaxation électronique dans les semiconducteurs.

Le cadre théorique de cette partie est explicité dans l'annexe B et dans les publications citées.

Les mécanismes de désexcitation électroniques sont importants tant du point de vue du comportement des céramiques sous irradiation, que pour le transport dans les nanodispositifs. Or, comprendre les mécanismes de relaxation implique l'étude du couplage électron-phonon dans la bande de conduction.

Jusqu'à récemment, ce couplage était évalué dans les semiconducteurs avec des modèles ajustés sur l'expérience. Le postdoc de J. Sjakste a permis de développer la théorie *ab initio* du couplage de deux états électroniques de

la bande de conduction avec un phonon de vecteur d'onde fini [5]. Ce travail a été mené en collaboration avec le Prof. V. Tyuterev, de l'Université Pédagogique de Tomsk, Russie. J'ai orienté les recherches vers l'interprétation d'expériences de spectroscopie résolue en temps [5, 31]. Ces dernières donnent accès aux processus d'interaction microscopique fondamentaux tel le couplage électron-phonon.

Dans les semiconducteurs présentant différents minima (vallées) dans la bande de conduction, le couplage électronique aux phonons de longueur d'onde finie permet le transfert électronique d'une vallée à l'autre et contrôle le transport électronique. Dans GaAs, nous avons d'abord montré que nous pouvions prédire les constantes de couplage à 10% près pour la diffusion de la vallée Γ à la vallée X, responsable de l'effet Gunn [32]. Ceci est une avancée considérable par rapport aux écarts trouvés dans la littérature expérimentale.

Enfin, dans GaP, nos calculs ont permis d'évaluer ce temps de vie de l'excitation, et de rectifier les connaissances actuelles, en montrant quels phonons limitent réellement le temps de vie de l'exciton [5].

Ces succès dus aux trois membres de l'équipe permettent d'envisager différentes directions futures (section 1.4).

1.3.3 Etudes des matériaux riches en bore.

Le cadre détaillé de cette activité peut être trouvé dans les références [33, 34]. Les derniers résultats publiés sont donnés dans le chapitre 5.

Le noyau de bore ^{10}B est un excellent absorbeur de neutron et cela a initié mon intérêt pour le bore et les matériaux riches en bore. D'autre part, les éléments B, C, N forment des matériaux ultradurs à cause des liaisons covalentes fortement directionnelles.

Citant (et traduisant) R.B. Kaner et al. [35], "les composés riches en bore (...) sont des matériaux très durs qui méritent des études continues". Une forte activité de recherche a lieu sur ces matériaux, particulièrement au Japon. Dans ces recherches, les calculs *ab initio*, au nombre desquels ceux que j'ai menés pendant ma thèse [33, 34, 36–40], jouent un grand rôle.

Dans le passé, je me suis en effet intéressée - en collaboration avec R. Lazzari, J.M. Besson, S. Baroni et G. Zérah, aux propriétés vibrationnelles du bore [33, 34, 36, 37] et du carbure de bore [38–40]. Ces travaux sont bien cités dans la littérature. La comparaison de nos calculs *ab initio* obtenus sur des structures hypothétiques, avec les données de l'expérience mesurées en diffusion Raman et en absorption infrarouge, nous a permis de lever les incertitudes sur la localisation des atomes de carbone dans la structure

de bore et de déterminer la structure atomique du carbure de bore B_4C, comme un icosaèdre $B_{11}C^p$ et une chaîne CBC. Ce qui me permet de mettre en questions les résultats récents de la Ref. [41].

Plus récemment, en étudiant les spectres de résonance magnétique nucléaire, en collaborant avec F. Mauri, de l'IMPMC -Institut de Minéralogie et de Physique des Milieux Condensés- Université Paris VI P.M. Curie, la structure atomique du carbure de bore B_4C que j'avais déterminée pendant ma thèse [33, 34, 38–40], a été confirmée par ces nouvelles études [42], et le défaut de structure le plus courant dans ce matériau a été identifié [42].

Enfin, il est maintenant connu que le bore pur à haute pression métallise et devient supraconducteur [43]. L'origine de cette transition est cependant encore à l'état d'hypothèse, une nouvelle phase B_{28} venant d'être découverte [44]. Pour le carbure de bore, nous avons prédit pour ce matériau que le dopage par des trous le rend métallique à pression ambiante, avec une température de supraconductivité élevée pour un supraconducteur BCS, proche de celle de MgB_2 [6].

L'analyse de la littérature récente [45–47] montre que l'étude de la formation des carbures de bore et de leur stabilité soulève un intérêt continu, et que la question n'est pas résolue. J'ai récemment [48] calculé, en collaboration avec Jelena Sjakste et Emmanuel Betranhandy, l'énergie de formation de différentes structures atomiques. Ces énergies calculées montrent de façon inattendue que la plupart des carbures de bore étudiés ont une tendance à se décomposer en bore + graphite. A part le carbure de bore B_4C, nous avons trouvé seulement cinq structures qui sont stables et peuvent se former [48] (cf. Chapitre 5). Ces structures sont métastables par rapport au carbure de bore B_4C. C'est le cas de la maille élémentaire de $B_{13}C_2$, lorsqu'elle est modélisée par un icosaèdre B_{12} et une chaîne C-B-C. Nous en avons conclu que cette métastabilité explique la difficulté à synthétiser des échantillons propres de $B_{13}C_2$. Elle explique aussi l'absence d'échantillon monocristallin.

Bien que B_4C présente la limite élastique d'Hugoniot (HEL) la plus importante connue parmi les céramiques (HEL $\approx$ 17 GPa), son utilisation comme matériau de blindage reste délicate car il ne peut résister à la propagation d'une onde de choc, comme le démontrent les données expérimentales récentes [49, 50]. Cependant, à l'heure actuelle , le mécanisme même de réponse à une compression dynamique n'est pas compris : ainsi la perte de résistance a pu être associée à une baisse de la contrainte de cisaillement [50], mais cette interprétation a été contestée par la suite par une expérience d'impacts de projectiles sur cibles [49]. Dans cette dernière expérience, la modification du comportement sous conditions extrêmes n'a pas pu être comprise: elle peut être attribuée à une propriété physique intrinsèque du carbure de bore B_4C, ou à une ou plusieurs transitions de phase [49].

D'autre part, un processus d'amorphisation de B_4C a été suggéré à partir de l'observation de zones d'endommagement dans les zones entre les grains de B_4C afin d'expliquer les modifications des propriétés mécaniques observées lors d'une compression dynamique [50]. Ces zones ont également été observées lors d'expériences de nanoindentation [51], ou sur des échantillons ayant subi une compression non hydrostatique allant jusqu'à 50 GPa [52]. Les zones de dommage observées ne concernent cependant qu'une faible fraction du volume du matériau, et les interprétations de l'amorphisation qui sont données sont contradictoires entre elles : certaines se basent sur la présence de bore et du carbone amorphe [51], d'autres y voient du carbure de bore B_4C amorphe [50, 52, 53]. De plus, les expériences d'impact sur cibles de Vogler et al. [49] n'induisent pas la présence de phases amorphes.

L'étude en cours a permis entre autres de calculer le comportement sous très haute pression des phases précédemment identifiés comme stables [48]. Nous avons trouvé que la présence de lacunes de bore dans la chaîne CBC induit une modification du comportement mécanique du carbure de bore. Cela n'avait jamais été étudié auparavant. Nous avons montré que

i B_4C tel que décrit ci-dessus peut soutenir des pressions de l'ordre de 1 Mbar sans altération des propriétés mécaniques.

ii La présence de lacune de bore dans la chaîne induit une modification des propriété's mécaniques par formation d'une liaison C-C (chaîne à deux atomes).

Notre interprétation va à l'encontre de celle d'un papier très récent [52] selon lequel une pression uniaxiale plie la chaîne C-B-C et provoque une modification des propriétés mécaniques dans B_4C pur. Nos premiers résultats concernant l'application d'une déformation uniaxiale démentent ces résultats. Ce débat un peu technique a d'importantes conséquences : dans notre cas, on peut pallier la mauvaise tenue mécanique sous pression en améliorant la synthèse du matériau, alors que dans le cas de la Ref. [51] la mauvaise tenue mécanique est une propriété intrinsèque du matériau. Nos études en cours sont destinées à clarifier ce point.

1.4 Projet de recherche à quatre ans

Dans le cadre de l'objectif général donné en première section 1.1, une première direction de recherche a été peu évoquée et concerne les propriétés de l'état fondamental. Elle implique de comprendre les limites de la DFT dans sa précision sur l'énergie totale.

J'ai trouvé dans les calculs que la phase d'équilibre n'est pas la phase observée, dans des métaux tels le titane ou le zirconium, ou un oxyde tel

que TiO_2, et d'autres ont trouvé un problème avec la zircone (cf. la fin de l'annexe A). En d'autres termes le diagramme de phase prédit par le calcul est erroné. Les différences d'énergies entre les phases des matériaux cités sont très petites.

Mon hypothèse, élaborée lors de la thèse de V. Trinité Quéquet sur le titane [54], co-encadrée avec Marc Hayoun et Jean-Claude Toledano, et après de nombreuses discussions scientifiques avec diverses personnalités, est que la prédiction des différences d'énergie en DFT est limitée par l'incertitude des approximations du potentiels d'échange et de corrélation pour les électrons de valence. Aller au-delà pour les métaux en utilisant un potentiel basé sur de l'échange exact est une tâche ambitieuse, qui présente de réelles difficultés, et nécessite des développements théoriques et des simulations très précises. Ce travail est en cours, en collaboration avec V. Trinité, maintenant chercheure permanent à Thalès.

Les premiers résultats obtenus en Décembre 2008 montrent qu'une fonctionnelle de type PBE0 à base d'échange exact ne permet de stabiliser la phase α. J'ai en projet d'étudier s'il se produit des modifications significatives de l'équation d'état calculée.

Les études sur les borures (sous-section 1.3.3) vont se poursuivre. B_4C est très utilisé dans l'industrie et dans l'armement. Sa dureté vient juste après celle du diamant, et permet son utilisation courante dans les outils de coupe et de blindage. Nous avons réfléchi à combiner les propriétés de dureté et de supraconductivité en dopant en trous le carbure de bore [6]. Il convient d'étudier les carbures de bore sous l'angle de leur stabilité, qui permettrait de comprendre la stabilité du matériau lors du dopage. Ce dopage permettra de combiner dureté et supraconductivité. La combinaison dans un même matériau de la supraconductivité et d'une forte dureté est extrêmement intéressante tant du point de vue fondamental que des applications qui pourraient en découler. Un projet franco-japonais avec Koun Shirai, de l'Université d'Osaka, a démarré, pour doper le bore -hypothèse nippone [55]- ou le carbure de bore -hypothèse française [6] . Le doctorant japonais Haruhiko Dekura a été reçu en 2008, et sera encore accueilli pendant plusieurs mois au LSI en 2009.

D'autre part, les études sur les borures (sous-section 1.3.3) vont se continuer avec un premier objectif de comprendre la structure atomique des carbures de bore riches en bore. Il s'agit de trouver une caractéristique spectroscopique aux lacunes, afin de pouvoir les détecter dans les échantillons. Une collaboration avec Sciences Chimiques de Rennes (J.F. Hallet et L. Le Pollès) est envisagées, ainsi qu'avec T. Mori pour la synthèse des échantillons (Senior Researcher au National Institute for Materials Science (NIMS), WPI Materials Nanoarchitechtonics Center (MANA), Senior Operations Officer, Strategic Office, NIMS, Tsukuba 305-0044, Japan, et guest

Scientist, National Institute of Science and Technology Policy (NISTEP) du NIMS. Un deuxième enjeu est d'améliorer la tenue sous choc de ces matériaux, en y introduisant des dopants appropriés.

L'étude sur la désexcitation électronique (sous-section 1.3.2) va continuer, et cette thématique va se renforcer, en particulier grâce au recrutement par le CNRS de J. Sjakste, en section 5 en Octobre 2008. Cette thématique a reçu le soutien de l'ANR par le financement PNANO 2008 du projet ACCATTONE, avec F. Mauri (IMPMC -Institut de Minéralogie et de Physique des Milieux Condensés- Université Paris VI P.M. Curie.), et Natalio Mingo (CEA Grenoble - LITEN).

Ces études vont devoir être étendue au carbure de silicium et aux isolants, matériaux d'intérêt au CEA. De plus, les phonons de grande longueur d'onde interviennent dans la relaxation électronique et dans le transport thermique, et nous savons que l'un des enjeux de la nanoélectronique est la solution des problèmes d'échauffement. Nous avons en projet :

i d'étendre la méthode au couplage avec les phonons acoustiques de centre de zone. La théorie doit être étendue car ces phonons sont accompagnés d'une déformation élastique.

ii d'étudier le couplage avec le champ électrique créé par les phonons optiques dans les matériaux polaires (couplage de Fröhlich).

iii d'étudier les effets de la nanostructuration sur le couplage électron-phonon, d'abord sur des superréseaux, puis sur des fils semiconducteurs.

Ces deux derniers points sont fondamentaux dans le projet de J. Sjakste au CNRS. D'autre part, l'apport d'une nouvelle méthode pour calculer les éléments de matrice du couplage électron-phonon avec les fonctions de Wannier devra permettre d'accélérer le calcul (M. Calandra, IMPMC - Université Paris VI P.M. Curie). Ces fonctions de Wannier sont maintenant utilisées également dans le calcul de quasiparticule en GW, ce qui permet un gain important dans le temps d'éxécution des programmes [56, 57].

Enfin, les excitations électroniques (sous-section 1.3.1), et les spectres de perte d'énergie électronique, sont toujours d'intérêt, par une nouvelle méthode en TDDFT, beaucoup plus efficace, qui s'appuie sur la résolution de l'équation de Liouville [58]. Selon moi, l'intérêt à long terme de cette orientation est que la solution de l'équation de Liouville est la base d'une équation de Bolzmann complètement quantique, permettant de modéliser à la fois le transport électronique incohérent (auquel nos constantes de couplage électron-phonon contribuent) et le transport cohérent [59]. D'autre part, elle peut être couplée avec les déplacements atomiques.

L'ambition à terme est en effet de prédire la relaxation atomique produite par l'excitation électronique: on aura alors une description *ab initio* des effets d'irradiation, et des défauts produits par irradiation.

1.5 Plan de ce manuscrit

La section suivante regroupe la bibliographie propre à ce chapitre uniquement.

Par commodité, et également pour entériner le fait que l'anglais est notre langue de travail, les chapitres suivants sont en anglais.

Le chapitre 2 regroupe différentes notes de travail qui permettent de comprendre comment est calculée la fonction diélectrique inverse en TDDFT, et quel est le lien avec la fonction de perte électronique observée. J'ai voulu redériver les principaux résultats, n'ayant trouvé nulle part dans la littérature le cheminement complet. Mon souhait est que ces notes soient utiles dans la formation des jeunes scientifiques que j'encadrerai.

Le chapitre 3 donne les principaux résultats théoriques sur la fonction diélectrique inverse dans des oxydes non corrélés. Les résultats de ce chapitre permettent de comprendre que la TDDFT, et l'approximation plus simple de la phase aléatoire ou RPA, sont des approximations adéquates pour calculer les spectres de perte d'énergie électronique des électrons de valence. L'amélioration de la résolution des expériences de perte d'énergie électronique est primordiale pour étudier de façon fine la réponse des électrons de valence, par exemple lorsque le cristal présente différentes phases cristallines.

Le chapitre 4 donne les principaux résultats théoriques pour les calculs de spectres d'absorption optique. J'y présente une nouvelle interprétation de travail sur le noyau permettant de modéliser les effets excitoniques en théorie de la fonctionnelle de la densité dépendante du temps.

Enfin, le chapitre 5 résume les derniers calculs menés sur les carbures de bore. Ce chapitre est en fait un article de revue écrit suite à une conférence invitée au 16^{th} International Symposium on Boron, Borides and Related Materials September 7-12 , 2008, Matsue, Shimane, Japan.

Enfin, dans les annexes, je décris les différentes phases de la zircone (Annexe A), je redérive la règle d'or de Fermi (Annexe B), je précise mon curriculum vitae (Annexe C) et ma liste de publications (Annexe D), avant de donner la bibliographie générale, qui regroupe celle de ce chapitres et des suivants.

1.6 Bibliographie de ce chapitre

[1] W. Kohn. *Nobel Lectures, Chemistry 1996-2000.* World Scientific Publishing Co., Singapore, 2003.

[2] R. O. Jones and O. Gunnarsson. The density functional formalism, its applications and prospects. *Reviews of Modern Physics*, 61:689, 1989.

[3] P. Giannozzi, S. de Gironcoli, P. Pavone, and S. Baroni. *Ab initio* calculation of phonon dispersions in semiconductors. *Phys. Rev. B*, 43:7231, 1991.

[4] F. Mauri, O. Zakharov, S. de Gironcoli, S.G. Louie, and M.L. Cohen. Phonon softening and superconductivity in tellurium under pressure. *Phys. Rev. Lett.*, 77:1151, 1996.

[5] J. Sjakste, N. Vast, and V. Tyuterev. *Ab initio* method for the electron-phonon scattering times in semiconductors: application to GaAs and GaP. *Physical Review Letters*, 99:236405, 2007. Selected by the American Physical Society for the January 2008 issue of Virtual Journal of Ultrafast Science. http://www.vjultrafast.org.

[6] Matteo Calandra, Nathalie Vast, and Francesco Mauri. Superconductivity from doping boron icosahedra. *Phys. Rev. B*, 69:224505, 2004.

[7] E. Runge and E.K.U. Gross. Density-functional theory for time-dependent systems. *Phys. Rev. Lett.*, 52:997, 1984.

[8] E. K. U. Gross and W. Kohn. Local density-functional theory of frequency-dependent linear response. *Phys. Rev. Lett.*, 55:2850, 1985.

[9] Silvana Botti, Francesco Sottile, Nathalie Vast, Valerio Olevano, Lucia Reining, Hans-Christian Weissker, Angel Rubio, Giovanni Onida, Rodolfo Del Sole, and R. W. Godby. Long-range contribution to the exchange-correlation kernel of time-dependent density functional theory. *Phys. Rev. B*, 69:155112, 2004.

[10] G. Onida, L. Reining, and A. Rubio. Electronic excitations: Density functional versus many body green's functions approaches. *Rev. Mod. Phys.*, 74:601, 2002.

[11] R. W. Godby, M. Schlüter, and L. J. Sham. Self-energy operators and exchange-correlation potentials in semiconductors. *Phys. Rev. B*, 37:10159, 1988.

[12] M. Lannoo, M. Schlüter, and L. J. Sham. Calculation of the kohn-sham potential and its discontinuity for a model-semiconductor. *Phys. Rev. B*, 32:3890, 1985.

[13] L. Hedin and B.I. Lundqvist. Solid state physics. volume 23, page 1. Academic Press, New York, 1969.

[14] L. Hedin. *Phys. Rev.*, 139:A796, 1965.

[15] S. Albretch, L. Reining, R. Del Sole, and G. Onida. *Phys. Rev. Lett.*, 80:4510, 1998.

[16] L. Benedict, E. Shirley, and R.B. Bohn. Theory of optical absorption in diamond, Si, Ge, and GaAs. *Phys. Rev. B*, 57:R9385, 1998.

[17] L. Benedict, E. Shirley, and R.B. Bohn. Optical absorption of insulators and the electron-hole interaction: An ab initio calculation. *Physical Review Letters*, 80:4514, 1998.

[18] M. Rohlfing and S. Louie. Electron-hole excitations in semiconductors and insulators. *Phys. Rev. Lett.*, 82:1959, 1998.

[19] N. Vast, L. Reining, V. Olevano, P. Schattschneider, and B. Jouffrey. Local field effects and the anisotropy of the electron energy loss spectrum of titanium dioxide TiO_2. *Phys. Rev. Lett.*, 88:37601, 2002.

[20] A.G. Marinopoulos, L. Reining, A. Rubio, and N. Vast. Optical and loss spectra of carbon nanotubes: depolarization effects and intertube interactions. *Phys. Rev. Lett.*, 91:046402, 2003.

[21] S. Botti, N. Vast, L. Reining, V. Olevano, and L. C. Andreani. *Ab initio* calculation of the dielectric tensor of GaAs/AlAs superlattices. *Phys. Rev. Lett.*, 89:216803, 2002.

[22] S. Botti. *Semiempirical and* ab initio *calculations of optical properties in semiconductor superlattices.* PhD thesis, Università di Pavia, Italie, 2002.

[23] S. Botti, N. Vast, L. Reining, V. Olevano, and L. C. Andreani. *Ab initio* and semi-empirical dielectric response of superlattices. *Phys. Rev. B*, 70:045301, 2004.

[24] L.K. Dash, Nathalie Vast, Philippe Baranek, Marie-Claude Cheynet, and Lucia Reining. Electronic structure and electron energy-loss spectroscopy of ZrO_2 zirconia. *Physical Review B*, 70:245116, 2004.

[25] F. Sottile, F. Bruneval, A.G Marinopoulos, L. Dash, S. Botti, V. Olevano, N. Vast, A. Rubio, and L. Reining. TDDFT from molecules to solids: the role of long-range interactions. *Int. J. Quant. Chem.*, 102:684, 2005.

[26] L.K. Dash, Fabien Bruneval, Virginie Trinité, Nathalie Vast, and Lucia Reining. Electronic excitations: *ab initio* calculations of electronic spectra and application to zirconia ZrO_2, titania TiO_2 and cuprous oxide Cu_2O. *Comp. Mat. Sci.*, 38:482, 2006.

[27] S. Faleev, M. van Schilfgaarde, and T. Kotani. All-electron self-consistent GW approximation: Application to Si, MnO, and NiO. *Phys. Rev. Lett.*, 93:126406, 2004.

[28] F. Bruneval. *Echange et Corrélation dans la Structure Electronique des Solides, du Silicium à l'Oxyde Cuivreux: Approximation GW et au-delà.* PhD thesis, Ecole Polytechnique, Palaiseau, France, 2005.

[29] Fabien Bruneval, Nathalie Vast, Lucia Reining, M. Izquierdo, F. Sirotti, and N. Barrett. Exchange and correlation effects in electronic excitation of Cu_2O. *Phys. Rev. Lett.*, 97:267601, 2006. and refererences herein.

[30] Fabien Bruneval, Nathalie Vast, and Lucia Reining. Effect of self-consistency on quasiparticles in solids. *Phys. Rev. B*, 74:045102, 2006.

[31] J. Sjakste, V. Tyuterev, and N. Vast. Intervalley scattering in GaAs: *ab initio* calculation of the effective parameters for Monte Carlo simulations. *Applied Physics A*, 86:301, 2007.

[32] J. Sjakste, V. Tyuterev, and N. Vast. emphAb initio study of $\Gamma - X$ intervalley scattering in GaAs under pressure. *Phys. Rev. B*, 74:235216, 2006.

[33] N. Vast. *Propriétés vibrationnelles du bore α et du carbure de bore B_4C.* PhD thesis, Université Paris VI, France, 1998.

[34] Nathalie Vast. Propriétés vibrationnelles du bore α et du carbure de bore B_4C. *Thèse de doctorat. Université Paris VI, France et rapport CEA-R-5842*, 1999.

[35] R.B. Kaner, J.J. Gilman, and S.H. Tolbert. Designing superhard materials. *Sciences*, 308:1268, 2005.

[36] N. Vast, S. Baroni, G. Zérah, J. M. Besson, A. Polian, J.C. Chervin, and M. Grimsditch. Lattice-dynamics of α-boron from *ab initio* calculation and Raman scattering under high pressure. *Phys. Stat. Sol. (b)*, 198:115, 1996.

[37] N. Vast, S. Baroni, G. Zérah, J. M. Besson, A. Polian, M. Grimsditch, and J. C. Chervin. Lattice dynamics of icosahedral α-boron under pressure. *Phys. Rev. Lett.*, 78:693, 1997.

[38] R. Lazzari, N. Vast, J.M. Besson, S. Baroni, and Andrea Dal Corso. Structural and vibrational properties of icosahedral B_4C boron carbide. *Phys. Rev. Lett.*, 83:3230, 1999.

[39] R. Lazzari, N. Vast, J.M. Besson, S. Baroni, and Andrea Dal Corso. Erratum: structural and vibrational properties of icosahedral B_4 boron carbide. *Phys. Rev. Lett.*, 85:4194, 2000.

[40] N.Vast, J.M. Besson, S.Baroni, and A. Dal Corso. Atomic structure and vibrational properties of icosahedral α-boron and B_4C boron carbide. *Comp. Mat. Sci.*, 17:127, 2000.

[41] G. Fanchini, J.W. McCauley, and M. Chhowalla. *Phys. Rev. Lett*, 97:035502, 2006. Les résultats de ce papier sont erronés. La forme du carbure de bore B_{12}-C-C-C est quasi inexistante selon nos calculs.

[42] F. Mauri, N. Vast, and C. J. Pickard. Atomic structure of icosahedral B_4C boron carbide from a *first-principles* analysis of NMR spectra. *Phys. Rev. Lett.*, 87:085506, 2001.

[43] M. I. Eremets, V. V. Struzhkin, H. Mao, and R. J. Hemley. *Science*, 293:272, 2001.

[44] A. R. Oganov, J. Chen, d Y. Ma C. Gatti a, C. W. Glass, Z. Liu, T. Yu, O. O. Kurakevych, and V. L. Solozhenko. *Nature*, 457:863, 2009.

[45] J.E. Saal, S. Shang, and Z.-K. Liu. The structural evolution of boron carbide via *ab initio* calculations. *Appl. Phys. Lett.*, 91:231915, 2007.

[46] A. Masago, K. Shirai, and H. Katayama-Yoshida. *Phys. Rev. B*, 73:104102, 2006.

[47] N. G. Szwacki, A. Sadrzadeh, and B. I. Yakobson. *Phys. Rev. Lett.*, 98:166804, 2007.

[48] N. Vast, J. Sjakste, and E. Betranhandy. Boron carbides from first principles. *Journal of Physics: Conference proceedings*, 2009. Review article with 3 referees. To be published.

[49] T.J. Vogler, W.D. Reinhart, and L.C. Chhabildas. Dynamic behavior of boron carbide. *J. Appl. Phys.*, 95:4173, 2004.

[50] M. Chen, J.W. McCauley, and K.J. Hemker. Shock-induced localized amorphization in boron carbide. *Science*, 299:1563, 2003.

[51] D. Ghosh, G. Subhash, C.H. Lee, and Y.K. Yap. Strain-induced formation of carbon and boron clusters in boron icarbide during dynamic indentation. *Applied Physics Letters*, 91:061910, 2007.

[52] X.Q. Yan, Z. Tangi, L. Zhang, J.J. Guo, C.Q. Jin, Y. Zhang, T. Goto, J.M. McCaulay, and M.W. Chen. Depressurization amorphization of single-crystal boron carbide. *Phys. Rev. Lett.*, 102:075505, 2009.

[53] X.Q. Yan, W.J. Li, and M.W. Chen. Raman spectroscopy of pressure-induced amorphous boron carbide. *Appl. Phys. Lett.*, 88:131905, 2006.

[54] V. Trinité. *Etude théorique des phases du titane.* PhD thesis, Ecole Polytechnique, Palaiseau, France, 2006.

[55] H. Dekura, K. Shirai, and H. Katayama-Yoshidai. Valence control of α-rhombohedral boron by electronic doping. *J. Phys. Cond. Matter*, 19:365, 2007.

[56] P. Umari, G. Stenuit, and S. Baronu. Bridging the size gap between density-functional and many-body perturbation theory. cond-mat/0811.1453.

[57] D.R. Hamann and D. Vanderbilt. *Phys. Rev. B*, 79:045109, 2009.

[58] B. Walker, A. M. Saitta, R. Gebauer, and S. Baroni. Efficient approach to time-dependent density-functional perturbation theory for optical spectroscopy. *Phys. Rev. Lett.*, 96:11300, 2006.

[59] K. Burke, R. Car, and R. Gebauer. Density functional theory of the electrical conductivity of molecular devices. *Phys. Rev. Lett.*, 97:146803, 2005.

Chapter 2

A key quantity : the inverse of the microscopic dielectric function

In this chapter I describe the theoretical basis I will be using in the following chapters.

When describing the response to an excitation, the applied macroscopic field and the total field on the microscopic scale are not equal. The microscopic field rapidly varies over the unit cell. In the standard definition of the dielectric constant ϵ, called the test-charge response, the microscopic field consists of the applied potential δV_{bare} and of the (Hartree) potential $\delta V_{Hartree}$ that comes from the charge density induced by the external field. The Hartree field includes the so called *local fields* which determines the polarization of the electronic system [60].

Instead, I will be using the electron-electron dielectric constant $\tilde{\epsilon}$ in the following sections (except the final one). Then, the microscopic field is the Kohn-Sham effective potential which contains an additional term with respect to above definition : the exchange and correlation potential.

Linear response yields, to first order, the relation between the external (applied) perturbing potential δV_{bare} and the total potential δV at the microscopic scale. The inverse of the microscopic dielectric function $\tilde{\epsilon}^{-1}$ also known as the screening function is the key quantity linking δV_{bare} and δV [60–62],

$$\delta V(\mathbf{r}, \mathbf{r}', t) = \int \tilde{\epsilon}^{-1}(\mathbf{r}, \mathbf{r}', t)\delta V_{bare}(\mathbf{r}', t)d\mathbf{r}'. \tag{2.1}$$

In the following sections I will step by step derive equation 2.1, and show how the inverse dielectric function is calculated in the computer program which has been used to obtain the results of the next chapters.

2.1 Ground state

Let $H^{(0)}$ be the (periodic in space) unperturbed Hamiltonian, and

$$H^{(0)}|\psi^{(0)}_{n\mathbf{k}}>=\varepsilon^{(0)}_{n\mathbf{k}}|\psi^{(0)}_{n\mathbf{k}}>, \tag{2.2}$$

where $\varepsilon^{(0)}$ and $\psi^{(0)}$ are eigenvalues and eigenvectors of $H^{(0)}$ labelled with the band index n and the Brillouin zone wave vector $\mathbf{k}$.

The Hamiltonian of equation 2.2 can describe a many-bodied system, or simply be an Hamiltonian for a single particle. In the latter case, one often expresses $H^{(0)}$ in the framework of density functional theory (DFT) [63, 64],where it consists respectively of the kinetic operator, the electron-ion potential V_{Ie}, and the self-consistent potential :

$$H^{(0)}=\frac{-\hbar^2}{2m}\nabla^2+V_{Ie}+V_{scf}, \tag{2.3}$$

where $\hbar$ is Planck's constant (divided by 2π), and m the electronic mass. V_{Ie} is often treated in the pseudopotential approximation [65], and V_{scf} consists of the classical electrostatic potential $V_{Hartree}$ and the quantum exchange and correlation potential, V_{xc}.

In the absence of any perturbation, the time propagation of the electronic wave function is given by

$$|\phi^{(0)}_{n\mathbf{k}}(t)>=e^{-i\varepsilon^{(0)}_{n\mathbf{k}}\frac{t}{\hbar}}|\psi^{(0)}_{n\mathbf{k}}>. \tag{2.4}$$

and the set of $|\phi^{(0)}(t)>$ forms a basis of stationary states for the unperturbed system [66].

2.2 Effect of a perturbation

Electronic excitations are time dependent processes. Following Ref. [66], together with the introduction of a time dependent perturbation $\delta V(t)$, conservation of total energy breaks down, and there are no longer any stationary states. The system can make a transition from the initial stationary state $|\psi^{(0)}_{n\mathbf{k}}>$ to any other state.

The transition probability might be calculated in several cases [66]. For instance, if the perturbation is applied adiabatically, and the initial state $|\psi^{(0)}_{n\mathbf{k}}>$ is a non degenerate stationary state, the system may remain in this state. Another extreme case is the application of $\delta V(t)$ in a very short time: the system has no time to change and might stay in the state $|\psi^{(0)}_{n\mathbf{k}}>$, which, however, is no longer a stationary state of the new Hamiltonian.

Let us call $\delta V(\mathbf{r},t)$ the *total* time dependent perturbation, consisting of the external (applied) potential δV_{bare} plus the electronic response δV_{scf}. Within the density functional theory, the latter consists of the variation of the electrostatic potential $\delta V_{Hartree}$ plus the variation of the exchange and correlation potential, δV_{xc} :

$$\delta V(\mathbf{r},t) = \delta V_{bare}(\mathbf{r},t) + \delta V_{Hartree}(\mathbf{r},t) + \delta V_{xc}(\mathbf{r},t). \tag{2.5}$$

The total Hamiltonian is $H(t) = H^{(0)} + \delta V(t)$, and to calculate the properties of the excited state, one has to solve Schrödinger's equation :

$$i\hbar \frac{d|\psi(t)}{dt} = H(t)|\psi(t)> . \tag{2.6}$$

Then, one has to calculate the wave functions in the basis of the stationary states of the unperturbed system given by eq. 2.4 [66].

$$|\psi(t)>= \sum_{n\mathbf{k}} a_{n\mathbf{k}} e^{-i\varepsilon^{(0)}_{n\mathbf{k}}\frac{t}{\hbar}} |\psi^{(0)}_{n\mathbf{k}}> . \tag{2.7}$$

2.3 Time dependent perturbation theory

Keeping the $a_{n\mathbf{k}}$ coefficients to first-order, the wave function reads

$$|\psi(t)>= \sum_{n\mathbf{k}} a^{(0)}_{n\mathbf{k}} e^{-i\varepsilon^{(0)}_{n\mathbf{k}}\frac{t}{\hbar}} |\psi^{(0)}_{n\mathbf{k}}> + \sum_{n\mathbf{k}} a^{(1)}_{n\mathbf{k}}(t) e^{-i\varepsilon^{(0)}_{n\mathbf{k}}\frac{t}{\hbar}} |\psi^{(0)}_{n\mathbf{k}}> + ... \tag{2.8}$$

The solution of eq. 2.6 to zeroth order results in the zeroth-order $a^{(0)}_{n\mathbf{k}}$ being time-independent.

One is left with eq. 2.6 to first-order

$$i\hbar \sum_{n\mathbf{k}} \frac{da^{(1)}_{n\mathbf{k}}(t)}{dt} e^{-i\varepsilon^{(0)}_{n\mathbf{k}}\frac{t}{\hbar}} |\psi^{(0)}_{n\mathbf{k}}>= \sum_{n\mathbf{k}} a^{(0)}_{n\mathbf{k}} e^{-i\varepsilon^{(0)}_{n\mathbf{k}}\frac{t}{\hbar}} \delta V(t) |\psi^{(0)}_{n\mathbf{k}}> . \tag{2.9}$$

Projecting onto $< \psi^{(0)}_{m\mathbf{k}'}|$ one obtains

$$a^{(1)}_{m\mathbf{k}'}(t) = \frac{-i}{\hbar} \sum_{n\mathbf{k}} a^{(0)}_{n\mathbf{k}} \int_{t_0=0}^{t} e^{-i(\varepsilon^{(0)}_{n\mathbf{k}} - \varepsilon^{(0)}_{m\mathbf{k}'})\frac{\tau}{\hbar}} < \psi^{(0)}_{m\mathbf{k}'}|\delta V(\tau)|\psi^{(0)}_{n\mathbf{k}}> d\tau. \tag{2.10}$$

We will now compute the integral in eq. 2.10 for a given form of the perturbing potential.

2.4 Solution for a time periodic perturbation

Following Ref. [60] let us suppose that the *applied* perturbation is Hermitian and time periodic, i.e.,

$$\delta V_{bare}(\mathbf{r},t) = (\delta V_{bare} e^{i\omega t} + c.c.)e^{\alpha t}, \tag{2.11}$$

where the term $e^{\alpha t}$ is understood with a real, positive and small α which guarantees an adiabatic switch on of the perturbation. The first term on the right-hand side stands for a photon emission, and $c.c.$ stands for the complex conjugate term, a photon absorption.

Let us moreover suppose that the applied perturbation is a (in space) slowly varying external potential [60–62],

$$\delta V_{bare}(\mathbf{r},t) = \delta V_{bare}(\mathbf{q},\mathbf{r},\omega)e^{-i(\mathbf{q}.\mathbf{r}-\omega t)}e^{\alpha t} + c.c., \tag{2.12}$$

where the wavelength of the perturbation is $2\pi/|\mathbf{q}|$, and the wavevector length $|\mathbf{q}|$ is small compared to the reciprocal lattice vector length $|\mathbf{G}|$.

Neglecting memory effects, the *total* potential is, to first order, also time periodic,

$$\delta V(t) = (Fe^{i\omega t} + F^{\dagger}e^{-i\omega t})e^{\alpha t}. \tag{2.13}$$

With $F = F^{\mathbf{q}} = F^0(\mathbf{q},\mathbf{r},\omega)e^{-i(\mathbf{q}.\mathbf{r})}$, eq. 2.13 reads

$$\delta V(\mathbf{r},t) = [F^0(\mathbf{q},\mathbf{r},\omega)e^{-i(\mathbf{q}.\mathbf{r}-\omega t)} + F^{0\,\dagger}(\mathbf{q},\mathbf{r},\omega)e^{i(\mathbf{q}.\mathbf{r}-\omega t)}]e^{\alpha t}. \tag{2.14}$$

One expresses F^0 in terms of its Fourier components in the spaces dual to $\mathbf{r}$ and t,

$$X(\mathbf{r},t) = \int d\omega \sum_{\mathbf{G}} X(\mathbf{G},\omega)e^{-i\mathbf{G}.\mathbf{r}}e^{i\omega t} \tag{2.15}$$

Because of local fields, the total potential will in general contain rapidly varying terms with wavevector $\mathbf{q}+\mathbf{G}$

$$\delta V(\mathbf{r},t) = \sum_{\mathbf{G}}[F^0(\mathbf{q},\omega,\mathbf{G})e^{-i(\mathbf{q}+\mathbf{G}).\mathbf{r}+i\omega t)} + F^{0\,*}(\mathbf{q},\omega,\mathbf{G})e^{i(\mathbf{q}+\mathbf{G}).\mathbf{r}-i\omega t)}]e^{\alpha t}. \tag{2.16}$$

Let us call

$$\mathcal{F}^{\mathbf{q}}_{m\mathbf{k}'n\mathbf{k}}(t) = (e^{i\omega t}\frac{<\psi^{(0)}_{m\mathbf{k}'}|F^{\mathbf{q}}|\psi^{(0)}_{n\mathbf{k}}>}{\varepsilon^{(0)}_{n\mathbf{k}} - \varepsilon^{(0)}_{m\mathbf{k}'} - \hbar\omega - i\hbar\alpha} + e^{-i\omega t}\frac{<\psi^{(0)}_{m\mathbf{k}'}|F^{\mathbf{q}\,\dagger}|\psi^{(0)}_{n\mathbf{k}}>}{\varepsilon^{(0)}_{n\mathbf{k}} - \varepsilon^{(0)}_{m\mathbf{k}'} + \hbar\omega - i\hbar\alpha})e^{\alpha t}. \tag{2.17}$$

Solution of eq. 2.10 yields

$$a^{\mathbf{q}\,(1)}_{m\mathbf{k}'}(t) = \sum_{n\mathbf{k}} a^{(0)}_{n\mathbf{k}}[e^{-i(\varepsilon^{(0)}_{n\mathbf{k}} - \varepsilon^{(0)}_{m\mathbf{k}'})\frac{t}{\hbar}}\mathcal{F}^{\mathbf{q}}_{m\mathbf{k}'n\mathbf{k}}(t) - \mathcal{F}^{\mathbf{q}}_{m\mathbf{k}'n\mathbf{k}}(t_0=0)], \tag{2.18}$$

and thus

$$|\psi^{\mathbf{q}}(t)>=\sum_{n\mathbf{k}} a^{(0)}_{n\mathbf{k}} e^{-i\varepsilon^{(0)}_{n\mathbf{k}}\frac{t}{\hbar}}|\psi^{(0)}_{n\mathbf{k}}>+\sum_{n\mathbf{k}m\mathbf{k}'} a^{(0)}_{m\mathbf{k}'}(t)[e^{-i\varepsilon^{(0)}_{m\mathbf{k}'}\frac{t}{\hbar}}\mathcal{F}^{\mathbf{q}}_{n\mathbf{k}m\mathbf{k}'}(t)-e^{-i\varepsilon^{(0)}_{n\mathbf{k}}\frac{t}{\hbar}}\mathcal{F}^{\mathbf{q}}_{n\mathbf{k}m\mathbf{k}'}(t_0=0)]|\psi^{(0)}_{n\mathbf{k}} \tag{2.19}$$

2.5 Zeroth order density matrix

The single particle density matrix reads

$$\rho^{\mathbf{q}}(t)=|\psi^{\mathbf{q}}(t)><\psi^{\mathbf{q}}(t)|. \tag{2.20}$$

To zeroth order, one has, with $|\psi^{\mathbf{q}}(t)>$ from eq. 2.19,

$$\rho^{(0)}=\sum_{n\mathbf{k}m\mathbf{k}'} a^{(0)*}_{m\mathbf{k}'}a^{(0)}_{n\mathbf{k}}e^{-i(\varepsilon^{(0)}_{n\mathbf{k}}-\varepsilon^{(0)}_{m\mathbf{k}'})\frac{t}{\hbar}}|\psi^{(0)}_{n\mathbf{k}}><\psi^{(0)}_{m\mathbf{k}'}|, \tag{2.21}$$

with [60]

$$\rho^{(0)}|\psi^{(0)}_{p\mathbf{k}''}>=f^{(0)}(\varepsilon^{(0)}_{p\mathbf{k}''})|\psi^{(0)}_{p\mathbf{k}''}>=\sum_{n\mathbf{k}} a^{(0)*}_{p\mathbf{k}''}a^{(0)}_{n\mathbf{k}}e^{-i(\varepsilon^{(0)}_{n\mathbf{k}}-\varepsilon^{(0)}_{p\mathbf{k}''})\frac{t}{\hbar}}|\psi^{(0)}_{n\mathbf{k}}>, \tag{2.22}$$

where $f^{(0)}(\varepsilon^{(0)}_{p\mathbf{k}''})$ stands for the occupation number, and as

$$<\psi^{(0)}_{l\mathbf{k}_1}|\rho^{(0)}|\psi^{(0)}_{p\mathbf{k}_2}>=f^{(0)}(\varepsilon^{(0)}_{p\mathbf{k}_2})\delta_{l\mathbf{k}_1;p\mathbf{k}_2}, \tag{2.23}$$

one gets the very important relation

$$a^{(0)*}_{p\mathbf{k}_2}a^{(0)}_{l\mathbf{k}_1}e^{-i(\varepsilon^{(0)}_{l\mathbf{k}_1}-\varepsilon^{(0)}_{p\mathbf{k}_2})\frac{t}{\hbar}}=f^{(0)}(\varepsilon^{(0)}_{p\mathbf{k}_2})\delta_{l\mathbf{k}_1;p\mathbf{k}_2}. \tag{2.24}$$

Eq. 2.24 will be used in the next section.

2.6 First order density matrix

One obtains the first order density matrix from eq.s 2.19 and 2.20

$$\rho^{\mathbf{q}\,(1)}=\sum_{n\mathbf{k}m\mathbf{k}'p\mathbf{k}''} a^{(0)*}_{m\mathbf{k}'}a^{(0)}_{p\mathbf{k}''}[e^{-i(\varepsilon^{(0)}_{p\mathbf{k}''}-\varepsilon^{(0)}_{m\mathbf{k}'})\frac{t}{\hbar}}\mathcal{F}^{\mathbf{q}}_{n\mathbf{k}p\mathbf{k}''}(t)-$$
$$e^{-i(\varepsilon^{(0)}_{n\mathbf{k}}-\varepsilon^{(0)}_{m\mathbf{k}'})\frac{t}{\hbar}}\mathcal{F}^{\mathbf{q}}_{n\mathbf{k}p\mathbf{k}''}(t_0=0)]|\psi^{(0)}_{n\mathbf{k}}><\psi^{(0)}_{m\mathbf{k}'}|+c.c. \tag{2.25}$$

The matrix elements then read, using eq. 2.24,

$$<\psi^{(0)}_{l\mathbf{k}_1}|\rho^{\mathbf{q}\,(1)}|\psi^{(0)}_{p\mathbf{k}_2}>=$$
$$f^{(0)}(\varepsilon^{(0)}_{p\mathbf{k}_2})[\mathcal{F}^{\mathbf{q}}_{l\mathbf{k}_1p\mathbf{k}_2}(t)-e^{-i(\varepsilon^{(0)}_{l\mathbf{k}_1}-\varepsilon^{(0)}_{p\mathbf{k}_2})\frac{t}{\hbar}}\mathcal{F}^{\mathbf{q}}_{l\mathbf{k}_1p\mathbf{k}_2}(t_0=0)]+$$
$$f^{(0)}(\varepsilon^{(0)}_{l\mathbf{k}_1})[\mathcal{F}^{\mathbf{q}\,*}_{p\mathbf{k}_2l\mathbf{k}_1}(t)-e^{-i(\varepsilon^{(0)}_{l\mathbf{k}_1}-\varepsilon^{(0)}_{p\mathbf{k}_2})\frac{t}{\hbar}}\mathcal{F}^{\mathbf{q}}_{p\mathbf{k}_2l\mathbf{k}_1}(t_0=0)]. \tag{2.26}$$

Remembering eq. 2.13, $\delta V^{\mathbf{q}}(\mathbf{r},t) = (F^{\mathbf{q}}e^{i\omega t} + F^{\mathbf{q}\,\dagger}e^{-i\omega t})e^{\alpha t}$, the matrix elements in terms of $F^{\mathbf{q}}$ and $F^{\mathbf{q}\,\dagger}$ operators read

$$\begin{aligned} < \psi^{(0)}_{l\mathbf{k}_1}|\rho^{\mathbf{q}(1)}|\psi^{(0)}_{p\mathbf{k}_2} > = e^{\alpha t} I_0^{\mathbf{q}} + \\ e^{\alpha t}e^{i\omega t}[f^{(0)}(\varepsilon^{(0)}_{p\mathbf{k}_2}) - f^{(0)}(\varepsilon^{(0)}_{l\mathbf{k}_1})]\frac{< \psi^{(0)}_{l\mathbf{k}_1}|F^{\mathbf{q}}|\psi^{(0)}_{p\mathbf{k}_2} >}{\varepsilon^{(0)}_{p\mathbf{k}_2} - \varepsilon^{(0)}_{l\mathbf{k}_1} - \hbar\omega - i\hbar\alpha} + \\ e^{\alpha t}e^{-i\omega t}[f^{(0)}(\varepsilon^{(0)}_{p\mathbf{k}_2}) - f^{(0)}(\varepsilon^{(0)}_{l\mathbf{k}_1})]\frac{< \psi^{(0)}_{l\mathbf{k}_1}|F^{\mathbf{q}\,\dagger}|\psi^{(0)}_{p\mathbf{k}_2} >}{\varepsilon^{(0)}_{p\mathbf{k}_2} - \varepsilon^{(0)}_{l\mathbf{k}_1} + \hbar\omega - i\hbar\alpha}. \end{aligned} \tag{2.27}$$

In the previous equation, the $I_0^{\mathbf{q}}$ term can be chosen such that, at initial time t_0, first order terms in the wavefunction and in the density vanish, $a^{\mathbf{q}\,(1)}_{n\mathbf{k}}(t_0 = 0) = 0$ and $\rho^{\mathbf{q}\,(1)}(t_0 = 0) = 0$,

$$\begin{aligned} I_0^{\mathbf{q}} = -e^{-i(\varepsilon^{(0)}_{l\mathbf{k}_1} - \varepsilon^{(0)}_{p\mathbf{k}_2})\frac{t}{\hbar}}[f^{(0)}(\varepsilon^{(0)}_{p\mathbf{k}_2}) - f^{(0)}(\varepsilon^{(0)}_{l\mathbf{k}_1})] \\ (\frac{< \psi^{(0)}_{l\mathbf{k}_1}|F^{\mathbf{q}}|\psi^{(0)}_{p\mathbf{k}_2} >}{\varepsilon^{(0)}_{p\mathbf{k}_2} - \varepsilon^{(0)}_{l\mathbf{k}_1} - \hbar\omega - i\hbar\alpha} + \frac{< \psi^{(0)}_{l\mathbf{k}_1}|F^{\mathbf{q}\,\dagger}|\psi^{(0)}_{p\mathbf{k}_2} >}{\varepsilon^{(0)}_{p\mathbf{k}_2} - \varepsilon^{(0)}_{l\mathbf{k}_1} + \hbar\omega - i\hbar\alpha}). \end{aligned} \tag{2.28}$$

Alternatively, if one uses the adiabatic switch at $t_0 = -\infty$ ($e^{\alpha t} \to 0$) and then the initial conditions expressed by $I_0^{\mathbf{q}}$ vanish.

The matrix elements of the first order density matrix in eq. 2.27 are key quantities to obtain the electronic response functions χ^0, χ and $\tilde{\epsilon}^{-1}$. To obtain them, we have linearized Schrödinger's equation 2.6, hence the name "Linear Response" given to this theoretical framework.

2.7 Conservation of crystal momentum

In above equations, matrix elements of the form $< \psi^{(0)}_{l\mathbf{k}_1}|F^{\mathbf{q}}|\psi^{(0)}_{p\mathbf{k}_2} >$ read

$$\sum_{\mathbf{G}} F^0(\mathbf{G},\mathbf{q},\omega)\sum_{\mathbf{G}_1}\psi^{(0)}_{p\mathbf{k}_2}(\mathbf{G}_1)\sum_{\mathbf{G}_2}\psi^{(0)\,*}_{l\mathbf{k}_1}(\mathbf{G}_2)\int d\mathbf{r}e^{-i(\mathbf{q}+\mathbf{G}).\mathbf{r}}e^{-i(\mathbf{k}_1+\mathbf{G}_1).\mathbf{r}}e^{i(\mathbf{k}_2+\mathbf{G}_2).\mathbf{r}}. \tag{2.29}$$

The integral yields the delta function

$$\delta(\mathbf{k}_2 + \mathbf{G}_2 - \mathbf{k}_1 - \mathbf{G}_1 - \mathbf{q} - \mathbf{G}), \tag{2.30}$$

and thus the law for the conservation of the crystal momentum

$$\mathbf{k}_2 = \mathbf{k}_1 + \mathbf{q} + \mathbf{G}, \tag{2.31}$$

where $\mathbf{G}$ is a reciprocal lattice vector. The Umklapp processes are included in the sum ($\mathbf{G} \neq \mathbf{0}$). They give rise to local field corrections [62].

From now on, $\mathbf{k}_2$ is assumed to satisfy the above conservation law, eq. 2.31.

2.8 Induced change in the electronic density

The induced change in the electronic density $\delta n^{\mathbf{q}}(\mathbf{r}, t)$ is the diagonal term of the first-order density matrix and reads

$$(-e)\delta n^{\mathbf{q}}(\mathbf{r}, t) = Tr[\rho^{\mathbf{q}\,(1)}(-e)\delta(\mathbf{r} - \hat{\mathbf{r}})], \tag{2.32}$$

where $\hat{\mathbf{r}}$ is the position operator, and $-e$ is the charge of one electron.

Developing previous equation on the basis of the unperturbed wavefunctions (closure relation) yields

$$\begin{aligned}\delta n^{\mathbf{q}}(\mathbf{r}) =& < \mathbf{r}|\rho^{\mathbf{q}\,(1)}|\mathbf{r} > \\ &= \sum_{l\mathbf{k}_1 p\mathbf{k}_2} < \mathbf{r}|\psi^{(0)}_{l\mathbf{k}_1} >< \psi^{(0)}_{l\mathbf{k}_1}|\rho^{\mathbf{q}\,(1)}|\psi^{(0)}_{p\mathbf{k}_2} >< \psi^{(0)}_{p\mathbf{k}_2}|\mathbf{r} > \\ &= \sum_{l\mathbf{k}_1 p\mathbf{k}_2} \psi^{(0)\,*}_{p\mathbf{k}_2}(\mathbf{r}) < \psi^{(0)}_{l\mathbf{k}_1}|\rho^{\mathbf{q}\,(1)}|\psi^{(0)}_{p\mathbf{k}_2} > \psi^{(0)}_{l\mathbf{k}_1}(\mathbf{r}).\end{aligned} \tag{2.33}$$

$\delta n^{\mathbf{q}}$ has the form

$$\delta n^{\mathbf{q}}(\mathbf{r}, t) = \delta n^0 + \delta n^{\mathbf{q}}(\mathbf{r}) e^{i\omega t} e^{\alpha t} + \delta n^{\mathbf{q}\dagger}(\mathbf{r}) e^{-i\omega t} e^{\alpha t}, \tag{2.34}$$

where δn^0 reads

$$\delta n^0 = \sum_{l\mathbf{k}_1 p\mathbf{k}_2} \psi^{(0)\,*}_{p\mathbf{k}_2}(\mathbf{r}) \psi^{(0)}_{l\mathbf{k}_1}(\mathbf{r}) e^{\alpha t} I^0_{\mathbf{q}}, \tag{2.35}$$

and vanishes in the adiabatic approximation.

In equation 2.34, $\delta n^{\mathbf{q}}(\mathbf{r})$ reads

$$\delta n^{\mathbf{q}}(\mathbf{r}) = \sum_{l\mathbf{k}_1 p\mathbf{k}_2} \psi^{(0)\,*}_{p\mathbf{k}_2}(\mathbf{r}) \psi^{(0)}_{l\mathbf{k}_1}(\mathbf{r}) [f^{(0)}(\varepsilon^{(0)}_{p\mathbf{k}_2}) - f^{(0)}(\varepsilon^{(0)}_{l\mathbf{k}_1})] \frac{< \psi^{(0)}_{l\mathbf{k}_1}|F^{\mathbf{q}}|\psi^{(0)}_{p\mathbf{k}_2} >}{\varepsilon^{(0)}_{p\mathbf{k}_2} - \varepsilon^{(0)}_{l\mathbf{k}_1} - \hbar\omega - i\hbar\alpha} \tag{2.36}$$

2.9 Poisson's equation

In addition, Poisson's equation links the electronic density to the Laplacian of the electrostatic potential [67]. Expanded to the first order, it links the induced change in the electronic density to the Laplacian of the change in the electrostatic potential $\delta V^{\mathbf{q}}_{Hartree}$:

$$\nabla^2_{\mathbf{r}}\, \delta V^{\mathbf{q}}_{Hartree}(\mathbf{r}, t) = -4\pi e^2 \delta n^{\mathbf{q}}(\mathbf{r}, t). \tag{2.37}$$

Fourier transformation of the Hartree potential yields the following equation, remembering that the induced potential contains terms with wavevector $\mathbf{q} + \mathbf{G}$ (local fields),

$$\delta V^{\mathbf{q}}_{Hartree} = (F^{\mathbf{q}}_{Hartree} e^{i\omega t} + c.c) e^{\alpha t}, \tag{2.38}$$

$$F^{\mathbf{q}}_{Hartree} = \sum_{\mathbf{G}} F^{0}_{Hartree}(\mathbf{q},\mathbf{G},\omega) e^{-i(\mathbf{q}+\mathbf{G}).\mathbf{r}}, \tag{2.39}$$

The Fourier transform of the equation 2.36 reads

$$\delta n^{\mathbf{q}}(\mathbf{r}) = \sum_{\mathbf{G}} \delta n(\mathbf{q}+\mathbf{G},\omega) e^{-i(\mathbf{q}+\mathbf{G}).\mathbf{r}}. \tag{2.40}$$

In the adiabatic approximation, one obtains the relationship between the Fourier components of the Hartree potential and of the density as

$$F^{0}_{Hartree}(\mathbf{q},\mathbf{G},\omega)|\mathbf{q}+\mathbf{G}|^2 = 4\pi e^2\, \delta n(\mathbf{q}+\mathbf{G},\omega). \tag{2.41}$$

For any $\mathbf{G}$ component other than $\mathbf{G}=\mathbf{0}$, one has

$$\delta n(\mathbf{q}+\mathbf{G},\omega) = F^{0}_{Hartree}(\mathbf{q},\mathbf{G},\omega)\frac{|\mathbf{q}+\mathbf{G}|^2}{4\pi e^2}. \tag{2.42}$$

For long wavelength ($\mathbf{q}=\mathbf{0}$) perturbation and $\mathbf{G}=\mathbf{0}$, $\delta n(\mathbf{q}+\mathbf{G},\omega)=\mathbf{0}$. In other words the induced change in density has no macroscopic component - the total macroscopic electronic density is kept constant in the excited state.

2.10 Response function χ^0

Replacing, in eq. 2.33, the matrix elements of $\rho^{\mathbf{q}\,(1)}$ with eq. 2.27, and defining I^0 and χ^0 as

$$\begin{aligned}\delta n(\mathbf{q}+\mathbf{G},\omega) = &\sum_{\mathbf{G}'} F^0(\mathbf{q},\mathbf{G}',\omega)\chi^0(\mathbf{q}+\mathbf{G},\mathbf{q}+\mathbf{G}',\omega) + \\ &\sum_{\mathbf{G}'} F^{0\,*}(\mathbf{q},\mathbf{G}',\omega)\chi^0(\mathbf{q}+\mathbf{G},-\mathbf{q}-\mathbf{G}',-\omega) \\ + \sum_{\mathbf{G}'} F^0(\mathbf{q},\mathbf{G}',\omega) I^0(\mathbf{q}+\mathbf{G},\mathbf{q}+\mathbf{G}',\omega) &+ \sum_{\mathbf{G}'} F^{0\,*}(\mathbf{q},\mathbf{G}',\omega) I^0(\mathbf{q}+\mathbf{G},-\mathbf{q}-\mathbf{G}',-\omega),\end{aligned} \tag{2.43}$$

one obtains the I^0 term, whose effect vanishes in the adiabatic limit $t_0 = -\infty$, ,

$$\begin{aligned}I^0(\mathbf{q}+\mathbf{G},\mathbf{q}+\mathbf{G}',\omega) = -\sum_{l\mathbf{k}_1 p\mathbf{k}_2} e^{-i(\varepsilon^{(0)}_{l\mathbf{k}_1}-\varepsilon^{(0)}_{p\mathbf{k}_2})\frac{t}{\hbar}}[f^{(0)}(\varepsilon^{(0)}_{p\mathbf{k}_2}) - f^{(0)}(\varepsilon^{(0)}_{l\mathbf{k}_1})] \\ \frac{< \psi^{(0)}_{l\mathbf{k}_1}|e^{i(\mathbf{q}+\mathbf{G}).\mathbf{r}}|\psi^{(0)}_{p\mathbf{k}_2} >< \psi^{(0)}_{p\mathbf{k}_2}|e^{-i(\mathbf{q}+\mathbf{G}').\mathbf{r}}|\psi^{(0)}_{l\mathbf{k}_1} >}{\varepsilon^{(0)}_{p\mathbf{k}_2} - \varepsilon^{(0)}_{l\mathbf{k}_1} - \hbar\omega - i\hbar\alpha}.\end{aligned} \tag{2.44}$$

The electronic response function χ^0 reads

$$\chi^0(\mathbf{q}+\mathbf{G},\mathbf{q}+\mathbf{G}',\omega) = \sum_{l\mathbf{k}_1 p\mathbf{k}_2} [f^{(0)}(\varepsilon^{(0)}_{p\mathbf{k}_2}) - f^{(0)}(\varepsilon^{(0)}_{l\mathbf{k}_1})] \frac{< \psi^{(0)}_{l\mathbf{k}_1}|e^{i(\mathbf{q}+\mathbf{G}).\mathbf{r}}|\psi^{(0)}_{p\mathbf{k}_2} >< \psi^{(0)}_{p\mathbf{k}_2}|e^{-i(\mathbf{q}+\mathbf{G}').\mathbf{r}}|\psi^{(0)}_{l\mathbf{k}_1} >}{\varepsilon^{(0)}_{p\mathbf{k}_2} - \varepsilon^{(0)}_{l\mathbf{k}_1} - \hbar\omega - i\hbar\alpha}. \tag{2.45}$$

The electronic response function χ^0 links the variation of the electronic charge density to the *total* potential through equation 2.43.

2.11 Response function χ

To obtain the relation between the variation of the electronic charge density and the *external* potential, one looks for the response function χ such as :

$$\begin{aligned}\delta n(\mathbf{q}+\mathbf{G},\omega) = &\sum_{\mathbf{G}'} \delta V_{bare}(\mathbf{q},\mathbf{G}',\omega)\chi(\mathbf{q}+\mathbf{G},\mathbf{q}+\mathbf{G}',\omega) + \\ &\sum_{\mathbf{G}'} \delta V^*_{bare}(\mathbf{q},\mathbf{G}',\omega)\chi(\mathbf{q}+\mathbf{G},-\mathbf{q}-\mathbf{G}',-\omega) \\ + \sum_{\mathbf{G}'} \delta V_{bare}(\mathbf{q},\mathbf{G}',\omega) I(\mathbf{q}+\mathbf{G},\mathbf{q}+\mathbf{G}',\omega) &+ \sum_{\mathbf{G}'} \delta V^*_{bare}(\mathbf{q},\mathbf{G}',\omega) I(\mathbf{q}+\mathbf{G},-\mathbf{q}-\mathbf{G}',-\omega),\end{aligned} \tag{2.46}$$

where, according to eq. 2.12, the external potential does not vary over a unit cell, so that

$$\delta V_{bare}(\mathbf{q},\mathbf{G},\omega) = \delta(\mathbf{G},\mathbf{0})\delta V_{bare}(\mathbf{q},\omega). \tag{2.47}$$

Fourier transforming equation 2.5, one has

$$F^0(\mathbf{q},\mathbf{G},\omega) = \delta V_{bare}(\mathbf{q},\mathbf{G},\omega) + F^0_{Hartree}(\mathbf{q},\mathbf{G},\mathbf{q},\omega) + F^0_{xc}(\mathbf{q},\mathbf{G},\omega), \tag{2.48}$$

where $F^0_{Hartree}$ has been defined in 2.42. The variation of the exchange and correlation potential $\delta V_{xc}[\delta n(\mathbf{G})]$ also depends on the variation of the electronic density.

Then, in the simplest approximation, the exchange and correlation potential is taken to follow the time dependence of the density. For instance within the local density approximation, the generalized gradient approximation[68] or the adiabatic local density approximation[69], the exchange and correlation kernel f_{xc} is defined as

$$f_{xc}(\mathbf{r},t) = \frac{\delta V_{xc}(\mathbf{r},\mathbf{t})}{\delta n(\mathbf{r}',\mathbf{t}')}\delta(\mathbf{r}-\mathbf{r}')\delta(t-t') \tag{2.49}$$

so that

$$\delta V_{xc}(\mathbf{r}, t) = f_{xc}(\mathbf{r}, t)\delta n(\mathbf{r}, \mathbf{t}). \tag{2.50}$$

In the above simplest approximations, the kernel is chosen to be local in space and time.

Using above definition together with eq. 2.42 one obtains that

$$F^0(\mathbf{q}, \mathbf{G}\omega) = \delta V_{bare}(\mathbf{q}, \mathbf{G}, \omega) + \sum_{\mathbf{G}'}[\frac{4\pi e^2}{|\mathbf{q}+\mathbf{G}'|^2}\delta(\mathbf{G}'-\mathbf{G}) + f_{xc}(\mathbf{G}'-\mathbf{G})]\delta n(\mathbf{q}+\mathbf{G}', \omega). \tag{2.51}$$

We now make eq.s 2.43 and 2.46 equal, and with the help of eq. 2.51, we obtain the term dealing with initial conditions, which vanishes in the adiabatic limit,

$$I(\mathbf{q}+\mathbf{G}, \mathbf{q}+\mathbf{G}', \omega) = I^0(\mathbf{q}+\mathbf{G}, \mathbf{q}+\mathbf{G}', \omega) +$$
$$I^0(\mathbf{q}+\mathbf{G}, \mathbf{q}+\mathbf{G}', \omega)\sum_{\mathbf{G}''}[\frac{4\pi e^2}{|\mathbf{q}+\mathbf{G}''|^2}\delta(\mathbf{G}'-\mathbf{G}'') + f_{xc}(\mathbf{G}'-\mathbf{G}'')]\chi(\mathbf{q}+\mathbf{G}', \mathbf{q}+\mathbf{G}'', \omega). \tag{2.52}$$

For the response function χ, one is left with a Dyson-like equation [70]

$$\chi(\mathbf{q}+\mathbf{G}, \mathbf{q}+\mathbf{G}', \omega) = \chi^0(\mathbf{q}+\mathbf{G}, \mathbf{q}+\mathbf{G}', \omega) +$$
$$\chi^0(\mathbf{q}+\mathbf{G}, \mathbf{q}+\mathbf{G}', \omega)\sum_{\mathbf{G}''}[\frac{4\pi e^2}{|\mathbf{q}+\mathbf{G}''|^2}\delta(\mathbf{G}'-\mathbf{G}'') + f_{xc}(\mathbf{G}'-\mathbf{G}'')]\chi(\mathbf{q}+\mathbf{G}', \mathbf{q}+\mathbf{G}'', \omega). \tag{2.53}$$

Evaluation of the response function χ requires both the knowledge of the response function χ^0 (eq. 2.45) and of the exchange and correlation kernel f_{xc} (eq. 2.49).

2.12 The inverse dielectric function $\tilde{\epsilon}^{-1}$

To obtain the relation between the external potential δV_{bare} and the total potential δV, one uses the fact (eq.s 2.34 and 2.40) that

$$\delta n(\mathbf{q}+\mathbf{G}, \omega) = \sum_{\mathbf{G}'}\delta V_{bare}(\mathbf{G}', \mathbf{q}, \omega)\chi(\mathbf{q}+\mathbf{G}, \mathbf{q}+\mathbf{G}', \omega), \tag{2.54}$$

so that equation 2.51 reads

$$F^0(\mathbf{q}, \mathbf{G}, \omega)) = \sum_{\mathbf{G}'}\delta V_{bare}(\mathbf{q}, \mathbf{G}', \omega)\{\delta(\mathbf{G}-\mathbf{G}') +$$
$$\sum_{\mathbf{G}''}[\frac{4\pi e^2}{|\mathbf{q}+\mathbf{G}''|^2}\delta(\mathbf{G}-\mathbf{G}'') + f_{xc}(\mathbf{G}-\mathbf{G}'')]\chi(\mathbf{q}+\mathbf{G}'', \mathbf{q}+\mathbf{G}', \omega)\}. \tag{2.55}$$

The inverse dielectric function $\tilde{\epsilon}^{-1}$ is the key quantity,

$$\tilde{\epsilon}^{-1}(\mathbf{q}+\mathbf{G},\mathbf{q}+\mathbf{G}',\omega) = \delta(\mathbf{G}-\mathbf{G}')+$$
$$\sum_{\mathbf{G}''}[\frac{4\pi e^2}{|\mathbf{q}+\mathbf{G}''|^2}\delta(\mathbf{G}-\mathbf{G}'') + f_{xc}(\mathbf{G}-\mathbf{G}'')]\chi(\mathbf{q}+\mathbf{G}'',\mathbf{q}+\mathbf{G}',\omega), \quad (2.56)$$

where $\mathbf{q}$ is the wavevector for momentum transfer within the first Brillouin zone.

$\tilde{\epsilon}^{-1}$ links, on the microscopic scale, the external potential to the total potential inside the crystal

$$F^0(\mathbf{q},\mathbf{G},\omega) = \sum_{\mathbf{G}'} \delta V_{bare}(\mathbf{q},\mathbf{G}',\omega)\tilde{\epsilon}^{-1}(\mathbf{q}+\mathbf{G},\mathbf{q}+\mathbf{G}',\omega). \quad (2.57)$$

2.13 Linear response in real space

In real space, equations of linear response theory read [60–62]

$$\delta V_{tot}(\mathbf{r},\omega) = \int \tilde{\epsilon}^{-1}(\mathbf{r},\mathbf{r}',\omega)V_{bare}(\mathbf{r}',\omega)d\mathbf{r}'. \quad (2.58)$$

$$\delta n(\mathbf{r},\omega) = \int \chi^0(\mathbf{r},\mathbf{r}',\omega)\delta V_{tot}(\mathbf{r}',\omega)d\mathbf{r}', \quad (2.59)$$

$$\delta n(\mathbf{r},\omega) = \int \chi(\mathbf{r},\mathbf{r}',\omega)V_{bare}(\mathbf{r}',\omega)d\mathbf{r}'. \quad (2.60)$$

In latter equations, memory effects in time were omitted.

χ^0 reads

$$\chi_0(\mathbf{r},\mathbf{r}',\omega) = \sum_{i,j}(f_i - f_j)\frac{\psi_i(\mathbf{r})\psi_j^*(\mathbf{r})\psi_j(\mathbf{r}')\psi_i^*(\mathbf{r}')}{\omega_{ij}-\omega-i\hbar\alpha}, \quad (2.61)$$

where i and j are global indexes for the band number and crystal wave vector, and $\omega_{ij} = \varepsilon_i - \varepsilon_j$.

2.14 Average dielectric function by electron energy-loss spectroscopy

When a charged particle collides with electrons and atoms, it behaves differently according to its mass. If its mass is larger than the electronic mass, a collision with electrons will lead to energy loss, whereas a collision with atoms will be elastic with a deflection of the trajectory. If the incident particle is an electron, there will be both inelastic scattering and deflection

of the electron [67].

In the type of experiment considered here, transmission electron energy-loss spectroscopy, a high energy beam is transmitted through a thin sample, and experiences both elastic scattering, quasi-elastic scattering with excitation of a phonon, or inelastic scattering, where the Coulomb field of the incident electron interacts with the electrons in the solid, and gives rise to longitudinal collective excitations, the plasmons [71].

The incident electron faces a very long-ranged Coulombian interaction from the valence electrons of the solid. This interaction is responsible for the energy loss, and has been shown to be too long-ranged to be treated in perturbation theory [72]. Therefore the theoretical scheme for EELS is different from those for photoemission or absorption spectra.

According to Hubbard [73], as the interaction length is very big, one can treat the solid as a homogeneous medium, and rely on a dielectric treatment of these long-range interactions. In that case, the potential created by the electron moving at a constant velocity $\mathbf{v}$ is given by Poisson's equation. At variance with equation 2.37, the dielectric function $\epsilon_{av}^{\mathbf{q}}$ of the medium considered as homogeneous is now inserted in Maxwell's equation for the electric displacement, yielding , for Poisson's equation,

$$\epsilon_{av}(t,\mathbf{q})\nabla_{\mathbf{r}}^2\, V(\mathbf{r},t) = -4\pi e^2 n^{\mathbf{q}}(\mathbf{r},t), \tag{2.62}$$

where $n = e\delta(\mathbf{r}-\mathbf{v}t)$ is the charge of the incident electron. In the above equation the dielectric function is an average over $\mathbf{r}$, due to the very long range nature of the interaction. This macroscopic quantity is, however, time dependent, and depends on the direction and module of the transferred momentum $\mathbf{q}$.

The double differential inelastic scattering cross section for fast electrons reads :

$$\frac{\partial^2\sigma}{\partial\Omega\partial\omega} = D\frac{4\pi\epsilon_0}{(e\pi a_0)^2}\Im\left(\frac{-1}{\mathbf{q}\epsilon_{av}\mathbf{q}}\right) \tag{2.63}$$

where $\epsilon_{av} = \epsilon_{av}(\omega = E_{\text{loss}}, q)$ is the diagonal element of the inverse microscopic dielectric function, D is the sample thickness, a_0 is the Bohr radius, and $\mathbf{q}$ is the scattering vector. -$\Im(\epsilon_{av}^{-1})$ is called the loss function, that depends on the loss of kinetic energy E_{loss} of the transmitted electron beam.

The relationship between the average function $\epsilon_{av}(\omega,\mathbf{q})$ and the microscopic function is

$$\epsilon_{av}(\omega,\mathbf{q}) = \frac{1}{\epsilon^{-1}(\mathbf{q}+\mathbf{G},\mathbf{q}+\mathbf{G}',\omega)_{\mathbf{G}=\mathbf{G}'=\mathbf{0}}}, \tag{2.64}$$

where ϵ^{-1} is now for a test-charge response, given by the standard definition of the microscopic dielectric function,

$$\epsilon^{-1}(\mathbf{q}+\mathbf{G},\mathbf{q}+\mathbf{G}',\omega) = \delta(\mathbf{G}-\mathbf{G}') + \frac{4\pi e^2}{|\mathbf{q}+\mathbf{G}|^2}\chi(\mathbf{q}+\mathbf{G},\mathbf{q}+\mathbf{G}',\omega). \quad (2.65)$$

With respect to eq. 2.56 for the electron-electron dielectric function, only the electrostatic potential has been included in eq. 2.65. Indeed, it has been taken into account that in such an experiment, the probe is an electron with a very high energy. In that case (1keV-1MeV) electron-electron exchange can be ignored, and we are left with the Coulomb crystal potential in eq. 2.65 [74]. Electron-electron exchange is possible only when the two electrons have the same energy [66].

Finally, one notes that the test-charge definition of eq. 2.65 and the electron-electron response of eq. 2.56 can not coincide at a very high energy, because the exchange and correlation kernel is not frequency-dependent in any adiabatic approximations.

Chapter 3

Theoretical results : electron energy loss spectra

The interpretation and prediction by the theory of electronic spectra obtained by the excitation of valence electrons in $3d$ metal oxides is a very important subject, combining both the difficulty of the excited state with the challenge of properly describing $3d$ elements in the simulation. This is a formidable task, even if one leaves apart the problem of strong electronic correlation, which is the focus of the dynamical mean field theory (DFMT) [75].

In what follows I will concentrate on ZrO_2 and TiO_2, materials in which the $3d$ levels are nearly empty. These materials are important for nuclear applications. Zirconia is described in the appendix A.

In these oxides no strong electronic correlations are expected to occur. It is nonetheless an important task to understand, among the theoretical methods reviewed in chapter 2, which level of theory is appropriate for these oxides.

In this chapter I explain through some examples which level of description is necessary for electron energy loss spectra. More details and results can be found in my bibliography [19, 24, 26]. I also explain in some detail the different structures which appear in the real and imaginary parts of the dielectric function. I believe that these guiding fingerprints are essential and relevant for many transition metal oxides.

3.1 Random phase approximation

3.1.1 Theory

As seen in the previous chapter, the polarizability for independent particles χ^0 in equation 2.45 can be written to first order in perturbation as a sum over independent transitions between unperturbed states. We take density

functional theory as our starting point for the unperturbed ground state, with wavefunctions ψ_i and values of the transition energy $\omega_{ij} = \varepsilon_i - \varepsilon_j$ being the difference between the DFT eigenvalues for states ψ_i and ψ_j :

$$\chi_0(\mathbf{q}+\mathbf{G},\mathbf{q}+\mathbf{G}',\omega) = \sum_{i,j}(f_i - f_j)\frac{<\psi_j|e^{i(\mathbf{q}+\mathbf{G}).\mathbf{r}}|\psi_i><\psi_i|e^{-i(\mathbf{q}+\mathbf{G}').\mathbf{r}'}|\psi_j>}{\omega_{ij}-\omega-i\hbar\alpha}, \tag{3.1}$$

where the sum runs over all DFT states and occupation numbers $f_{i,j}$ are smaller than or equal to unity.

In a first step, neglecting local field effects and approximating χ by χ_0, the microscopic inverse dielectric function can be directly calculated from χ_0 as[24]

$$\epsilon^{-1}_{RPA}(\mathbf{q}+\mathbf{G},\mathbf{q}+\mathbf{G}',\omega) = \delta(\mathbf{G}-\mathbf{G}') + \frac{4\pi e^2}{|\mathbf{q}+\mathbf{G}|^2}\chi^0(\mathbf{q}+\mathbf{G},\mathbf{q}+\mathbf{G}',\omega). \tag{3.2}$$

The above equation is the Random Phase Approximation without local field effects. The standard definition of the scalar dielectric function is[69]

$$\epsilon_{RPA}(\mathbf{q}+\mathbf{G},\mathbf{q}+\mathbf{G}',\omega) = \delta(\mathbf{G}-\mathbf{G}') - \frac{4\pi e^2}{|\mathbf{q}+\mathbf{G}|^2}\chi^0(\mathbf{q}+\mathbf{G},\mathbf{q}+\mathbf{G}',\omega). \tag{3.3}$$

3.1.2 Results in zirconia

In figure 3.1, I report the dielectric function ϵ for cubic ZrO_2 calculated in the RPA without local fields (dashed lines) : the real part ϵ_1 is shown in the top panel, the imaginary part ϵ_2 (corresponding to the absorption spectrum) in the center panel, and in the bottom panel I show the loss function, defined as $-\mathrm{Im}(\epsilon^{-1})$, which in this approximation is equal to $\epsilon_2/(\epsilon_1^2+\epsilon_2^2)$. Three regions can be distinguished.

Firstly, I observe that the valence excitation region extends up to 18.5 eV. The real part of ϵ behaves mainly as a double (classical) oscillator [76]. It vanishes (from positive to negative value) around 8.8 and 16.5 eV/ and correspondingly, ϵ_2 shows maxima of absorption at these frequencies. The real part ϵ_1 vanishes (from negative to positive) at 13.7 and at 16.5 eV (not seen in the figure because of the small broadening). The loss function consequently shows two peaks at these values of the energy. In the absorption spectrum ϵ_2, the strong absorption below 9.5 eV stems from transitions from the valence band to the E_g states. The absorption band extending beyond 9.5 up to 16 eV is associated with transitions from the valence band to T_{2g} states in the conduction band. The small absorption peak at 16 eV comes from valence band to A_{1g} excitations. More details are given in Ref. [24].

Secondly, I see that above 28 eV, corresponding to the zirconium $4p$ excitations, ϵ_1 also behaves as a triple classical oscillator : it vanishes (from

positive to negative) at 30.4, 32.8 and 34.0 eV. Consequently ϵ_2 shows strong absorption at 30.5 eV and between 32.9 and 34.1 eV. Peaks are observed in the loss function when ϵ_1 vanishes (from negative to positive) at 31.5, 33.4 and 37.7 eV.

Thirdly, I would like to point out that the region between the valence plasmons and the $4p$ plasmons, i.e. around 16 to 28 eV, cannot be interpreted in terms of classical oscillators. Between 22 and 28 eV, ϵ_1 and ϵ_2 are dominated by linear features, increasing for ϵ_1 and decreasing for ϵ_2. The corresponding loss function exhibits a broadened peak at 24.9 eV which I assign *not* to plasmons but to other forms of collective excitations : The plasmon is defined by a vanishing real part of the dielectric function and a minimum of the imaginary part, which is not the case for this peak. Such linear behavior for ϵ_1 and ϵ_2 has already been observed in the theoretical EELS of rutile TiO_2 [19]. However, I note that here the oscillators associated with the O $2s$ electrons are present (ϵ_1 vanishes from positive to negative around 20.0 eV, and vanishes from negative to positive around 24.7 eV) but are overwhelmed by the linear behaviour of ϵ_1 and ϵ_2, which is the cause of the main peak at 24.9 eV.

3.2 Local field effects

3.2.1 Theory

To include local fields, one first has to evaluate χ^0, as in the previous section, and then to calculate the full response function χ (eq. 2.53). The inverse dielectric function is then computed from eq. 2.65, and the macroscopic limit is taken (eq. 2.64).

The way I introduced local field effects was to take into account the off-diagonal elements $\mathbf{G} = \mathbf{G}'$ of the various matrices χ^0, χ and ϵ^{-1} in matrix inversions of eqs. 2.53 and 2.64. These additional components correspond to a coupling between longitudinal and transverse disturbances [62].

The mixing of the formerly independent transitions could alternatively be described by the concept of an electron-hole exchange [77–79].

3.2.2 Results

The local-field effects reflect the inhomogeneity of the material in the response function, and have the effect of mixing the formerly independent transitions. In ZrO_2, $4p$ states are atomic like, but they "feel" the interaction with neighboring atoms and do hybridize slightly[24]. Local field effects are found to be strong at these values of the energy. They introduce

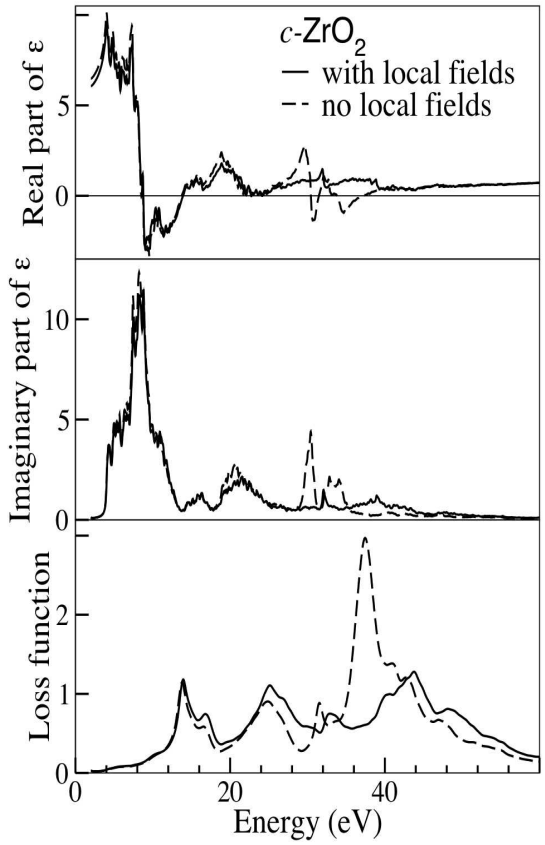

Figure 3.1: cubic ZrO_2 : theoretical dielectric function at $\mathbf{q}=\mathbf{0}$. Top panel : real part. Center : imaginary part. Bottom panel : the loss function. Solid lines : RPA with local fields. Dashed line : RPA without local fields. The real and imaginary parts of the dielectric function (resp. the loss function) are broadened with a Lorentzian of HWHM (half width at half maximum) of 0.1 eV (resp. 0.5 eV). From Ref. [24]. From Ref. [26].

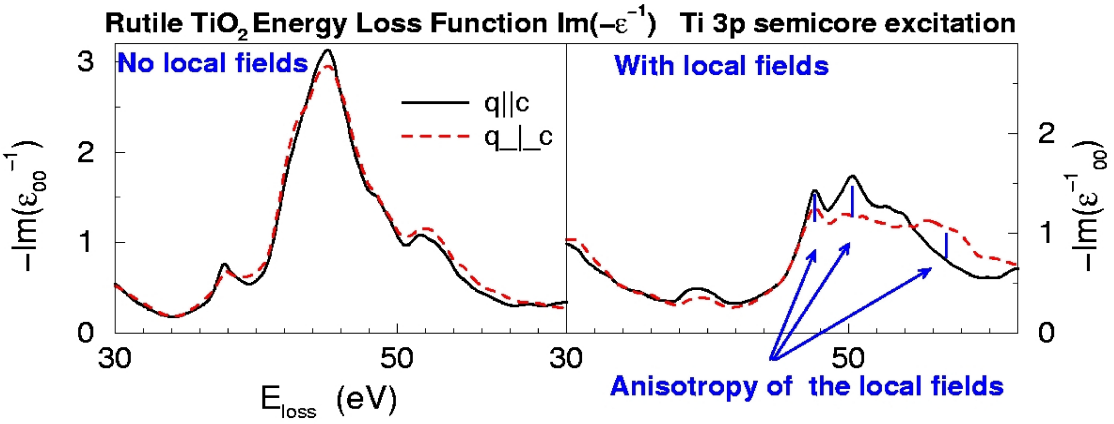

Figure 3.2: TiO_2 : loss function in the region of the $3p$ electronic excitations. Left panel : without local fields. Right panels : with local fields. Unpublished.

the "surroundings" in an otherwise local environment.

As shown in the solid lines of Fig. 3.1 (ZrO_2) and in Fig. 3.3, the effects on ϵ_1 and ϵ_2 are weak below 25 eV. At higher energy, however, they drastically modify the triple p plasmons, both in lineshape and peak position. In ZrO_2, the peak formerly at 31.5 eV is shifted towards higher energy by 1.4 eV, while the main peak is shifted by as much as 6.4 eV (!).

3.2.3 Local field effect and anisotropy

Large effects on excitations from a quasi-atomic level due to local fields have similarly been found for the $3p$ excitations in rutile TiO_2 [19]. Although rutile is a tetragonal crystal, where the symmetry is decreased with respect to the cubic one, the spectra for a momentum transfer parallel or perpendicular to the tetragonal axis are very close (Fig. 3.2, left panel). Local field effects increase the difference in the EELS spectrum taken for a momentum transfer parallel or perpendicular to the tetragonal axis (Fig. 3.2, right panel). Thus local field effects increase the anisotropy in the EELS spectra. In other words, the anisotropy observed in the 40-60 eV range in rutile TiO_2 mainly comes from local field effects.

3.3 Comparison with experiments

Comparison with experiments is not straightforward. In experiments, the observed intensity depends on an integration of the signal over the collection

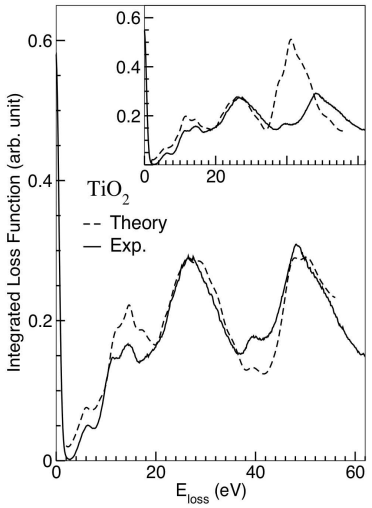

Figure 3.3: TiO_2 : loss function at finite momentum transfer Dashed : RPA with local field effects. Solid line : Experiment. Insert, dashed : RPA without local field effects. From Ref. [19].

angle β [80], which for a cubic phase is expressed by the formula

$$I(E) \propto -\pi \mathrm{Im}\left[\varepsilon^{-1} \ln\left(1+\frac{\beta^2}{\theta_E^2}\right)\right], \tag{3.4}$$

where $\theta_E = E_{\mathrm{loss}} m/\hbar^2 k_0^2$ is the characteristic angle depending on the energy loss E_{loss}, and on the relativistic mass m and wave vector k_0 of the incident electron beam. This has to be taken into account to produce a theoretical "integrated loss function" which depends on the symmetry of the crystal and on the experimental conditions [19, 24].

When this is done, relative peak positions between the collective excitation at mid energy between the valence and p plasmons is well reproduced, both in rutile [19] and in zirconia [24]. The theoretical spectral intensity of the valence plasmon at 12-14 eV is however too weak (Fig. 3.3). This might partly be attributed to the difficulty in the experiment in extracting the inelastic part from the large elastic peak (zero loss contribution). At vanishingly small momentum transfer, this might also partly come from excitonic effects beyond the RPA [81].

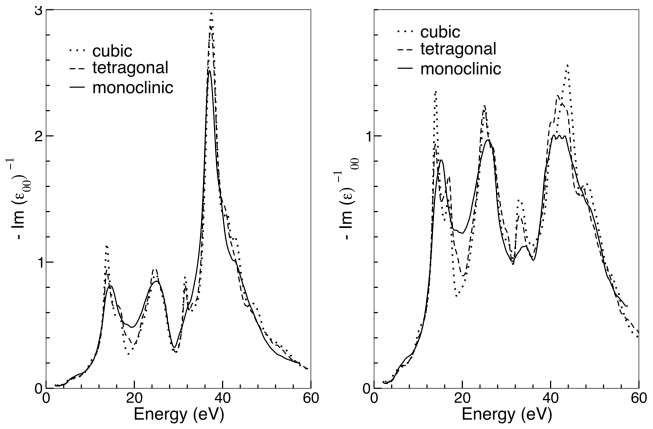

(a) (b)

Figure 3.4: Theoretical loss function (a) within the RPA without local fields, and (b) with local field effects. Dotted line: c-ZrO_2. Dashed line: t-ZrO_2. Solid line: m-ZrO_2. The loss function is broadened with a Lorentzian of HWHM of 0.5 eV. From Ref. [24].

3.4 Comparison among different crystal phases

The effects of anisotropy seen in previous section have been further studied by comparing EELS spectra of crystals with the same composition but with a different crystal symmetry. To this end, comparison of EELS spectra between different phases of zirconia has been undertaken [24].

I have found that, in the calculations, the valence plasmon(s) as well as the $4p$ plasmons differ both in peak position and shape in the three low pressure phases of zirconia (figure 3.4). These differences have two origins : for the valence plasmon, the difference in the lineshape directly arises from differences in the band structure between the phases, like the gap in the conduction states [24]. For the $4p$ peak ($N_{2,3}$ edge), the difference is brought in *via* the local-field effects.

These differences are not observed in the experiment (figure 3.5), partly because the accuracy of the measurements is not yet high enough for these differences to be seen, partly because of the difficulty to synthesize appropriate samples. The particular phase diagram of zirconia, with many phase transition lines, makes it difficult to grow monoclinic or tetragonal single crystals. In this respect, core spectroscopy, such as electron energy-loss near-edge spectroscopy [82, 83] seems to have a greater potential for the characterization of different phases.

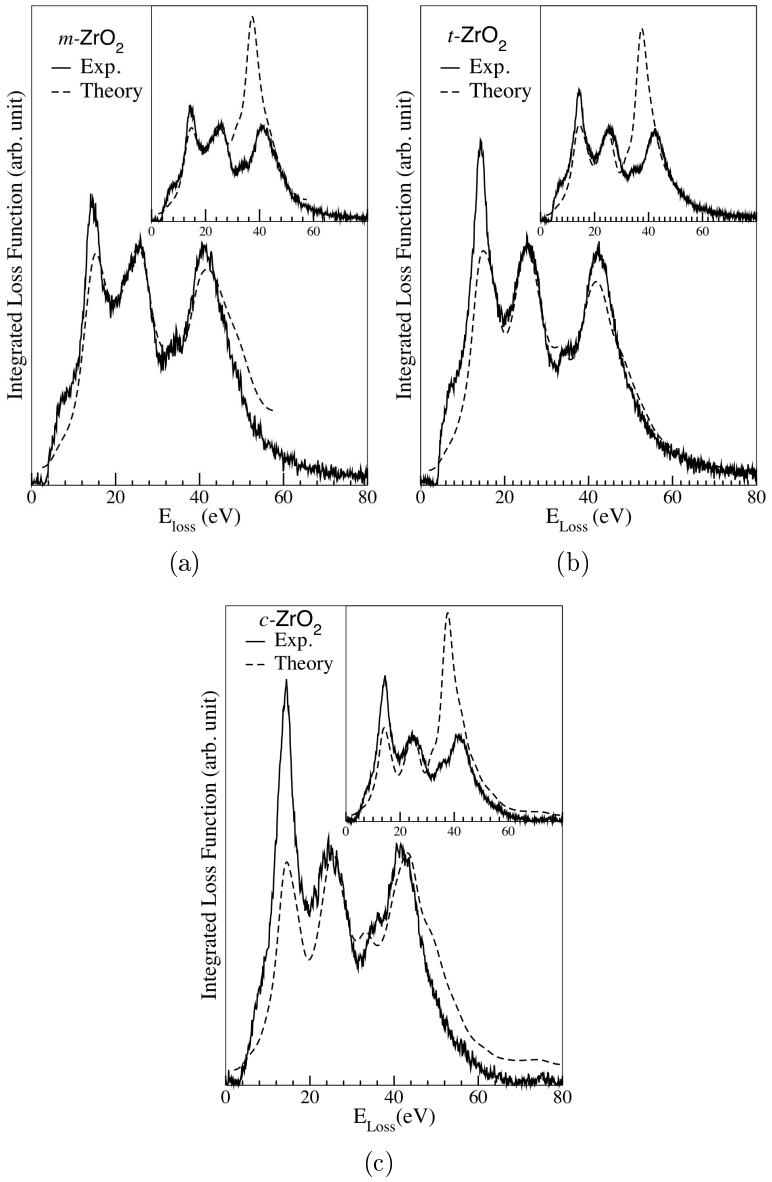

Figure 3.5: Integrated loss function (see text) for pure zirconia: (a) monoclinic, (b) tetragonal and (c) cubic phases. Solid line: experiment. Dashed line: theory with local fields. Insert: theory without local fields The theoretical curves have been convoluted with a Voigt profile: Gaussian of HWHM of 1 eV, and Lorentzian function of HWHM of 1 eV. In the experiment, cubic zirconia is yttria stabilized. From Ref. [24].

3.5 The Random Phase Approximation is a good approximation for EELS

In the preceding sections, I have reported EELS spectra calculated within the RPA at vanishing momentum transfer $\mathbf{q}$ for ZrO_2 in satisfactory agreement with experimental data, and this is true in many systems. The RPA is however not sufficient for absorption spectra [10].

In the calculation of both $\mathbf{q} = \mathbf{0}$ EELS and absorption spectra, the ingredients are similar : the components of the independent-particle response function and the bare Coulomb potential, and therefore the discrepancy is at first sight intriguing. The discrepancy has recently been understood in the following way [10].

EELS can be shown to be mathematically proportional to :

$$-\Im[\lim_{\mathbf{q}\to\mathbf{0}} v_0(\mathbf{q})\chi_{00}(\mathbf{q},\omega)], \tag{3.5}$$

where v_0 is the $\mathbf{G} = \mathbf{0}$ component of bare Coulomb potential, and χ_{00} is the microscopic response function, as stated in Eqs. 2.65 and 2.45. Within the RPA, Eq. 2.53 becomes :

$$\chi = \chi_0 + \chi_0 v \chi, \tag{3.6}$$

and all the components of the bare Coulomb potential v enter in Eq. 3.6, the short-range as well as the $\mathbf{G} = \mathbf{0}$ long-range ones.

On the other hand, the imaginary part of the macroscopic dielectric function can be shown to be proportional to a modified equation :

$$-\Im[\lim_{\mathbf{q}\to\mathbf{0}} v_0(\mathbf{q})\tilde{X}_{00}(\mathbf{q},\omega)], \tag{3.7}$$

where the modified response function $\tilde{X}$ verifies a modified Dyson equation :

$$\tilde{X} = \chi_0 + \chi_0 \bar{v} \tilde{X}, \tag{3.8}$$

where now only the short range components of the bare Coulomb potential enter :

$$\bar{v}(\mathbf{G} = \mathbf{0}) = 0, \tag{3.9}$$

$$\bar{v}(\mathbf{G}) = v(\mathbf{G}). \tag{3.10}$$

Excitonic effects are a long-range effect. Therefore, the introduction in the calculation of the excitonic effects only slightly weakly modifies the theoretical EELS spectra whereas it considerably modifies the absorption spectrum[81]. This is because an electron energy loss spectrum already contains a long-range part whereas an absorption spectrum does not contain

any long-range part within the RPA approximation. In fact, near the plasmon energy, there is a cancellation between the long range term and the quasiparticle shift, i.e., the shift in the one electron energy produced by the self-energy taking into account the fact that electrons move in a medium, see subsection 4.2.2.

3.6 Conclusion

I have presented the theoretical framework to calculate electronic energy-loss spectra. The random phase approximation is shown to be adequate for EELS, both through examples on ZrO_2 and TiO_2 and on mathematical grounds. I have also addressed elsewhere, either directly or in collaboration, the effects of the inclusion of semi-core states in the valence in TiO_2 and Cu_2O [26].

Chapter 4

Theoretical results : optical absorption experiment

In what follows, I will compare the absorption spectrum of a polycrystal of zirconia (see. appendix A) with the theoretical description taken at various levels [26], and the absorption spectrum of a single crystal of Cu_2O with theoretical descriptions taken beyond one-particle theory [28–30].

We consider an optical absorption experiment. In this case, one measures the absorption coefficient,

$$\alpha(\omega) = \frac{\omega \Im(\varepsilon_M(\omega))}{n_1(\omega)c}, \tag{4.1}$$

where c is the light velocity, ω is the energy of the absorbed photon, n_1 is the real part of the index of refraction, and $\Im(\varepsilon_M(\omega))$ is the imaginary part of the macroscopic dielectric function.

We need to calculate the macroscopic dielectric function, which reads

$$\varepsilon_M(\omega) = \lim_{\mathbf{q}\to\mathbf{0}} \frac{1}{\varepsilon^{-1}_{\mathbf{G}=0G'=0}(\mathbf{q},\omega)}. \tag{4.2}$$

The theoretical absorption spectrum is then given by the imaginary part of equation (4.2).

4.1 Within independent transition theory

The absorption of a photon allows one electron of the valence band to be promoted to a conduction state. In an independent particle approximation, we write an expression for the macroscopic dielectric function

$$\varepsilon_M \approx 1 - v\chi_0(\mathbf{G} = \mathbf{G}' = 0; \mathbf{q} \to 0), \tag{4.3}$$

which can be used to calculate the theoretical absorption spectrum.

The imaginary part of the macroscopic dielectric function ε_M reads:

$$\Im(\varepsilon_M(\omega)) = \frac{4\pi}{\omega^2} \sum_{v,c} |\langle\psi_c| - i\mathbf{A}.\nabla|\psi_v\rangle|^2 \delta(\omega - \varepsilon_c + \varepsilon_v) \tag{4.4}$$

where $-i\mathbf{A}\cdot\nabla$ describes the coupling of the electron with the vector potential $\mathbf{A}$ of the electromagnetic field. We treat this term within the dipolar approximation. The sum is performed both on the initial valence and final conduction states, which in Eq. 4.4 are Bloch states of the periodic potential in the solid.

This Fermi's golden rule (see appendix B) comes from the fact that one treats the transitions between states, independently. Using equation 2.45 or equation 2.61 for the polarizability, and taking the limit $\mathbf{G} = \mathbf{G'} = 0; \mathbf{q} \to 0$, the response function χ_0 of section 2.10 amounts to the Fermi's golden rule of eq. 4.4.

4.1.1 Joint density of states.

The simplest approach to the absorption spectrum consists of the evaluation of the joint density of states. As a first attempt to obtain theoretical electronic spectra, we can use the eigenvalues ε_i of the DFT Hamiltonian to calculate the joint density of states (JDOS) $\sum_{v,c} \delta(\omega - \varepsilon_c - \varepsilon_v)$, where ε_v is the energy of a state in the valence band, and ε_c is the energy of a state in the conduction band. This approximation supposes that the matrix elements $|\langle\psi_c| - i\mathbf{A}\cdot\nabla|\psi_v\rangle|^2$ are kept constant in equation 4.4. The quantity

$$\Im(\epsilon_{JDOS}(\omega)) = \frac{\sum_{v,c} \delta(\omega - \varepsilon_c + \varepsilon_v)}{\omega^2}, \tag{4.5}$$

reported in ZrO_2 is related to the joint density of states (Fig. 4.1, dashed line). The JDOS does not satisfy conservation rules and therefore the calculated spectrum is in arbitrary units.

The JDOS shows a good overall agreement, although it is not sufficient to interpret the details of the experimental data (circle symbols), especially between 6 and 8 eV, and around 29–33 eV. In particular the overall shape of the spectrum is not reproduced.

4.1.2 Effect of matrix elements

The simplest level of approximation one can make beyond the JDOS is to treat the particles, and the transitions between states, independently, with equation 4.3.

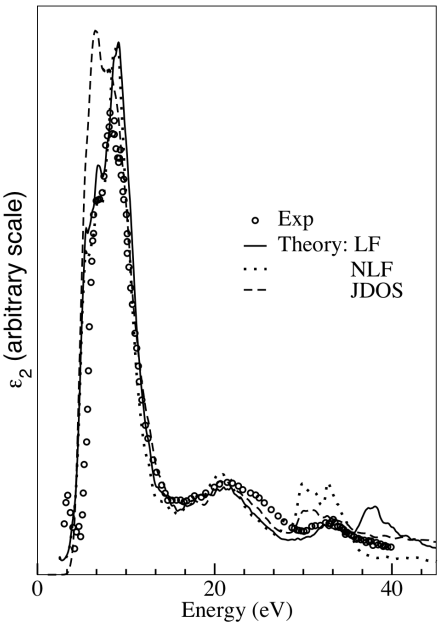

Figure 4.1: Absorption spectrum for monoclinic ZrO_2 calculated using the RPA with local fields (solid line), RPA without local fields (dotted line), and with the ratio of the JDOS by the squared frequency, compared with experimental results from French *et al.* (reference [84]). The theoretical curves have been scaled to the intensity of the experimental peak around 20 eV. From Ref. [26].

This approximation is sometimes sufficient for systems with weak inhomogeneities, or with metallic screening. Among recent examples one can cite the absorption spectrum of small diameter nanotubes when the light is polarized along the nanotube axis [20, 85].

The computation of the matrix elements $|\langle\psi_f| - i\mathbf{A}\cdot\nabla|\psi_i\rangle|^2$ in Eq. 4.4 is necessary to impose the selection rules. In optical absorption this is of importance when one has a monocrystal and wants to study the effects of the polarization of light.

Even when we average the absorption spectrum over the polarizations, are matrix elements of primary importance. In figure 4.1, we see that the overall shape of the absorption spectrum has been greatly modified by the inclusion of matrix elements.

4.2 Beyond independent transition theory

The microscopic dielectric function $\varepsilon(\mathbf{r}, \mathbf{r}', \omega)$ can be written, Fourier transformed, as the matrix with elements $\varepsilon_{\mathbf{G}\mathbf{G}'}(\mathbf{q}, \omega)$ of equation 2.56 [60–62].

Summarizing equation 2.56, we write the inverse dielectric function as

$$\varepsilon^{-1}_{\mathbf{G}\mathbf{G}}(\mathbf{q}, \omega) = 1 + v(\mathbf{q} + \mathbf{G})\chi_{\mathbf{G}\mathbf{G}}(\mathbf{q}, \omega), \tag{4.6}$$

where v is the Coulomb potential and χ the polarizability of the system (section 2.11).

In order to calculate these functions, we need to formulate an expression for the polarizability of the system, χ. It can be calculated by Dyson's like equation 2.53 or 3.6, which is apparently far from Fermi's golden rule (Appendix B). Nonetheless, one can show that when LFE are expressed as an electron-hole exchange [77–79] the imaginary part of the dielectric functions is given by equation 4.12.

4.2.1 Local field effects

The inhomogeneities of the system give rise to the crystal local-field effects. In our calculations, these local-field effects arise from the way the Coulomb term v is treated in section 2.11.

We can neglect the local-field effects entirely by including only the long-range part of the Coulomb potential (i.e. $v_{\mathbf{G}=0}(\mathbf{q})$), as done in section 4.1.2, which clearly ignores the microscopic components of the induced field. In this case we only need to calculate the head of the dielectric matrix, i.e. $\varepsilon_{\mathbf{G}=0,\mathbf{G}'=0}$, giving us the RPA without local fields of section 4.1.2.

Once we include the full Coulomb potential $v_{\mathbf{G}}(\mathbf{q})$ we need to calculate the full dielectric matrix, including the off-diagonal elements $\varepsilon_{\mathbf{G},\mathbf{G}'\neq\mathbf{G}}$—thus the inversion of this matrix has the effect of mixing the previously independent transitions.

However, just including the local-field effects does not guarantee that the results will be significantly closer to experiment than calculations where they are neglected. This is especially true in the case of absorption spectra for our transition-metal oxide systems. For example, in figure 4.1 we have plotted experimental results for monoclinic ZrO_2 against theoretical RPA calculations both with Hartree local-field effects, and without them. We can see that there is a clear difference between the results of the two theoretical approximations, and in particular they also differ in the high energy region, for values of the energy larger than 28 eV.

In an optical absorption experiment, $\mathbf{q}$ is close to zero. Exchange and correlation local field effects have been shown to have a small influence in $Ti0_2$ for vanishing $\mathbf{q}$ [19], and therefore they have not been taken into account in the calculations of figure 4.1.

4.2.2 Quasiparticles effects

For absorption spectra, the quasiparticle energy shifts that one can calculate in the GW approximation [13, 14] is necessary, but usually it is not sufficient [10].

The GW approximation consists of solving an equation similar to the system of equations in DFT, in which the local exchange and correlation potential $v_{xc}(\mathbf{r})$ is replaced by a non-local and dynamical self-energy operator $\Sigma(\omega, \mathbf{r}, \mathbf{r}')$:

$$H^{KS}\psi_n(\mathbf{r}) - v_{xc}(\mathbf{r})\psi_n(\mathbf{r}) + \int d^3\mathbf{r}'\Sigma(\omega, \mathbf{r}, \mathbf{r}')\psi_n(\mathbf{r}') = \varepsilon_n^{QP}\psi_n(\mathbf{r}). \qquad (4.7)$$

In the simplest formulation, the self-energy $\Sigma(\omega, \mathbf{r}, \mathbf{r}')$ is evaluated at $\omega = \varepsilon_n^{QP}$. It is approximated by the product of the Green's function and of the screened Coulomb interaction $W = \epsilon^{-1}v$, hence the name GW for this approximation. In a first step, eigenvalues are corrected by equation 4.7, while the wavefunctions are unchanged and are usually those obtained from DFT.

Including quasiparticle effects in the electronic spectra corrects the DFT bandgaps. Indeed, LDA calculations typically give band gaps which are much too small with respect to the photoemission gap. These results can be improved upon using methods such as the GW approximation [10]. A GW estimation of the band gap in monoclinic ZrO_2 gives a result of 5.4 eV [86] instead of the LDA value of 3.6eV [24].

When $3d$ electrons come into play, however, the simplest GW approximation is no longer sufficient, as has been shown for Cu_2O [28, 29]. A GW estimation of the band gap yields 1.3 eV, to be compared with 2.17 eV in the experiment. Therefore, one needs to go one step further in the theoretical framework and use the values of the quasiparticle energy in the expression of the inverse dielectric function ϵ^{-1}, to recalculate the screened Coulomb interaction W. The self-consistent GW approximation [27], was developed and accelerated by F. Bruneval during his PhD. thesis with the help of the so-called COHSEX approximation [30]. The gap of Cu_2O is calculated to be 2.4 eV in the scf COHSEX approximation, and 2. eV in the self-consistent GW.

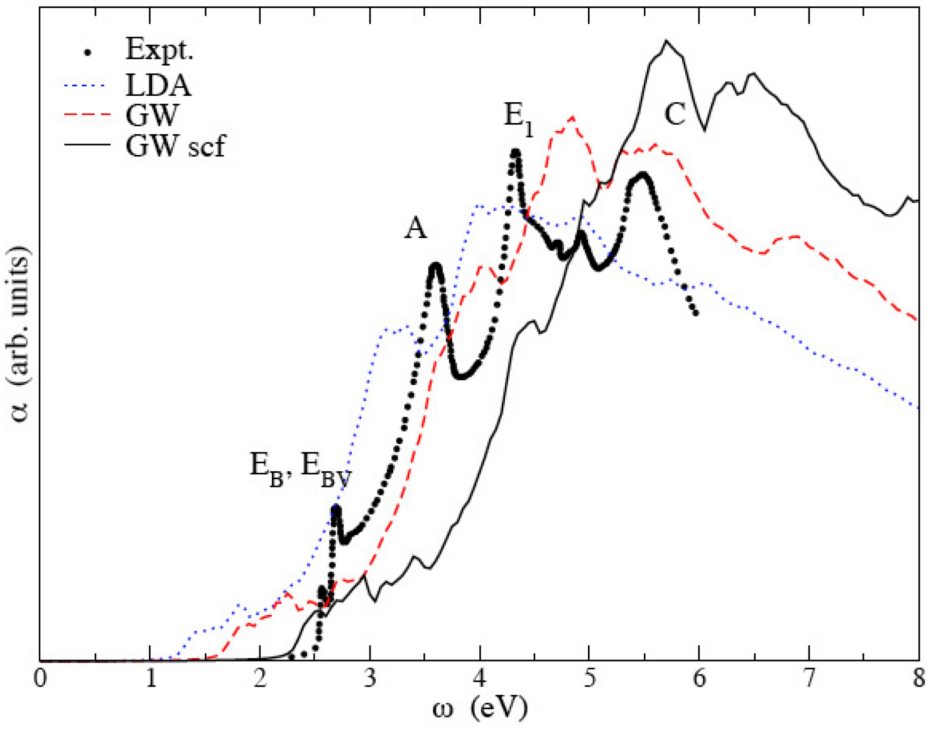

Figure 4.2: Absorption spectrum for Cu_2O without excitonic effects, calculated using the RPA with local fields at the DFT level (dotted line), at the *GW* level (dashed line) and with the self-consistent GW (solid line), compared with experiment of Ref. [87] (filled circles). From Ref. [28].

To illustrate this fact, I show in figure 4.2 theoretical spectra calculated with equations 4.6 and 4.2, together with experimental data. In equation 4.6 the values of the energy and wavefunctions of the initial and final states have been calculated at different levels of approximation : at the DFT-LDA level, as in figure 4.1; at the *GW* level; and at the level of a self-consistent *GW* approximation [30]. Only at the latter level is the theoretical absorption edge closer to the experimental one (black line and filled circles around 2.5 eV).

For absorption spectra, the quasiparticle energy shift that one can calculate in the *GW* approximation is usually necessary but not sufficient. This is seen in the overall shape of the theoretical spectra (figure 4.2). In fact, a major modification is brought in the absorption spectrum by excitonic effects. This is because, at variance with an EELS spectrum (see section 3.5), an absorption spectrum does not contain any long range part within the RPA approximation. Excitonic effects thus considerably modify an absorption spectrum, as illustrated in the next section.

4.3 Excitonic effects

Taking into account the excitonic effects is complex and has been nicely elaborated by Albrecht in its PhD thesis [79]. I can only recommend the reading of this PhD thesis. It amounts to solving a Bethe-Salpeter equation for a four point polarisability P

$$P = P_0 + P_0 \Xi P \tag{4.8}$$

Ξ is the interacting kernel and consists of the exchange effect (the local field of above section 4.2.1) and of the Coulomb electron-hole interaction screened with the potential W of the previous section 4.2.2.

The above equation 4.8 amounts to diagonalizing an effective Hamiltonian. The resonant part of the Hamiltonian consists of the free electron-hole pair energy plus the two above-mentioned interactions (exchange and screened Coulomb electron-hole) expressed in the kernel Ξ :

$$H^{exc}_{cv;c'v'} = (\varepsilon_c - \varepsilon_v)\delta_{vv'}\delta_{cc'} - i\Xi_{cv;c'v'}. \tag{4.9}$$

The values of the excitonic energy E_λ and wavefuntion coefficients A^{cv}_λ are the eigenvalues and eigenvectors of the effective two-particled Hamiltonian for the electron-hole pairs H^{exc},

$$H^{exc}_{e_1,h_1;e_2;h_2} A^{e_2,h_2}_\lambda = E_\lambda A^{e_1,h_1}_\lambda, \tag{4.10}$$

in which e_i labels an electronic state in the conduction band, and h_i labels a hole state in the valence band.

The Hamiltonian is expressed in the basis of electron-hole wave functions $|\psi_v\psi_c>$. The electron-hole pair wave function is usually expressed as $|\psi_v\psi_c>$, where $|\psi_v>$ and $|\psi_c>$ are (single particle) solutions of the DFT equations. The exciton amplitude is expressed as [79]

$$\Psi_\lambda(\mathbf{r},\mathbf{r}') = \sum_{(c,v)} A^{c,v}_\lambda \psi^*_c(\mathbf{r})\psi_v(\mathbf{r}'). \tag{4.11}$$

In the dielectric function, the excitonic effect induced by the screened Coulomb electron-hole interaction leads to a mixing of the formally independent transitions with the same energy [79]

$$\Im(\varepsilon_M(\omega)) = 2\pi \lim_{\mathbf{q}\to\mathbf{0}} v_{\mathbf{G}=\mathbf{0}}(\mathbf{q}) \sum_\lambda |\sum_{v,c} |\langle\psi_c| - i\mathbf{A}.\nabla|\psi_v\rangle A^{cv}_\lambda|^2 \delta(\omega - E_\lambda + i\alpha). \tag{4.12}$$

The wavefunction coefficients A^{cv}_{λ} mix the formally independent transitions and induce coherent effects in Fermi's golden rule.

Limiting Ξ to the exchange effect (local field effects) is strictly equivalent to section 4.2.1. Taking into account both the exchange effect and the screened Coulomb electron-hole interaction in Ξ induces drastic changes in the optical spectra (figure 4.3). Effects of the electron-hole interaction can be seen by comparing the dashed line of figure 4.2 and the dot-dashed line of panel (a) of figure 4.3.

Although the above scheme has been shown to be sufficient for *s-p* bonded semiconductors, it is not sufficient to interpret the experimental spectrum of Cu_2O (panel (a) of figure 4.3). Inserting the improved values of the quasiparticle energy obtaoned from a self-consistent *GW* calculation in the free electron-hole Hamiltonian $(\varepsilon_c - \varepsilon_v)\delta_{vv'}\delta_{cc'}$ is also not sufficient (dash-dotted line of panel (b) of figure 4.3). Bruneval has shown that one needs to go one steep further for materials with *d* electrons, because the values of the DFT energy are not sufficient to properly evaluate the screening function ϵ^{-1} needed to obtain the screened Coulomb electron-hole interaction *W*. When ϵ^{-1} is properly evaluated also in the expression of Ξ (solid line in panel (b) of figure 4.3), then the theory is helpful in understanding the experimental spectrum (or *vice versa* in present the case).

4.3.1 Modelisation of excitonic effects

The solution of the quasiparticle and of the Bethe-Salpeter equation are very cumbersome calculations.

We have made an attempt to model the excitonic effect within the framework of time-dependent density functional theory by including an approximation of the long range kernel as $\frac{\alpha}{|\mathbf{q}|^2}$, with α being an empirical parameter deduced from the static dielectric screening [9].

In my understanding, this amounts to inserting a long-range part $\frac{\alpha}{|\mathbf{q}|^2}$ in equation 2.51

$$F^0(\mathbf{q},\mathbf{G}\omega) = \delta V_{bare}(\mathbf{q},\mathbf{G},\omega) + \sum_{\mathbf{G}'}[\frac{4\pi e^2}{|\mathbf{q}+\mathbf{G}'|^2}\delta(\mathbf{G}'-\mathbf{G}) + f_{xc}(\mathbf{G}'-\mathbf{G})]\delta n^0(\mathbf{q}+\mathbf{G}',\omega),$$

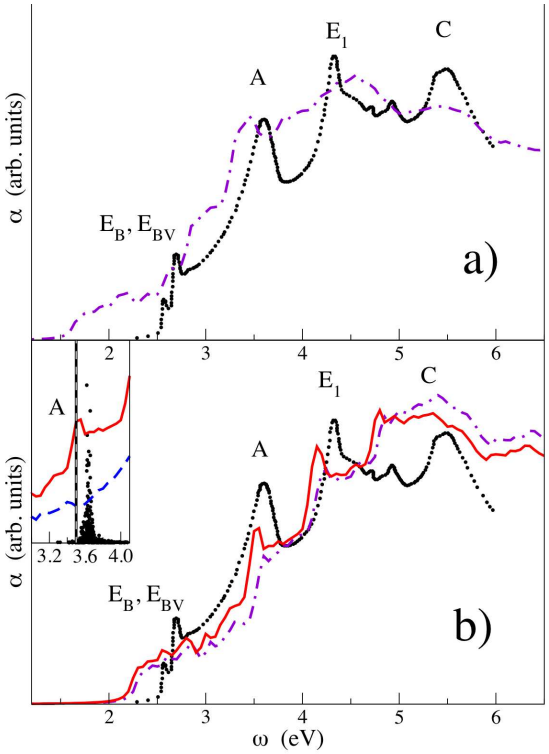

Figure 4.3: Absorption spectrum for Cu_2O calculated with excitonic effects with (a) the standard GW eigenvalues and the DFT wavefunctions in ϵ^{-1} and in the free electron-hole Hamiltonian $(\varepsilon_c - \varepsilon_v)\delta_{vv'}\delta_{cc'}$ (dot dashed line); (b) The quasiparticle corrections to the energy obtained from a self consistent GW calculation are inserted in the free electron-hole Hamiltonian $(\varepsilon_c - \varepsilon_v)\delta_{vv'}\delta_{cc'}$ (dash-dotted line), or both in the free electron-hole Hamiltonian and ϵ^{-1} (solid lines). The inset panel (b) shows the transition analysis for peak A : contributing transitions (dots) and optical absorption spectrum calculated with the self-consistent GW values of the energy but without excitonic effects (dashed line). Experiment of Ref. [87] (filled circles). From Ref. [29].

yielding

$$F^0(\mathbf{q},\mathbf{G}\omega) = \delta V_{bare}(\mathbf{q},\mathbf{G},\omega) + \sum_{\mathbf{G}'}[\frac{4\pi e^2}{|\mathbf{q}+\mathbf{G}'|^2}\delta(\mathbf{G}'-\mathbf{G}) + f_{xc}(\mathbf{G}'-\mathbf{G}) + \frac{4\pi\alpha e^2}{|\mathbf{q}+\mathbf{G}'|^2}\delta(\mathbf{G}'-\mathbf{G})]\delta n^0(\mathbf{q}+\mathbf{G}',\omega). \quad (4.13)$$

In its static form, it is not possible to create a Rydberg series in a finite system with this model, but it is convincing in modifying the optical spectra obtained in time-dependent density functional theory [9].

Excitonic effects are thought to be derived from the non-local exchange operator [88]. If this is so, Poisson's equation of 2.9 should be solved only with the Hartree potential. We have seen that for a long wavelength perturbation ($\mathbf{q}=\mathbf{0}$) and $\mathbf{G}=\mathbf{0}$, one has $\delta n(\mathbf{q}+\mathbf{G},\omega)=\mathbf{0}$. The induced change in the density has no macroscopic component - the total macroscopic electronic density is kept constant in the excited state, $\lim_{\mathbf{q}\to\mathbf{0}}\int[n(r)- < n >]e^{-i\mathbf{q}.\mathbf{r}} \to 0$. In such a case the kernel model $\frac{\alpha}{|\mathbf{q}|^2}$ should have no effect, because in equation 4.13 it is multiplied by $\delta n(\mathbf{q},\mathbf{G}\to\mathbf{0},\omega)$.

A recent attempt by myself and Marco Saitta (IMPMC -Institut de Minéralogie et de Physique des Milieux Condensés- Université Paris VI P.M. Curie) to introduce the model kernel in the TDDFPT equations of Ref. [58] has failed. In my understanding, this failure is connected to the fact that, in this case, the change in density is designed to have no macroscopic component. This is not the case in the DP program package used in Ref. [9], in which no check of the induced density is performed.

In my understanding, introducing a model kernel as done in Ref. [9] amounts to modifying Poisson's equation. This might have a justification if we consider that the perturbation is no longer taken as adiabatic. I am now going to elaborate on this point.

4.3.2 Non adiabatic effects

In such a case, one should take into account the component δn^0 defined by equation 2.35 in Poisson's equation 2.37.

Defining first the quantity A which appears in δn^0 (eq. 2.35) and in $\delta n^{\mathbf{q}}(\mathbf{r})$ (eq. 2.36) , one has

$$A_{l\mathbf{k}_1 p\mathbf{k}_2}(\mathbf{r}) = \frac{B_{l\mathbf{k}_1 p\mathbf{k}_2}}{\varepsilon^{(0)}_{p\mathbf{k}_2} - \varepsilon^{(0)}_{l\mathbf{k}_1} - \hbar\omega - i\hbar\alpha}, \quad (4.14)$$

with B equals to

$$B_{l\mathbf{k}_1 p\mathbf{k}_2}(\mathbf{r}) = \psi^{(0)*}_{p\mathbf{k}_2}(\mathbf{r})\psi^{(0)}_{l\mathbf{k}_1}(\mathbf{r})[f^{(0)}(\varepsilon^{(0)}_{p\mathbf{k}_2}) - f^{(0)}(\varepsilon^{(0)}_{l\mathbf{k}_1})] < \psi^{(0)}_{l\mathbf{k}_1}|F^{\mathbf{q}}|\psi^{(0)}_{p\mathbf{k}_2} > . \quad (4.15)$$

Rewriting Poisson equation with δn^0 leads to

$$\sum_{\mathbf{G}} |(\mathbf{q}+\mathbf{G})|^2 \, F^0_{Hartree}(\mathbf{q},\mathbf{G},\omega) e^{-i(\mathbf{q}+\mathbf{G}).\mathbf{r}} e^{i\omega t} e^{\alpha t} + c.c. = \quad (4.16)$$

$$4\pi e^2 \sum_{l\mathbf{k}_1 p\mathbf{k}_2} A_{l\mathbf{k}_1 p\mathbf{k}_2}(\mathbf{r}) e^{\alpha t}(e^{i\omega t} - e^{-i(\varepsilon^{(0)}_{l\mathbf{k}_1} - \varepsilon^{(0)}_{p\mathbf{k}_2})\frac{t}{\hbar}}) + c.c., \quad (4.17)$$

where the terms $e^{-i(\varepsilon^{(0)}_{l\mathbf{k}_1} - \varepsilon^{(0)}_{p\mathbf{k}_2})\frac{t}{\hbar}}$ come from nonadiabatic terms.

Integrating on time, and taking the long wavelength limit, I find that

$$\lim_{\mathbf{q},\mathbf{G}\to\mathbf{0}} |(\mathbf{q}+\mathbf{G})|^2 \, F^0_{Hartree}(\mathbf{q},\mathbf{G},\omega) = 4\pi e^2 \lim_{\mathbf{q},\mathbf{G}\to\mathbf{0}} \delta n(\mathbf{q}+\mathbf{G},\omega) + \quad (4.18)$$

$$\frac{4\pi e^2}{\hbar\omega} \lim_{\mathbf{q},\mathbf{G}\to\mathbf{0}} \sum_{l\mathbf{k}_1 p\mathbf{k}_2} B_{l\mathbf{k}_1 p\mathbf{k}_2}(\mathbf{G}) \quad (4.19)$$

We see that a non adiabatic perturbation induces an additional term to the kernel coming from the Hartree potential :

$$\frac{4\pi e^2}{\hbar\omega} \lim_{\mathbf{q},\mathbf{G}\to\mathbf{0}} \frac{1}{|(\mathbf{q}+\mathbf{G})|^2} \sum_{l\mathbf{k}_1 p\mathbf{k}_2} B_{l\mathbf{k}_1 p\mathbf{k}_2}(\mathbf{G}). \quad (4.20)$$

This additional term has the behavior $\frac{\alpha}{|\mathbf{q}|^2}$ which has been fruitful in explaining excitonic effects [9].

Whether such a non adiabatic contribution could be the main explanation for the excitonic effect of Ref. [89] is left for future work.

4.4 Conclusion

In this chapter, I have presented different levels of approximation to calculate optical absorption spectra. The present status of the theory is very mature, and the role of excitonic effect is well understood. Lastly, I have presented an unpublished explanation on the long range kernel $\frac{\alpha}{|\mathbf{q}|^2}$, which could be interpreted as the contribution of a non adiabatic perturbation.

Chapter 5

Theoretical results on the stability of boron carbides

This chapter is a reproduction of the preprint [48]. It is a review article of my work on boron carbides, following an invitation to the 16th International Symposium on Boron, Borides and Related Materials September 7-12 , 2008, Matsue, Shimane, Japan. I am now going to present new results on the formation energy of boron carbides at carbon concentrations lower than 20% at. C. The paper has been written in collaboration with Jelena Sjakste and E. Betranhandy.
.

5.1 Introduction

The density functional theory (DFT) has become a crucial *from-first-principles* tool to investigate ground state properties of materials.[1, 63, 64] Theoretical results on boron carbides presented in this paper rely on DFT, and therefore we briefly recall in this introduction the main purpose of DFT and its limitations. DFT maps a system of interacting electrons on a system of noninteracting electrons in an effective potential, which contains the so-called exchange and correlation potential. In fact, DFT relies on assumptions for the exchange and correlation energy, which aim at modeling terms difficult to take into account in the mapping : *(i)* the difference in kinetic energy between a system of interacting electrons and noninteracting ones; *(ii)* all many-bodied electron-electron quantum interactions - such as Pauli's principle - beyond the Hartree energy (the classical electrostatic energy for interacting charge densities).

In the simplest local density approximation (LDA), each small volume of the system is expected to contribute to the energy of exchange and correlation as would an equal volume of a homogeneous electron gas at the same density.[90] Equilibrium properties calculated within DFT-LDA such as lattice parameters and internal atomic positions usually agree extremely

well -within 1%- with experiment. There are, however, a number of applications in which this accuracy is not high enough. It is worthwhile pointing out, for instance, that most of today's calculations of electronic spectra are performed at the experimental lattice constant to avoid a lattice misfit.[10]

Exchange and correlation functionals beyond LDA are thus required in order to evaluate the equilibrium volume with a greater accuracy. The generalized gradient approximations (GGA) have been developed with such an objective.[68] It is important for properties which explicitly depend on the equilibrium volume V_{eq}, such as the tensor of elastic constants C_{ijkl}, defined as the second order derivative of the (DFT) total energy E with respect to the strain tensor ε_{ij}, where i, j, k and l are cartesian indexes

$$C_{ijkl} = \frac{1}{V_{eq}} \left(\frac{\partial^2 E}{\partial \varepsilon_{ij} \partial \varepsilon_{kl}} \right)_{\varepsilon=0}. \tag{5.1}$$

In the above equation, the explicit dependence on the equilibrium volume V_{eq} makes the error bar on elastic constants much smaller when calculated within the generalized gradient approximation than within LDA.[54] Nuclear magnetic resonance (NMR) is another type of properties which directly probes the local atomic structure through the electronic response to an external magnetic field. For the same reasons, calculations of the chemical shift tensor performed with GGAs do show a more satisfactory agreement with experiment in comparison with those obtained by using the LDA.[91–93] We therefore used one of the GGAs [94, 95] for our NMR results spectra presented in subsection 5.2.4.

Among known limitations of DFT, forbidden energy gaps in insulators and semiconductors are underestimated. For energy gap calculations, theoretical frameworks beyond DFT are required, which take into account the electron-electron interaction beyond an energy-independant and local potential. Energy gaps are currently computed with a Green's function approach which allows for the calculation of quasiparticle corrections to the values of the DFT energy to first-order in perturbation.[13, 14, 30]

Excited states are also out of reach of DFT. They are treated either by the time-dependent density functional theory (TDDFT),[7, 8] or by the solution of the Bethe-Salpeter equation, when, like in optical absorption, it is necessary to take into account the electron-hole interaction.[10, 29] These methods nonetheless rely on DFT, for obtaining the ground state wavefunctions and values of the energy which are used, either as a starting point, or to calculate key quantities like the dielectric tensor.

Finally, it is not yet clear whether the above-mentioned many-body methods based on Green's functions are sufficient in materials where electronic correlations are of primary importance, like in oxides with multiply

occupied $3d$ orbitals. The dynamical mean field theory presents an alternative method to model the correlations.[75] It should be noted, however, that both classes of methods have been successfully applied to the electronic spectroscopy of vanadium dioxide.[96, 97]

Being sp bonded materials, boron-rich solids (BRS) are expected to have ground state properties well described by DFT based methods. The crystal symmetry of BRS is rhombohedral with the $R\bar{3}m$ space group. The atomic structure consists of one distorted icosahedron per primitive unit cell (Figure 5.1), eventually plus one multi-atomic chain. Each atom in the icosahedron is the apex of a pentagonal-based pyramid. Two crystallographic sites in the icosahedron are defined by the intericosahedral bonding. In polar site p, one atom is linked by a covalent two-center p-p bond to one atom in the polar site of a neighboring icosahedron. In the second site e, the equatorial atom is bonded to the chain-end atom of a multiatomic chain that links neighboring icosahedra. The intericosahedral chain can be absent like in α-boron. In most of the icosahedral solids, there is one chain per unit cell. The chain can be diatomic - as in $B_{12}P_2$ and $B_{12}As_2$ - or triatomic like in boron carbides (Figure 5.1).

The nature of the bonding makes boron-rich solids widely different from fullerenes, a class of materials with which they are nonetheless often compared. Due to electron deficiency,[98–100] a "standing alone" B_{12}, $B_{11}C$ or $B_{10}C_2$ neutral cluster is unstable. Thus BRS can not be compared to fullerene crystals.[38, 39]. The comparison of the respective compressibilities of the intra and interatomic bonds by *ab initio* methods has proved that neither α-boron nor icosahedral boron carbide with 20 % of carbon concentration (B_4C) are molecular crystals. Neither do they form an inverted molecular crystal, in which the intericosahedral bonds would be "stronger" than the intraicosahedral ones.[39, 101, 102] Icosahedral boron-rich solids form a special case of covalent materials adopting an unusual structure because of the electronic deficiency that is intrinsic to the boron atom.

The icosahedral sp bonding is by far more complex than sp bonding in diamond or other covalent materials with a tetrahedral coordination. The density functional theory is expected to be well suited to explain physical properties related to this complex sp bonding.

5.2 The atomic structure of B_4C from first principles

In this section, our aim is to review what has been established about the atomic structure of B_4C by comparing experimental data to results computed *from first principles*.

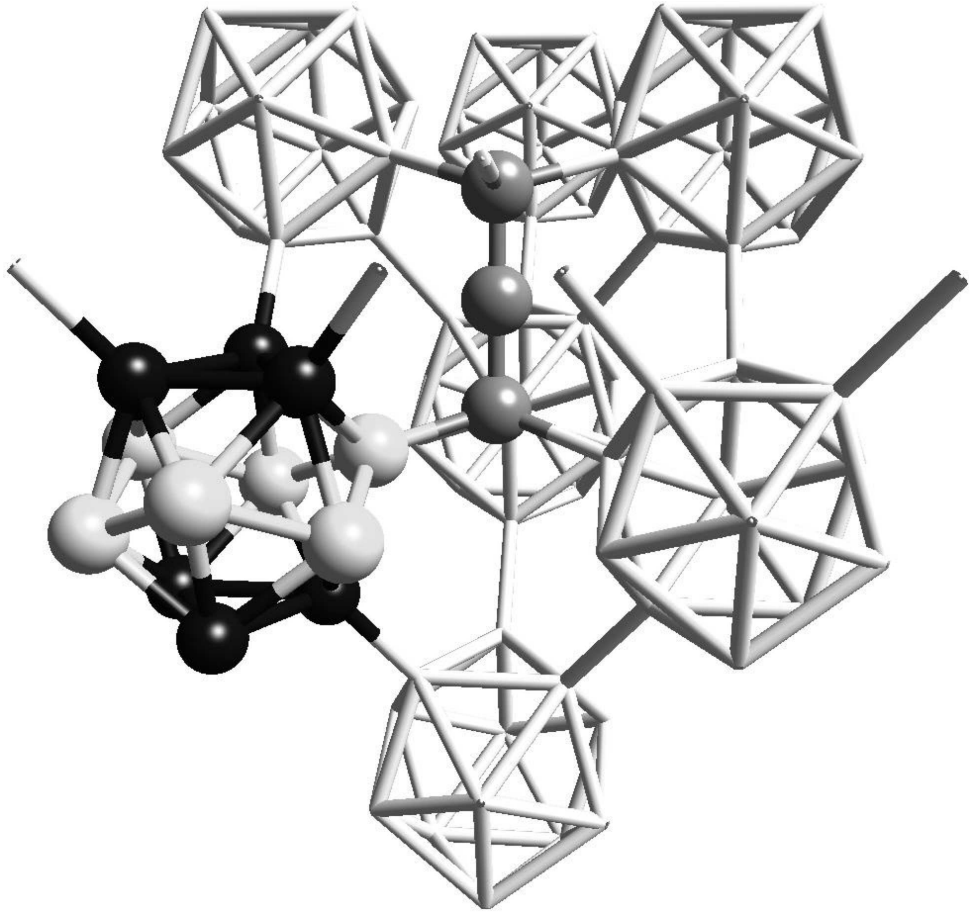

Figure 5.1: Atomic structure of icosahedral boron carbide from Ref. [42]. Seven distorted icosahedra are shown. The rhombohedral Bravais lattice vectors (not shown) link icosahedra centers. Black balls : atoms at the *p* polar site. Light grey balls : atoms at the *e* equatorial site. Dark grey balls : atoms at chain center and chain ends. Polar atoms are shown to be bonded to neighboring icosahedra *via* the covalent two-center *p*-*p* bonds. Equatorial atoms are linked to one atom at the end of the triatomic chain.

The atomic structure of $B_{12}C_3$ (B_4C) boron carbide contains 15 atoms in four occupied crystallographic sites (Figure 5.1). Two sites form a distorted icosahedron, the polar and equatorial sites, with 6 atoms *per* site. The third and fourth sites are respectively the center of the triatomic chain (one atom) and the chain ends (two atoms).

Experimentally, the three carbon atoms are difficult to distinguish from the twelve boron atoms. Indeed, the scattering length of a ^{13}C nucleus is very close to the scattering length of a ^{11}B nucleus, and only cell parameters have been measured by neutron diffraction.[103, 104] Atomic positions deduced from X-ray diffraction data indicate that the chain is C-B-C and that one carbon atom is substituted in the icosahedron.[105, 106] As the X-ray form factor scales like Z^2, where Z is the atomic number, the form factors for light neighboring elements like B and C are very close, and it is difficult to distinguish between boron and carbon atoms in the icosahedron. The picture provided by X-ray diffraction is the following one : the third carbon atom is statistically substituted on both polar and equatorial sites, with a predominance for the polar site. The formula is $(B_xC_{1-x})^p_6(B_yC_{1-y})^e_6$, in which $0.93 \leq x \leq 1$ for the polar site and $0.74 \leq y \leq 0.86$ for the equatorial site.[106, 107]

In order to gain knowledge of the atomic structure of boron carbide with a carbon concentration of 20%, we have investigated several structural models with *ab initio* methods based on DFT, with the purpose of comparing various computed physical properties with available experimental data. Calculations were performed within DFT using the plane-wave pseudopotential method. More details can be found in Refs. [38, 39, 42].

5.2.1 Structural models

In this subsection, all our structural models have a 20% carbon concentration and consist of one unit cell of 15 atoms, periodically repeated by translations of the Bravais lattice vectors. One exception is the *bipolar* model, which contains thirty atoms to keep the stoichiometry (Table 5.1). In the *polar* (resp. *bipolar*) model, the chain is C-B-C and the icosahedron has one (resp. two) carbon atom(s) in the polar site. In the *equatorial* model, the chain is C-B-C and one carbon atom is substituted in the equatorial site. We have also investigated a unit cell where the chain is C-C-C and the icosahedron is made of pure boron (*chain* model), or introduced some disorder in the chain, making it C-C-B instead of C-B-C (*disordered chain* model). A last model consists of a B-rich chain C-B-B (B-*rich chain* model) (Table 5.1).

The substitution of a carbon atom in the polar site of the icosahedra offers six possibilities, resulting in substitutional disorder. This makes the

observed symmetry of the unit cell *on average* rhombohedral. In our calculations, we do not take explicitly the substitutional disorder into account, as too large supercells would be required. Therefore, the periodic repetition of a carbon atom at a given position in the icosahedron induces a small distortion from the rhombohedral symmetry to a base-centered monoclinic cell. We have checked that this approximation does not modify the conclusions of this paper.

5.2.2 DFT total energy

The total energy obtained within DFT-LDA is reported in Table 5.1. The structure with the lowest energy is the *polar* model. We take this energy as our reference. The *bipolar* model comes second, with an energy higher by 0.25 eV per carbon atom change. This energy difference is very significant and corresponds in terms of thermal energy to a temperature higher than 2500 K. Furthermore, the DFT energetics allows the exclusion of the *equatorial* model, the *chain* model, the *disordered chain* model and the B-*rich chain* model. It shows that the chain is C-B-C. Exclusion of the *equatorial* and *chain* models will be further confirmed by inspecting the lattice dynamics and the NMR spectra. Moreover, the values of the formation energy of *disordered chain* and B-*rich chain* models show that these models are unstable (Table 5.5, rows 6 and 7 respectively).

The difference in total energy between our various structural models is much more important than actual accuracy of exchange and correlation functionals. The latter is indeed limited to 3 kcal/mol (10 meV/atom).[108] As our models differ only by the location of one carbon atom, the exchange-correlation functional limits the accuracy of our calculations to 10 meV per carbon atom change. Crystal phases differing by less than that amount can hardly be distinguished and this may lead to a wrong prediction of the most stable phase. We see that this is not the case in Table 5.1.

Furthermore the difference in total energy between our structural models is similar in LDA and in GGA (not shown, Ref. [42]) within 20 meV per change of carbon atom. This gives us confidence in the predictive ability of the DFT energetics for our models. We emphasize that LDA and GGA have the same physical content. Nonetheless, we note that by construction there is a cancellation of errors between the exchange energy and the correlation energy in LDA. This cancellation is not built-in in the GGA functionals,[109] which makes the computations both in LDA and in GGA worth performing and comparing. Moreover, by construction, GGA functionals tend to decrease the energy of the less dense phase, and hence to favor their stability.[110] Therefore, it is interesting to compute energy differences both in LDA and GGA, in order to obtain an error bar when the crystal density varies among the polymorphs. These differences in the construction of the functionals do not modify the relative stabilities of our

Table 5.1: Total energy (eV) *per* change of carbon atom location with respect to the *polar* model within DFT-LDA from Ref. [38, 39, 42].

Model	Chain	Icosahedron	Total energy (eV)
Polar	C-B-C	$B_{11}C^p$	(0)
Bipolar	$(C\text{-}B\text{-}C)_2$	$B_{10}C_2^p + B_{12}$	0.24
Equatorial	C-B-C	$B_{11}C^e$	0.53
Chain	C-C-C	B_{12}	1.05
Disordered chain	C-C-B	$B_{11}C^p$	2.5
B-*rich chain*	C-B-B	$B_{10}C_2^p$	3.9

structural models (Table 5.1 and Ref. [42]).

Our results for B_4C are robust against approximations. Contrastingly relative values of the energy of different crystal structures of pure carbon or of pure boron are much less robust. Graphite is found more stable than diamond by 145 meV/atom in DFT-GGA,[111] whereas diamond is found more stable than graphite in DFT-LDA by only 15 meV.[111] Zero-point motion might reverse the most stable phase. Clearly, the determination of the stability of pure carbon polymorphs is beyond the capacity of actual exchange and correlation functionals.[112] This is particularly true for graphite, because Van der Waals interactions are not properly taken into account in LDA nor in GGA.[113–117]

Turning to boron, in calculations for perfect crystals, α-B_{12} has been shown to be more stable than perfect 105-atoms-β-boron in DFT-LDA.[46] Recent calculations performed with a denser sampling of the Brillouin zone of α-boron yielded a total energy difference between α- and β-boron of 68 meV per atom in LDA and of 25 meV per atom in GGA, both predicting that α-B_{12} is more stable.[118] The difference between LDA and GGA is very important in this case. The 43 meV per atom energy difference yields an error bar of the exchange and correlation functionals.

On the other hand, calculations including defects predicted that defected β-boron is the most stable phase.[46, 119–123] The energy difference with respect to perfect α-boron is at most 20 meV/atom, far below the above-mentioned error bar of 43 meV. Also in this case, calculations reach the limit of exchange and correlation accuracy. We believe that the theoretical determination of the stability of pure carbon or pure boron polymorphs deserves further theoretical breakthroughs to overcome the intrinsic limitation of LDA and GGA functionals.

5.2.3 Lattice dynamics

Turning to lattice dynamics, we have computed [38] the phonon frequencies at the center of the Brillouin zone for the *polar*, *equatorial* and *chain* models (Table 5.1). We note that, in our case, the electronic structure and the lattice dynamics are performed within the same theoretical framework. This implies that changes in both Hartree potential and in exchange and correlation potential are calculated to first-order in perturbation theory. This response of the screening potential to the perturbing phonon is computed self-consistently, so that, at variance with semi-empirical models, the electronic density does not "rigidly shift" with the atomic motion. Compared to *e.g.* valence-force-field models, our computational scheme for phonon frequencies and displacement patterns does not contain any fitting parameter.

In Figure 5.2, we report the theoretical spectrum [38] for infrared absorption compared with data from Ref. [124]. Peak positions are clearly in better agreement for the *polar* model. With respect to the *equatorial* model, this is particularly true for the mode observed near 407 cm^{-1}. This is a vibration of the chain-center atom perpendicular to the chain axis.

The discrepancy between experimental peak positions and *chain* model ones is even more pronounced at high frequencies. The peak observed around 1560 cm^{-1} comes from the stretching of the chain, when the chain-end atoms vibrate antisymmetrically (*ungerade* vibration). The frequency is by far larger when the chain is C-C-C (Panel a) than when the chain is C-B-C (Panels b and c). We therefore conclude that the *chain* model can be disregarded : stretching of C-C-C chains does not occur in measured infrared spectra.

Turning to peak intensities in the *polar* model, we show in panel (d) a fit with one single parameter being the proportion between E_u and A_{2u} polarizations. Indeed, this proportion of polarizations is unknown in experiment. Our fit is in satisfactory agreement with experiment, showing that the tensor of effective charges is properly accounted for in the calculations.

If not silent, a vibration in B_4C is observed either in Raman diffusion or in infrared absorption. This is because the centre of the icosahedron is an inversion centre. The parity of a mode with respect to the inversion center is unique and the mode is either infrared active (ungerade E_u and A_{2u} modes) or Raman active (gerade E_g and A_{1g} modes). Therefore it is interesting to compare our computed phonon frequencies also to the peaks observed by Raman scattering. To our knowledge, only one Raman spectrum measured on a single crystal has been reported in the literature, and it is our reference in Figure 5.3. Observed peaks are broadened by disorder, and in the high frequency range, the theoretical frequencies of all our models [38] coincide with the experiment.

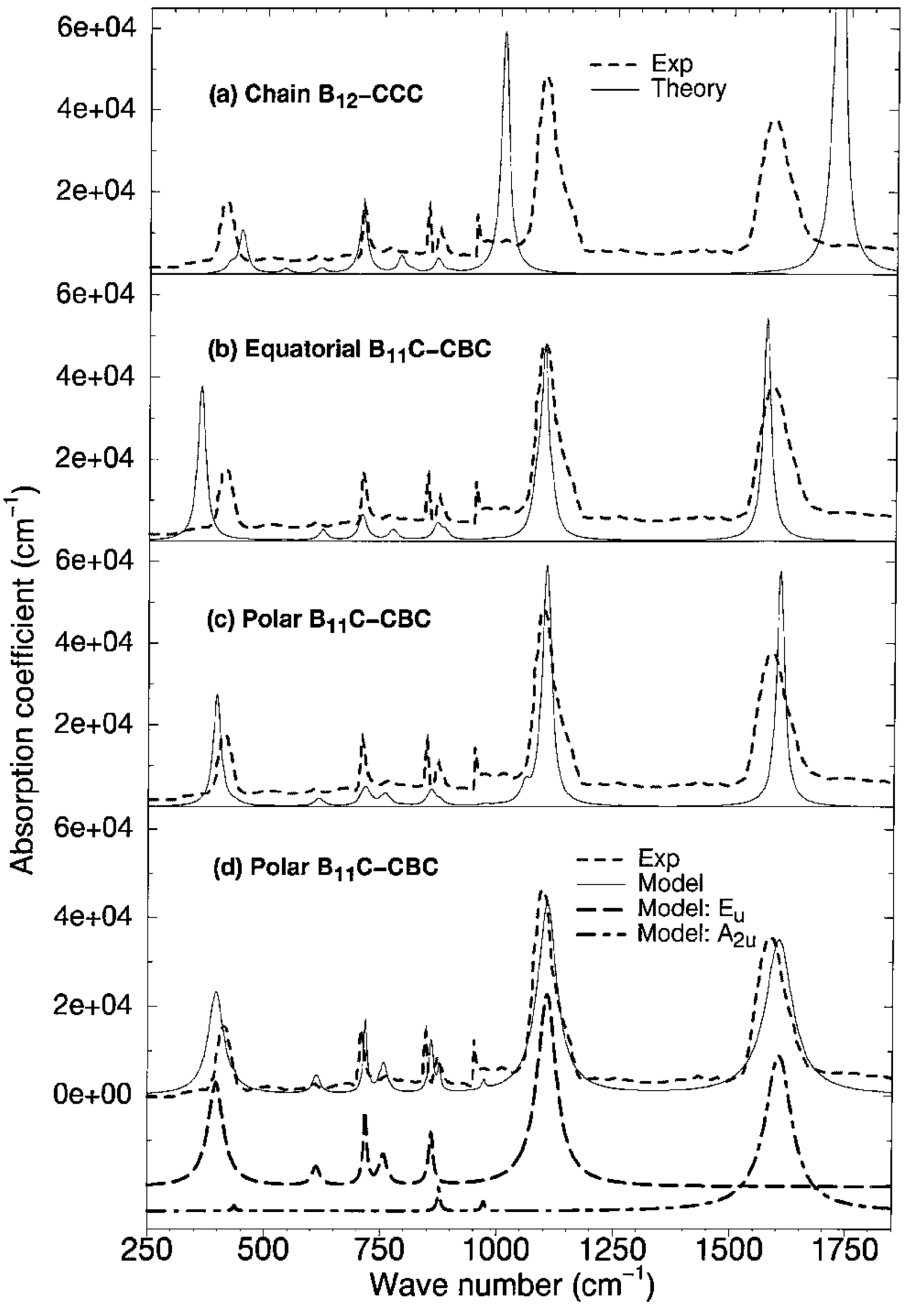

Figure 5.2: Infrared spectrum of B_4C from Ref. [38]. Dashed line : experiment.[124] Solid line: theoretical spectrum for the *chain* model (panel a); *equatorial* model (panel b); *polar* model (panel c). Panel d : spectrum for the *polar* model where the proportion of E_u and A_{2u} polarizations has been fitted with one single parameter to reproduce the unknown mixture of polarizations in the experiment (see text).

Nonetheless, two vibrational modes at 481 cm^{-1} and 534 cm^{-1} can be singled out. Both modes involve bond bending. The mode observed at 481 cm^{-1} corresponds in our calculations to a rotation of the chain-end atoms around the chain-center. The mode observed at 534 cm^{-1} corresponds to the libration of the icosahedron. This mode has been previously observed in α-boron and it was shown to be strongly harmonic.[37]

Compared with the disorder-induced broadening of other vibrations, the small widths of the two peaks indicate that the two above mentioned modes are harmonic in boron carbide. The frequency difference between them is therefore a quantity which is expected to be well reproduced in our calculations within the harmonic approximation. Figure 5.3 shows that the experimental frequency difference is reproduced only by the *polar* model. This difference is smaller by a factor of 2 in the *equatorial* model. Therefore the *equatorial* model can be disregarded as a possible structural model for B_4C.

Last but not least, we note that our calculations show no vibrational modes below 400 cm^{-1} (Figure 5.3). The Raman peaks which are observed below 400 cm^{-1} in most of the experiments [125–127] come from a lift of the selection rules for Raman scattering.[38] If ω is the phonon frequency, the intensity scales like a ω^4 power law at low frequency, which is the signature of a density of states of acoustic phonons. These phonons could be used to check the samples against structural disorder : they are expected to vanish in clean samples.

5.2.4 Nuclear Magnetic Resonance

In the previous subsection, the comparison of the calculated lattice dynamics with experiment allowed us to identify the atomic structure of B_4C as a C-B-C chain and a $B_{11}C^p$ icosahedron with the carbon atom substituted in the polar site. But we have also seen that experimental vibrational spectra do show a large broadening caused by substitutional disorder and/or structural defects. Therefore we have decided to compute NMR spectra, with the aim of learning more about these defects.[42]

Three values of the chemical shift of ^{13}C have been reported in the experimental literature (Table 5.2). Experiments [128–130] agree with one another about two signals around 1 and 82 ppm. Only one experimental work reports a signal at 101 ppm.[128] We note that this experiment yielded the best resolved spectrum. This additional peak may also be explained by a different route of synthesis of the sample, yielding more structural disorder.

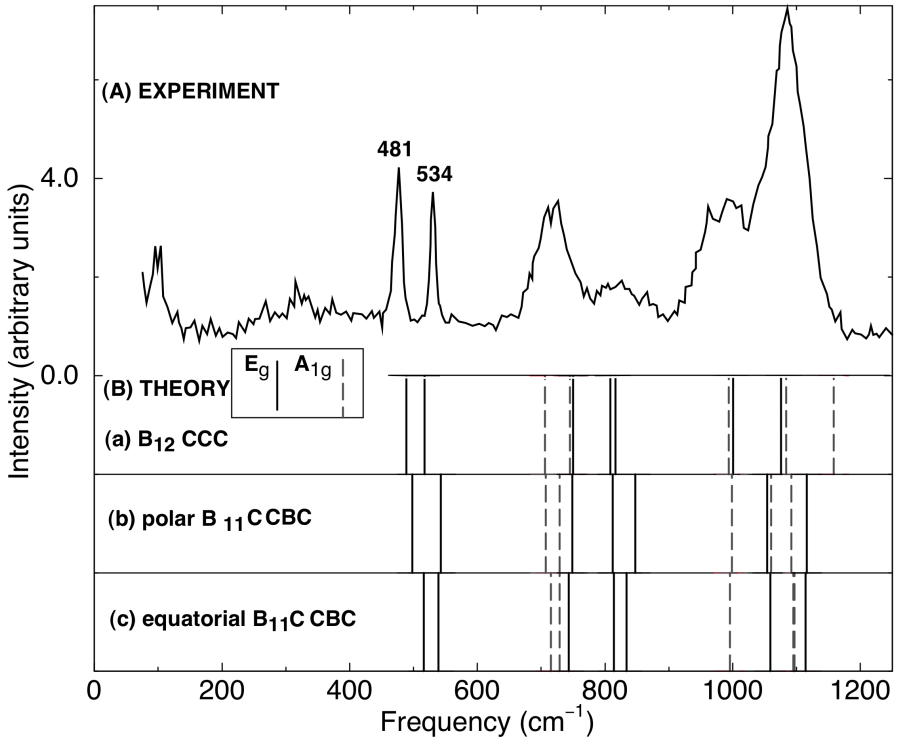

Figure 5.3: Raman spectrum of B_4C from Ref. [38]. Upper panel : experiment.[125] Lower panel : theory for *chain*, *polar* and *equatorial* models in subpanels a, b, and c respectively. Solid line : E_g mode. Dashed line : A_{1g} mode.

Our calculations show that the *polar* and *bipolar* models explain the experimental signals very well. Peaks around 1 and 82 ppm come from chain-end carbon atoms and from carbon atoms in the polar sites of the icosahedra, respectively (*polar* model). The *bipolar* model allows us to explain the signal at 101 ppm observed in Ref. [128], which comes from a different screening of the magnetic field when two carbon atoms are substituted in the same icosahedron. From the point of view of the total energy, the favorite relative location of two carbon atoms is in antipodal polar positions.[42] Furthermore, we note that a few percents of pure B_{12} icosahedra are necessary to keep the stoichiometry in our calculations.

Turning to the *equatorial* model, the width of the peak predicted by the theory that comes from chain-end carbon atoms is greater than 9.1 ppm (Table 5.2). This is significantly larger than in the experiment. Moreover, the calculated spectrum of the ^{11}B nucleus has a shoulder on the side of negative chemical shifts for the *equatorial* model (Figure 5.4). At variance with this finding, the observed spectrum shows a shoulder on the side of positive chemical shifts, in agreement with the *polar* model.[131] This al-

lowed us to disregard the substitution of one carbon atom in the equatorial site as a possible structure. Energetics, vibrational and NMR spectra thus agree on this point.

Furthermore, a carbon atom at the center of the chain would yield a chemical shift as large as 234 ppm in the ^{13}C spectrum. Such a signal is not observed (Table 5.2). Energetics, vibrational and NMR spectra agree on the fact that no C-C-C chains are present.

Finally, comparison of computed and observed NMR spectra allows us to draw the conclusion that the atomic structure of B_4C consists of a C-B-C chain and a $B_{11}C^p$ icosahedron with one carbon atom substituted in the polar site. A few percentages of the icosahedra have a $B_{10}C_2^p$ or a B_{12} atomic structure. We have estimated that 95% of the icosahedra are $B_{11}C^p$, 2.5% are $B_{10}C_2$ and 2.5% are B_{12} ones.[42]

Table 5.2: B_4C : ^{13}C NMR chemical shifts, δ_{TMS} (ppm), and the corresponding peak intensities (in brackets). Experiments from Ref. [128–130]. Note that the weak resonance at 101.3 ppm is visible only in the experiment of Ref. [128]. Theory : models as in Table 5.1.

Experiments			Theory			
Ref. [129]	Ref. [130]	Ref. [128]	*Bipolar*	*Polar*	*Equatorial*	*Chain*
13±15	-0.6	1.0	-1.7 & -1.1	-3.9 & 1.3	0.8 & 9.9	19.9
(66.7%)	(75.6%)	(66.9%)		(All models : 66.7%)		
85±10	79	81.9		81.6	79.1	233.8
(33.3%)	(24.4%)	(31.4%)		(These three models : 33.3%)		
		101.3	100.8 & 104.			
		(1.7%)	(33.3%)			

5.2.5 Conclusions

Inspection of both NMR and vibrational spectra yields the same picture for the atomic structure of B_4C : a C-B-C chain and a $B_{11}C^p$ icosahedron with one carbon atom substituted in the polar site.

There is no sign of the signature of a C atom at the chain center. This has important consequences : C-C-C chains can not be responsible for the boron carbide amorphization in shock-wave experiments.[41]

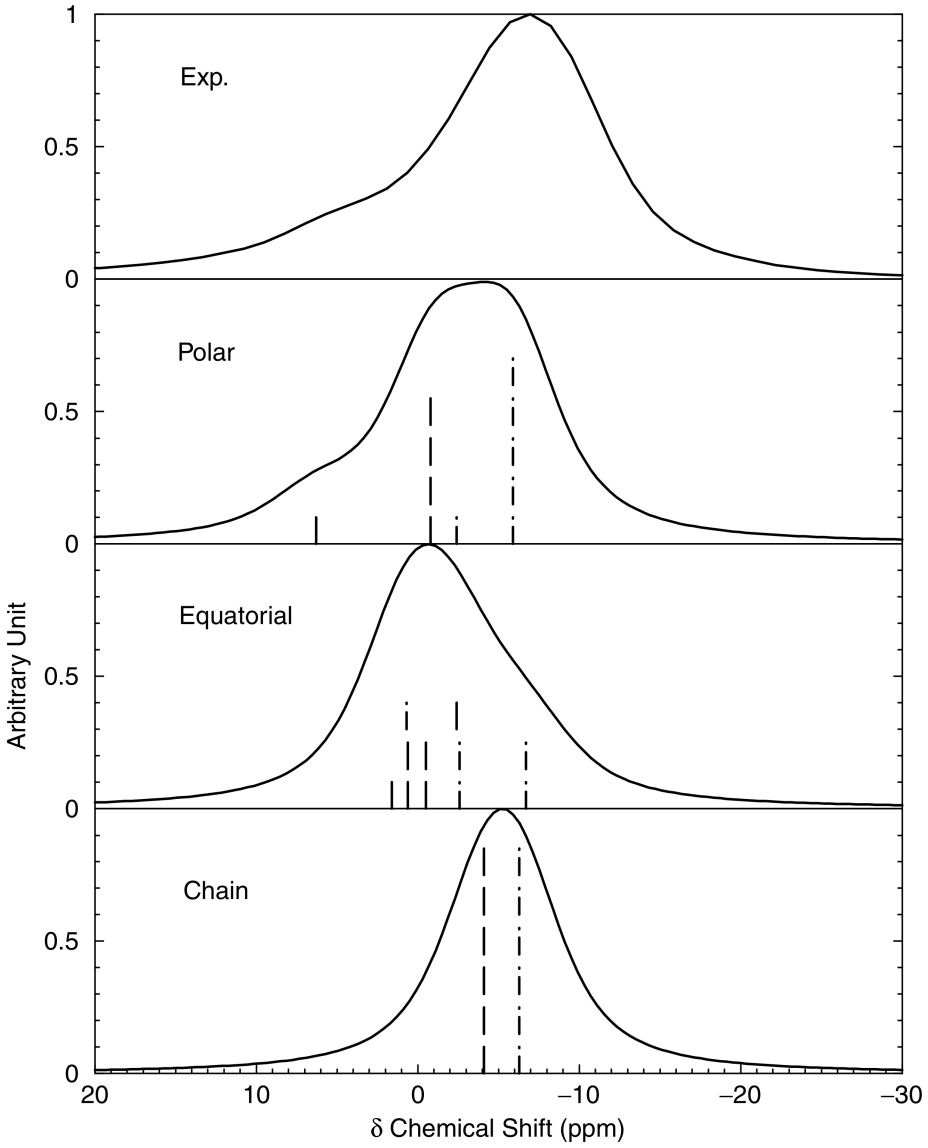

Figure 5.4: B_4C : ^{11}B NMR chemical shift spectrum. Experimental data is from Ref. [131] and theory for the *polar*, *equatorial* and *chain* models from Ref. [42].

Lastly, $B_{10}C_2^p$ icosahedra are present as defects in some B_4C samples. We have estimated that 2.5% of the icosahedra are $B_{10}C_2^p$. These defects have been experimentally observed. The presence of B_{12} icosahedra is inferred by us from the observed stoichiometry. To our knowledge, there are no direct observations of B_{12} icosahedra in B_4C samples.

5.3 Atomic structure of boron carbides at lower carbon concentrations.

At variance with the case of B_4C, knowledge about boron carbides at lower carbon concentrations must be improved both experimentally and theoretically. The atomic structures are not understood, nor are the phase stabilities.[132]

We have computed the equilibrium volume and formation energy of several structural models. Calculations were performed within DFT using the plane-wave pseudopotential method. Exchange and correlation energy was computed in the local density approximation. The pseudopotentials of boron and carbon were developed with the Troullier-Martin scheme.[133] For boron carbides, boron and diamond, plane waves up to a kinetic cutoff of 40 Ry have been included in the basis set. The irreducible wedge of the Brillouin zone has been sampled with 32 points when the unit cell was monoclinic (boron carbides with carbon atoms in the icosahedra), and 10 points when the unit cell was rhombohedral (*e.g.* for α-boron or boron carbides with B_{12} icosahedra) or cubic (diamond). Cell parameters and atomic degrees of freedom have been relaxed to minimize the total energy at the theoretical equilibrium.

5.3.1 Formation energy

Following present knowledge, α-boron (resp. diamond) is the most stable polymorph of pure boron (resp. carbon) within DFT-LDA for defect-free phases (see subsection 5.2.2). Firstly, values of the formation energy of boron carbides have been computed for a formation from α-boron + diamond.

We first considered a structural model as stable at 0 K when its formation energy E^f is negative with respect to a decomposition into α-boron + diamond, and when E^f is the smallest one among structures with the same carbon concentration. Among many structural models that have been investigated, only the five models of Table 5.3 are found stable.[134] At 20% carbon concentration, the *polar* model B_4C^p has the lowest formation energy. At approximatively 13 % carbon concentration, $B_{13}C_2$ is the most

stable phase. It consists of one B_{12} icosahedron and one C-B-C chain. A model combining both B_4C^p and $B_{13}C_2$, doubling the unit cell, is also stable (Table 5.3, 16.7 at. C %).

Secondly, we have tested our structural models against a decomposition into B_4C^p + α-boron (for a carbon concentration lower than 20%) or B_4C^p + diamond (for a carbon concentration greater than 20%). Surprisingly, no phases have been found stable against this decomposition in Table 5.4. For $B_{13}C_2$, we found $E^f_{B_4C}$=7 meV per atom. Our result is similar to previous calculations, -21 meV/atom at 0 K and -9 meV/atom at ambient temperature.[132] The model combining B_4C^p and $B_{13}C_2$ is also marginally unstable ($E^f_{B_4C}$ = 7 meV/atom, Table 5.4). These numbers are, however, within accuracy of actual exchange and correlation functionals (see subsection 5.2.2).

Replacing the chain-center atom by a vacancy in B_4C^p or in $B_{13}C_2$ yields two models with 21.3 or 14.3 % carbon concentration respectively. These crystals with vacancies are found to have a negative formation energy with respect to a formation from α-boron + diamond (Table 5.3). They have, however, a positive formation energy in Table 5.4 and should decompose into B_4C^p + α-boron or B_4C^p + diamond in thermodynamical conditions.

In conclusion, only B_4C^p is found to be thermodynamically stable in our calculations. Four other phases are found thermodynamically unstable under ambient conditions because : *(i)* at 0 K, they are energetically close to a decomposition into B_4C^p + α-boron or B_4C^p + diamond (Table 5.4); *(ii)* entropy effects are expected to further favor this decomposition at an ambient temperature. Having however negative values of the formation energy with respect to α-boron + diamond (Table 5.3), the four phases could nonetheless exist either in a metastable state, like diamond does; or as defects in an otherwise perfect crystal of B_4C^p, as $B_{10}C^p_2$ does (see subsection 5.2.4).

Turning to unstable structures,[134] our values of the formation energy with respect to α-boron + diamond are gathered in Table 5.5 together with previous studies.[45, 120, 132] Second in formation energy after B_4C^p, which is the most stable phase, come both our models for substitutional disorder (row 2) and the *bipolar* model (row 3). We have inferred from the broadening of the experimental vibrational modes that substitutional disorder is present, and inspection of NMR data tells us that the *bipolar* model is observed as a defect in actual samples. We now compare these two models. Our first approach to account for the effect of substitutional disorder (Table 5.5, row 2) is to double the cell and to substitute the carbon atom of the second icosahedron at different locations in the polar site. The effect of such a substitutional disorder on the formation energy is noticeable (row 2). In fact, starting from two identical icosahedra $B_{11}C^p$ + $B_{11}C^p$, one would

expect that the effect on the formation energy of exchanging one carbon atom and one boron atom in the same icosahedron, resulting in non identical $B_{11}C^{p}$ + $B_{11}C^{p'}$ (row 2) should be much smaller than that of a *bipolar* model, where one carbon atom and one boron atom are exchanged between two neighbouring icosahedra, yielding $B_{10}C_2^{p}$ + B_{12} (row 3). However this is not the case. The two models have a comparable formation energy (Table 5.5, rows 2 and 3). We then conclude that either our study of substitutional disorder lacks convergence with respect to the number of unit cells, and that larger cells should be studied; or that substitutional disorder might be energetically less favoured than a double substitution in the icosahedron.

At a carbon concentration of 20%, we found negative values of the energy for the *equatorial* and *chain* models previously discussed in subsection 5.2.2 (Table 5.5, rows 4 and 5). Nonetheless, these models have a much higher formation energy than the *bipolar* model, which is consistent with the fact that inspection of spectroscopic data enables us to exclude them. Moreover, we found positive formation energy for the *disordered chain* and B-*rich chain* models, which allows to exclude their formation in actual compounds (Table 5.5, rows 6 and 7).

At carbon concentrations other than 20%, all our unstable models show a positive energy of formation, larger than our expected accuracy on exchange and correlation functionals (see subsection 5.2.2). They can not be produced in a metastable state or as defects. For instance, insertion of carbon atoms in interstitial crystallographic sites is proved to be an inappropriate way of modeling boron-rich boron carbides (Table 5.5, rows 13 and 17). Another model which has been discussed in the scientific literature contains one atom at the centre of the icosahedron.[135] Such a model has a very high positive formation energy (Table 5.5, rows 8 and 14). Therefore we do not expect to observe materials in which boron icosahedra accommodate one atom at the icosahedron centre.

5.3.2 Discussion

Like B_4C, boron carbides at low carbon concentrations probably are mixtures of various building blocks. At carbon concentration other than 20%, the numerous structural models of Table 5.5 can be disregarded as possible candidates. Instead, models of Table 5.3 are useful guides towards a determination of actual atomic structures. The common thought that "intrinsic structural defects (...) originate from the energetically more favorable configuration compared to the ideal structures"[136] lacks theoretical justification. Indeed, the surprise comes from the small number of possible candidates (Table 5.3). Furthermore, the computation of the formation energy shows that these structures are not stable with respect to a decomposition into B_4C^{p} boron carbide + α-boron or B_4C^{p} + diamond (Table

5.4). This metastability explains why physical properties measured on different samples strongly depend on the synthesis route. More precisely, the instability of $B_{13}C_2$ with respect to a decomposition into B_4C^p + α-boron also explains the lack of an actual route to synthesize single crystals of $B_{13}C_2$.[137] Investigation with *ab initio* methods of an eventual stabilization under high pressure should shed some light on this question.

NMR data is crucially lacking for boron carbides at low carbon concentrations. To our knowledge, only the experiment of Ref. [128] yielded data on boron carbides at 13.3 and 10% carbon concentrations. This experiment showed two additional signals beside those of B_4C^p. The intensities of these additional peaks however barely vary between 13.3 and 10% atomic carbon concentrations, so that one can not simply consider them as fingerprints of boron-rich boron carbides. The precision of the NMR technique has drastically increased since 1991, and it would be of utmost importance to perform new experiments on boron carbides. DFT-based methods are mature enough to help the understanding of these experiments.

Finally, one should note that three models of Table 5.3 contain an odd number of electrons per unit cell, and hence are metals in any band theory. Contrastingly, boron carbides are thought to be semiconductors.[137] We think that actual experimental knowledge might be too sample dependent. A precise measurement of the resistivity on clean samples is lacking, and would be very helpful in discriminating among the models of Table 5.3. We show in the next section that the strength of the electron-phonon coupling combined with the high average vibrational frequency makes boron carbides very interesting if a metallic state can be achieved.

5.4 Strength of the electron-phonon coupling

Among possible candidates for the role of the main building block for boron carbides at low carbon concentrations, $B_{13}C_2$ is the favourite one. As described in previous section 5.3, it consists of one B_{12} icosahedron and one C-B-C chain. The odd number of electrons makes it metallic, while B_4C is semiconducting. $B_{13}C_2$ can be viewed as a B_4C crystal doped with one hole per unit cell, and any band theory in general, and DFT in particular, implies that $B_{13}C_2$ is a metal (Figure 5.5). 90% of the states at the Fermi level are icosahedral states. This was our main motivation to investigate electron-phonon coupling in this material, which is a prototype of metallic icosahedral structures.

We have therefore computed the electron-phonon coupling *ab initio*.[6, 91] By averaging around the Brillouin zone, we have obtained a coupling parameter equal to 0.8. This quantity is 0.9 in MgB_2.[6] The phonon density

Table 5.3: Formation energy of stable [134] boron carbides at $T = 0$ K, E^f (meV/atom). First column : model name as in Table 5.1. Second column : carbon content. In the third column, except for the *polar* model and the elements, the formula of the icosahedron (resp. chain) is given in (resp. out of) brackets. V stands for a vacancy. This work : E^f is computed in LDA for a formation from α-B_{12} + diamond. The values of the formation energy of pure carbon or boron phases are also given.

Model	at. % C	Materials	This work	Theory	Exp.
	100	Graphite		-24[1];0[2]	-35±10[5]
	100	Diamond	0		
	21.4	$(B_{11}C^p)$C-V-C	-15	-11[2]	
Polar	20	B_4C^p	-121	-112[2],-109[3][4]	-88±3[6]
					(119±24)[7]
	16.7	$(B_{11}C^p)$C-B-C+(B_{12})C-B-C	-94	[-92,-84][4]	
	14.3	(B_{12})C-V-C	-20	-35[2]; -33[4]	
	13.3	(B_{12})C-B-C	-74	-81[2], -79[4]	
	0	α-B_{12}	0	0[2]	

[1] Formation from graphene with Van der Waals forces, Ref. [113].
[2] Formation from graphite and α-B_{12} in GGA, Ref. [45].
[3] LDA, Ref. [132].
[4] GGA, Ref. [120]. Square brackets indicate an energy range for E^f.
[5] Cited in Ref. [113].
[6] Enthalpy of formation at 0 K[138].
[7] Energy of formation at ambient temperature, Ref. [139].

Table 5.4: The same as in Table 5.3 with $E^f_{B_4C}$ computed in LDA for a formation from B_4C^p + diamond for a carbon concentration larger than 20 %, and from B_4C^p+α-boron for a carbon concentration lower than 20 %.

Model	at. % C	Materials	$E^f_{B_4C^p+\alpha-B_{12}}$	$\Delta E^f_{B_4C^p+diamond}$
	21.4	$(B_{11}C^p)$C-V-C		104
Polar	20	B_4C^p	0	0
	16.7	$(B_{11}C^p)$C-B-C+(B_{12})C-B-C	7	
	14.3	(B_{12})C-V-C	66	
	13.3	(B_{12})C-B-C	7	

Table 5.5: Unstable [134] boron carbides. Formation energy E^f (meV/atom) from α-B_{12} + diamond. Square brackets indicates an energy range for E_f. Column 1 : model name as in Table 5.1 or row number. Column 2 : carbon concentration. Columns 3 and 4 : description of the chain and of the icosahedron, respectively. V stands for a vacancy. Column 5 indicates if additional atoms are in interstitial positions, and column 6 indicates if the icosahedron contains one atom at its centre.

Model or row number	at. % C	Chain	Icosahedron	Inter-stitial	Ico. center	This work	Theory
	26.7	C-B-C	$B_{10}C_2$			117	
(row 2)	20	$(C\text{-}B\text{-}C)_2$	$B_{11}C^p$+$B_{11}C^{p'}$			[-117,-81]	[-109,-70][1]
Bipolar	20	$(C\text{-}B\text{-}C)_2$	$B_{10}C_2{}^p$+B_{12}			-113	
Equatorial	20	C-B-C	$B_{11}C^e$			-84	-74[1]
Chain	20	C-C-C	B_{12}			-38	
Disordered chain	20	C-C-B	$B_{11}C^p$			55	
B-*rich chain*	20	C-B-B	$B_{10}C_2^p$			127	
(row 8)	18.8	C-B-C	B_{12}		C	648	
	15.4	C-V-V	$B_{11}C^p$				144[2]
	14.3	C-B-V	$B_{11}C^p$				48[2]
	14.3	B-V-C	$B_{11}C^p$				62[2]
	13.3	B-B-C	$B_{11}C^p$				45[2]
(row 13)	12.5	C-B-C	B_{12}	B		49	
(row 14)	12.5	C-B-C	B_{12}		B	504	
	12.5	none	$B_{11}C$+$B_{10}C_2$			579	
	11.1	C-B-C	$B_{11}C$+B_{12}			93	
(row 17)	10.	C-V-C	B_{12}	B_6		355	
	8.3	none	$B_{11}C^p$				127[2]
	7.7	B-V-V	$B_{11}C^p$				212[2]
	7.7	V-B-V	$B_{11}C^p$				212[2]
	7.4	C-B-C	B_{12}+B_{12}			75	
	7.1	C-B-V	B_{12}				65[2]
	7.1	B-V-C	B_{12}				67[2]
	7.1	B-B-V	$B_{11}C^p$				119[2]
	7.1	B-V-B	$B_{11}C^p$				119[2]
	6.7	C-V-V	B_{12}				77[2]
	6.7	B-B-C	B_{12}				14[2]; 16[1]; -58[3];
	6.7	B-B-B	$B_{11}C^p$				75[2]

[1] GGA, Ref. [120].
[2] From graphite and B_{12} in GGA, Ref. [45].
[3] LDA, Ref. [132].

of states reported in Figure 5.6, and the Eliashberg function in Figure 5.7, allow us to understand that the magnitude of the electron-phonon coupling mostly comes from a coupling with the vibrations of the icosahedron.

The pioneering theoretical method to compute the superconductivity now make possible the computation of the screened Coulomb interaction which is required to evaluate the critical temperature.[140, 141] In our calculation, we have instead used a parameter for the Coulomb repulsion in Mc Millan formula.[6] When this parameter is taken equal to the value of MgB_2, we obtain a critical temperature of 27.6 K, only slightly below the 30.7 K obtained for MgB_2.

To conclude this section, it has been shown that the critical temperature for metallic $B_{13}C_2$ is comparable to the Tc of MgB_2, and that superconductivity is linked to B_{12} building blocks. The difficulty comes from the synthesis of single crystals (see subsection 5.3.2). Extrapolating our results to heavily doped α-boron, its Tc is expected to be greater than the Tc of heavily doped diamond, silicon or silicon carbide, by more than one order of magnitude.

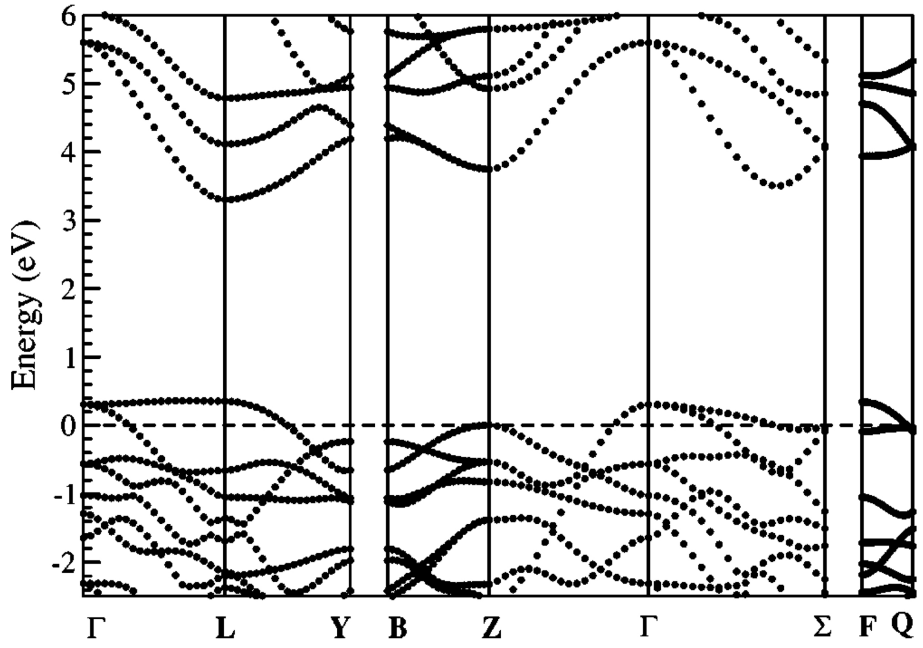

Figure 5.5: DFT-LDA band structure of $B_{13}C_2$ from Ref. [6]. The energy (eV) is referred to the Fermi level (dashed line).

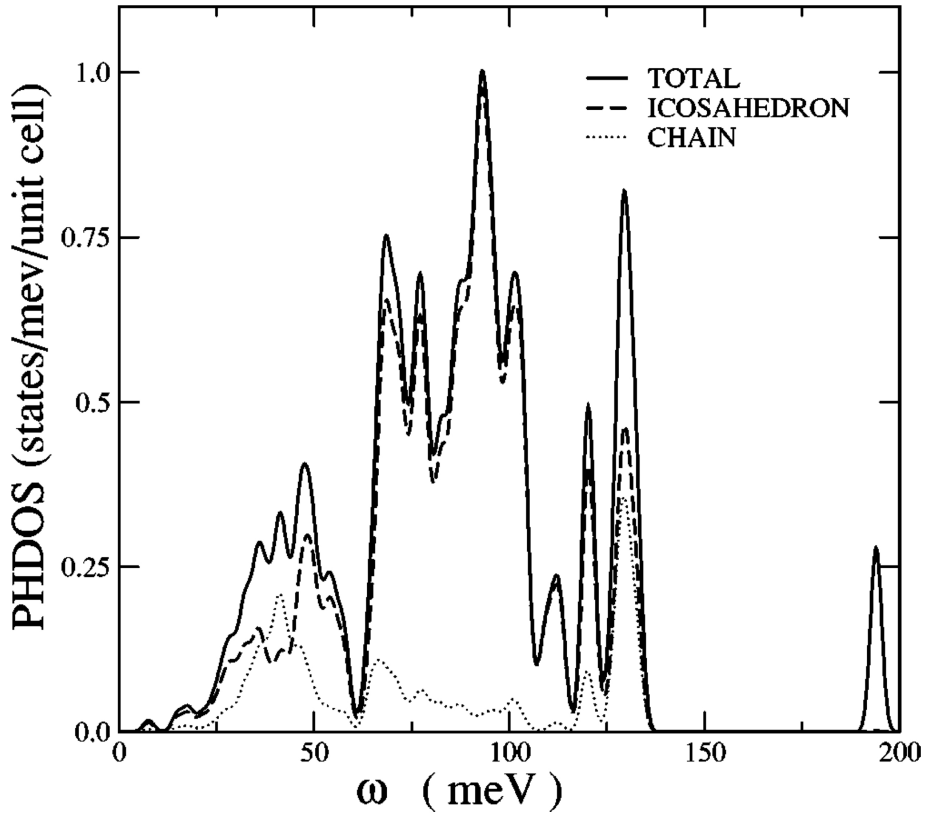

Figure 5.6: Phonon density of states of $B_{13}C_2$ from Ref. [6]. Solid line : total DOS. Dashed line : contribution from the vibrations of the icosahedron. Dotted line : contribution from the phonon modes of the chain.

5.5 Conclusion

In this work, we have reviewed actual understanding of the atomic structure of boron carbides gained from *ab initio* calculations. These computations allowed the unambiguous determination of the atomic structure of B_4C. Observed vibrational and NMR spectra are well explained by the *polar* model : one $B_{11}C^p$ icosahedron and one C-B-C chain per unit cell. We have shown that the main structural defect, apart from substitutional disorder of the carbon atom in the polar site, is a $B_{10}C_2^p$ icosahedron. These defects have been observed in one NMR experiment. Moreover stoichiometry implies the existence of B_{12} icosahedra.

In addition, this satisfactory agreement moreover gives us a great confidence in the ability of DFT to accurately predict the values of the formation energy of boron carbides at concentrations other than 20%. We have shown that very few structures can be regarded as possible candidates for being main structural blocks for boron carbides at carbon concentrations lower

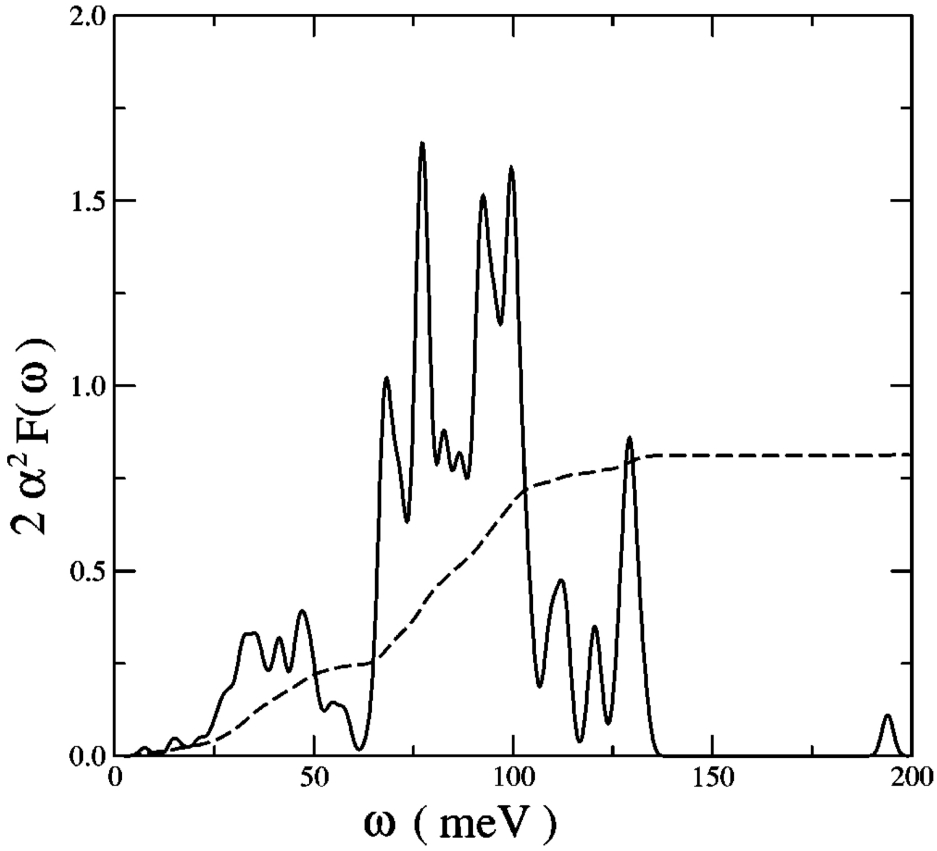

Figure 5.7: Solid line : Eliashberg function from Ref. [6]. Dashed line : average electron-phonon coupling parameter.

than 20%. This goes against the widely spread thought that intrinsic structural defects are energetically favourable with respect to the ideal structure. Rather, we find a metastability of any model with respect to B_4C^p + α-boron or B_4C^p + diamond. By shedding light on this metastability, we have explained actual difficulties in the synthesis of clean samples of boron carbides with carbon concentrations lower than 20%.

Lastly, we have shown that the strength of the electron-phonon coupling in a prototype icosahedral metal, $B_{13}C_2$, is comparable to electron-phonon coupling in MgB_2. From these considerations, we expect electron-phonon coupling in heavily doped α-boron to be more than one order of magnitude greater than that of heavily doped silicon. Combining superconductivity and the known remarkable mechanical properties of boron carbides can lead to materials of high industrial interest.

Chapter 6

Conclusion and outlook

In the long term, the ambitious objective is to understand and to predict the ways by which the electronic excitation yields changes in the atomic structure of a material and the processes by which structural defects are created.

In the chapters 2, 3 and 4 of this HDR thesis, I have presented the tools at our disposal to deal with the excitation of valence electrons and to understand the fingerprints that shows up in the electron energy loss spectra and in optical absorption spectra. I have reported results on various oxides. In the future, it will not be out of place to develop the theory of photoemission beyond its actual limitations. I have been involved in the project about the ARPES measurement on cuprous oxide and the computation of the corresponding band structure. [29] I have the feeling that whereas the theory of electron energy loss spectroscopy and of optical absorption has been developing to the point where it has reached a certain maturity, a lot a work is still needed to reach the same level of maturity in order to calculate the photocurrent, despite recent advances [142].

One way to make a progress in the above-cited objective is firstly to reach a deep understanding of a given material and of its defects, and secondly to understand which defects are developing under an irradiation, and why they do so. In the chapter 5, I have summarized my understanding of some physical properties of boron carbides, a material which I am a specialist of. I have reported which defects are predicted by the calculation to occur in this material. A study of how such defects are produced during a shock wave experiment and why they drastically modify the mechanical strength of this material is ongoing with Dr. Emmanuel Betranhandy. In the future, it will be of utmost importance to understand and predict by the calculation what kind of defects can develop under an electronic excitation in such a material.

The third subject left for the short-term future is the theory of electron-phonon coupling for the electronic relaxation in semiconductors. I consider this topics as an ongoing project, which we have well documented in the sci-

entific literature.[5, 31, 32, 143] Ongoing progress is made in the framework of the project ACCATTONE supported by the French Agence Nationale pour la Recherche. I hope that in the near future, this subject will be mature enough and recognized as very important. I hope that it will be soon developed in the HDR thesis of my collaborator Dr. Jelena Sjakste. The coupling of the electronic excitation to a phonon of a finite wavevector enables us to understand the lifetime of the electronic relaxation. The next step is to study the coupling with a phonon of vanishing wavevector (long wavelength) and the PhD thesis of Iurii Timrov is devoted to this point. The next step, left for future work, is to understand how such a coupling can modify the atomic structure.

Finally, I would like to thank the many people with whom I have been working. I hope they have been cited as they thought they should be, and I apologize if this it not the case. I deeply thank Professor Ulf von Barth for his detailed reading of the manuscript, and Jill Cottin for the corrections of the English language. I thank Prof. Ulf von Barth, Prof. Giulia Galli and Dr. Christophe Delerue to have accepted to review the manuscript and to participate to the jury of this HDR. I thank Prof. Maria Chamarro for having accepted to chair the jury, and Dr. Christian Colliex and Dr Guillaume Petite to have accepted to be members of the jury of this HDR. I thank Dr. Guillaume Petite, the former head of the laboratoire des Solides Irradiés, for his encouragements during these last nine years.

Appendices - Annexes

Appendix A

Description of zirconia

Zirconium dioxide is the only thermodynamically stable compound in the system Zr-O [144, 145].

Zirconia (ZrO_2) is a technologically important material due to its high strength and stability at high temperatures and its excellent dielectric properties, with an average static dielectric constant ε_0 of around 20 [146]. Zirconia thus shows a wide range of industrial applications, including uses in ceramic engineering (for example, to strengthen SiC ceramics [147]), or as an oxygen sensor in fuel cells [148]. It is also a technologically important catalytic support medium [149]. It is now proposed, together with hafnia, as a gate dielectric material in metal-oxide semiconductor devices [150, 151].

Furthermore, zirconia is one of the most radiation-resistant ceramics currently known [152, 153], and therefore has a particular importance in the nuclear industry, where it is used as a passivating medium for hydrogen ingress in pressure tubes. A proposed application of particular interest is the use of a ZrO_2 matrix which can be doped with radioactive nuclei (particularly actinides), and irradiated to force a transmutation process and form non-radioactive dopants in the irradiated and yet stable zirconia matrix.

The evolution of the structural and electronic properties of zirconia as a function of factors such as temperature and pressure in the polymorphs of pure zirconia (cubic, tetragonal or monoclinic phases), as well as their mixing with various oxides is therefore the subject of intensive experimental studies.

At low pressures, zirconia displays three phases : monoclinic, tetragonal and cubic. The ground state phase of zirconia, a baddeleyite structure with a monoclinic unit cell, is stable up to around 1480 K [154]. The monoclinic unit cell contains four ZrO_2 units (m-ZrO_2, Fig. A.1(c)). At 1480 K, monoclinic zirconia (m-ZrO_2) undergoes a first-order martensitic transition to transform into a tetragonal phase [155] (t-ZrO_2, Fig. A.1(b)). By increasing the temperature to 2650 K, a displacive transition takes place in t-ZrO_2 and

the cubic fluorite phase (c-ZrO_2, Fig. A.1(a)) is obtained [154, 156], which is then stable up to the melting temperature of 2983 K [144].

Coordination number of the zirconium atom is $Z = 8$ in the cubic and tetragonal structures, and $Z = 7$ in the monoclinic phase.

I have also studied an hypothetical rutile structure with $Z = 6$. This is the stable structure for TiO_2, which is isoelectronic with zirconia. I used the rutile phase as a tool to investigate effects of the crystal field in zirconia and better understand the properties of the complex monoclinic phase of zirconia.

In my calculations, I found that the energy of the phases follows the experimental phase diagram : the monoclinic phase is the most stable phase, than the tetragonal one, and finally the cubic one [24]. Nonetheless, G. Zanzotto has recently drawn my attention on the fact that the high pressure orthorombic phase shows an energy bigger than the energy of the monoclinic phase, and lower than the energy of the tetragonal one [157]. One could then suspect that the orthorombic phase could occur as an intermediate phase in the phase diagram of zirconia when the temperature is increased, thus yielding the order (monoclinic, orthorombic, tetragonal and cubic cristal), instead of the experimental order monoclinic, then tetragonal and finally cubic phase.

My personal view is that DFT fails in reproducing relative values of the total energy as soon as one compares cristal phases which have different numbers of electrons or numbers of atoms. So far, I encountered problems when comparing phase of Zr, Ti, TiO_2, and probably ZrO_2.

In the future, it will be necessary to clarify whether the DFT fails (also) in reproducing the phase diagram of zirconia, or whether it is not straightforward to 'guess' the behavior (when raising temperature) of these complex systems from the energetics of DFT.

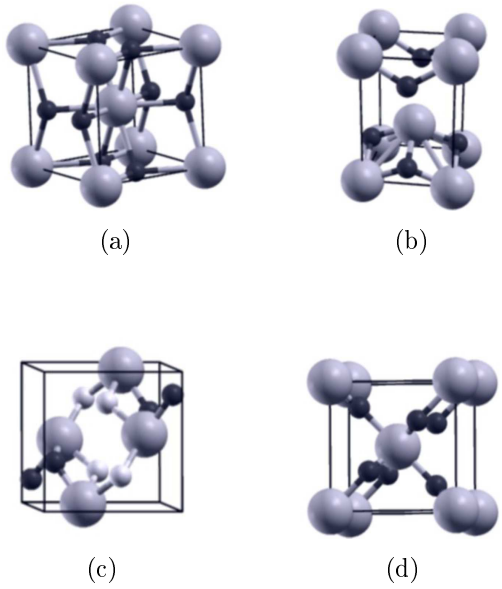

Figure A.1: The primitive unit cell of four atomic structures of zirconia. (a) cubic ZrO_2; (b) tetragonal ZrO_2; (c) monoclinic ZrO_2; (d) zirconia in the hypothetical rutile phase. Large sphere : zirconium atom. Small sphere : oxygen atom. For the monoclinic phase, the two different oxygen sites are shown in different shades. From [24].

Appendix B

A key rule: Fermi's golden rule

In this annex I describe one way to derive Fermi's golden rule.

Coming back to section 2.2, one wishes now to compute the probability for our system to make a transition from the unperturbed initial state $|\psi^{(0)}_{n\mathbf{k}}>$ to another final state $|\psi_f>$ under the influence of a perturbation. Following Ref. [66], we suppose the latter to be time periodic, and adiabatically switched at time $t=-\infty$ as in section 2.4.

Let us suppose that the energy of the perturbation is $\hbar\omega$, and that at initial time the system is in the state with energy $\varepsilon^{(0)}_{n\mathbf{k}}$, *i.e.* $a^{(0)}_{n\mathbf{k}}=1$ and $a^{(0)}_{p\mathbf{k}'}=0$ for $p\neq n$ or $\mathbf{k}'\neq\mathbf{k}$.

Examination of the denominators in eq. 2.17 shows that the values of the final energy for which these denominators are large are the resonant ones, for instance when $\varepsilon^{(0)}_f=\varepsilon^{(0)}_{n\mathbf{k}}+\hbar\omega$.

The quadrature 2.10 then reads

$$a^{(1)}_f(t)=\frac{-i}{\hbar}\int_{t_0=-\infty}^{t} e^{-i(\varepsilon^{(0)}_{n\mathbf{k}}-\varepsilon^{(0)}_f)\frac{\tau}{\hbar}}<\psi^{(0)}_f|F^{\mathbf{q}\,\dagger}|\psi^{(0)}_{n\mathbf{k}}>e^{-i\omega t}e^{\alpha t}d\tau, \qquad \text{(B.1)}$$

whose solution is

$$a^{(1)}_f(t)=\frac{e^{-i(\varepsilon^{(0)}_{n\mathbf{k}}-\varepsilon^{(0)}_f+\hbar\omega+i\hbar\alpha)\frac{t}{\hbar}}}{\varepsilon^{(0)}_{n\mathbf{k}}-\varepsilon^{(0)}_f+\hbar\omega+i\hbar\alpha}<\psi^{(0)}_f|F^{\mathbf{q}\,\dagger}|\psi^{(0)}_{n\mathbf{k}}>. \qquad \text{(B.2)}$$

The transition probability from the initial state $\psi^{(0)}_{n\mathbf{k}}$ to states $\psi^{(0)}_f$ whose energy lies within an energy range $d\nu_f$ reads

$$dw_{f;n\mathbf{k}}=|a^{(1)}_f(t)|^2 d\nu_f, \qquad \text{(B.3)}$$

where

$$|a^{(1)}_f(t)|^2=\frac{|<\psi^{(0)}_f|F^{\mathbf{q}\,\dagger}|\psi^{(0)}_{n\mathbf{k}}>|^2 e^{2\alpha t}}{(\varepsilon^{(0)}_{n\mathbf{k}}-\varepsilon^{(0)}_f+\hbar\omega)^2+(\hbar\alpha)^2}. \qquad \text{(B.4)}$$

One has

$$\frac{d|a_f^{(1)}(t)|^2}{dt} d\nu_f = \frac{2\alpha| < \psi_f^{(0)}|F^{\mathbf{q}\,\dagger}|\psi_{n\mathbf{k}}^{(0)} > |^2 e^{2\alpha t}}{(\varepsilon_{n\mathbf{k}}^{(0)} - \varepsilon_f^{(0)} + \hbar\omega)^2 + (\hbar\alpha)^2}. \tag{B.5}$$

Using the fact that

$$lim_{x\to 0} \frac{x}{\pi(\epsilon^2 + x^2)} = \delta(\epsilon), \tag{B.6}$$

one finds that

$$lim_{\alpha\to 0} \frac{d|a_f^{(1)}(t)|^2}{dt} = \frac{2\pi}{\hbar}| < \psi_f^{(0)}|F^{\mathbf{q}\,\dagger}|\psi_{n\mathbf{k}}^{(0)} > |^2 \delta(\varepsilon_{n\mathbf{k}}^{(0)} - \varepsilon_f^{(0)} + \hbar\omega) \tag{B.7}$$

Finally, the probability par time unit and par state amounts to Fermi's golden rule

$$\frac{dw_{f;n\mathbf{k}}}{d\nu_f} = \frac{2\pi}{\hbar}| < \psi_f^{(0)}|F^{\mathbf{q}\,\dagger}|\psi_{n\mathbf{k}}^{(0)} > |^2 \delta(\varepsilon_{n\mathbf{k}}^{(0)} - \varepsilon_f^{(0)} + \hbar\omega) \tag{B.8}$$

Appendix C

Curriculum vitae de N. Vast (Fr)

Nom :	**Nathalie VAST**
Poste :	Physicienne, Chercheure
	Expert senior CEA
Age :	43 ans
Indice H :	12 (au 8 aveil 2009)
HDR :	soutenance prévue le 13 juillet 2009
Email :	nathalie.vast@polytechnique.edu
Tel. :	+33 1 69 33 45 51

I. Données professionnelles

Affectation : CEA - DSM - IRAMIS
Labo. des Solides Irradiés
Ecole Polytechnique

II. Etat civil

Lieu de naissance : Lille, France
Nationalité: Française

III. Domaine d'expertise

Physique théorique et numérique pour la Matière Condensée
Etude *ab initio* des propriétés physiques des matériaux
Méthodes basées sur la Théorie de la Fonctionnelle de la densité (DFT),
http://nobelprize.org/nobel_prizes/chemistry/laureates/1998/kohn-lecture.html
et au-delà (effets à N-corps) pour

- la spectroscopie électronique et vibrationnelle
- les mécanismes d'excitation et de relaxation électronique, particulièrement la désexcitation par le couplage électron - phonon

Applications aux matériaux d'intérêt pour le CEA, spécialement :

- les diagrammes de phase du titane et du zirconium
- la spectroscopie des oxydes de métaux nobles et de transition : TiO_2, ZrO_2, Cu_2O par perte d'énergie électronique, photoémission, absorption optique
- les solides riches en bore
- les nanostructures semiconductrices

Spécialiste des carbures de bore et des matériaux riches en bore

IV. Formation

13 juillet 2009	Habilitation à diriger des recherches de l'Université P. et M. Curie
1994-1998	Thèse de doctorat de l'Université Pierre et Marie Curie (Paris VI)
	Science des matériaux (mention *félicitations du jury à l'unanimité*)
1987-1988	Diplôme d'études approfondies
	Université de Lille I, cité scientifique, Villeneuve d'Ascq, France
	Physique de l'état solide (mention *bien*)
1983-1988	Diplôme d'ingénieur ISEN, Institut Supérieur d'Electronique du Nord, Lille, France. Option physique de l'état solide.

V. Parcours professionnel

2008-	Echelon E5 du CEA (équivalent directrice de recherche CNRS)
2007-	Expert senior CEA
2000-	Chercheur à CEA-DSM-DRECAM-LSI
1991-2000	Chercheur à CEA-Direction des Applications Militaires Centre d'Etudes de Limeil-Valenton puis des Bruyères le Châtel Calculs *ab initio* de l'équation d'état de matériaux : dynamique moléculaire Car Parinello, structure électronique vibrations de réseau
1995-1997	Université de Marne La Vallée, Champs sur Marne Travaux dirigés de physique numérique (40 heures/an)

VI. Perspectives et collaborations

- Ces trois dernières années, j'ai développé une méthode *ab initio* pour calculer le temps de vie d'un électron excité dans la bande de conduction qui est limité par l'interaction avec les phonons de courte longueur d'onde. Quatre articles ont été écrits en collaboration avec avec J. Sjakste, postdoc, et V. Tyuterev, professeur à l'Université Pédagogique de Tomsk, Russie, visiteur au LSI.

Or, quand la taille des systèmes est réduite, à l'échelle nanométrique, le couplage électron-phonon devient très important pour le transport thermique. Je souhaite étendre la méthode aux phonons de grande longueur d'onde, importants pour le transport thermique, en collaboration avec nos collègues F. Mauri et M. Lazzeri, de l'Institut de Minéralogie et de Physique des Milieux Condensés, Université Paris VI P. et M. Curie, et Natalio Mingo, du CEA-LITEN, dans le cade du projet ANR-PNANO2008 ACCATTONE.

- Le travail sur les matériaux à base de bore a mené à une collaboration avec les expérimentateurs et les théoriciens de l'Université d'Osaka, Japon, pour rendre ces solides supraconducteur. Je vais recevoir le doctorant nippon H. Dekura au LSI cinq mois en 2008-2009. Le démarrage de la thèse de Iurii Timrov est prévu à la rentrée 2009, sous réserve de financement.

-Enfin, je suis internationalement reconnue comme une spécialiste des carbure de bore. Dans ce cadre, je bénéficie d'un contrat DGA pour comprendre la tenue mécanique de ces matériaux. Un grand progrès est en cours sur le rôle des lacunes dans la tenue mécanique de ce matériau, dont l'étude est actuellement menée avec E. Betranhandy.

VII. Coordination de projets scientifiques

Dans le projet **ANR** PNANO-2008 ACCATTONE (2009-2012),
-coordination du travail de l'équipe du LSI.

Dans le réseau d'excellence européen **NANOQUANTA** (2004-2007),
- **Participation** à l'écriture des rapports et aux revues de projet à Bruxelles
http://www.cmt.york.ac.uk/nanoquanta.

Suite coordination de projets scientifiques :

Dans le réseau d'excellence européen **NANOQUANTA**,

-**Participation** à la coordination de l'une des 4 équipes d'intégration scientifique *"Isolate a 0-dimensional structure (quantum dot ...) and conquer its environment"*.

-**Coordination** de l'équipe d'intégration (avec U. Von Barth et J. Sjakste) sur "society issues", in which "a comprehensive program has been formulated and implemented to deal with societal issues, including gender balance, ethical questions, scientific success and its measurement, family issues, contract questions, mentoring, and management training, all intended to help in particular the career development of young researchers".

VIII. Responsabilités scientifiques

Contrats

- Contrat **ANR** PNANO 2008 ACCATTONE, *"Ab initio Coupled Charge And Thermal TranspOrt in NanostructurEs"*. Financement postdoc 30 mois, 2009-2012 (E. Betranhandy).

- **Contrat DGA** sur *"l'étude théorique des carbures de bore"*.
Financement postdoc, 2008-2009 (E. Betranhandy) et 2007-2008 (J. Sjakste).

- **Contrat européen** du réseau d'excellence **Nanoquanta**
Financement d'un postdoc de trois ans, J. Sjakste, Dec. 2004-2007.

- **Postes d'accueil** de l'Ecole Polytechnique pour les visites de V. Tyuterev, pendant 18 mois répartis sur 2004-2009.

- **Contrat CEA-DEN**, dans le cadre du CPR ISMIR -Contrat Programme Recherche "**IS**olants, **M**odélisation de **I**rradiation" sur les "*excitationsélectroniques dans la zircone ZrO2*".
Financement d'un postdoc de 24 mois, 2002-2005 (Ph. Baranek, L. Dash).

- Chaque année, projet au conseil scientifique du calcul centralisé du CEA-DSM, projet p93.
"*Structure électronique et propriétés vibrationnelles des matériaux: calculs ab initio*".

- Depuis 2008, projet 2210 au Grand Equipement National de Calcul Intensif (GENCI)
"*Structure électronique et propriétés vibrationnelles des matériaux: calculs ab initio*".

Direction de thèse :

Etude théorique du couplage électron-phonon dans les matériaux : désexcitationi électronique, supraconductivité, I. Timrov, démarrage prévu à la rentrée 2009.

Suite responsabilités scientifiques :
Codirection de thèses :

- Accueil de H. Dekura, doctorant du Nanoscience and Nanotechnology Center, The Institute of Scientific and Industrial Research (ISIR), Osaka University, Japan, envoyé pour étudier la supraconductivité du bore et du bore dopé, (Nov 2008-Janvier 2009 et Juin-Juillet 2009).

Etude théorique des phases du titane, V. Trinité Quéquet, Ecole Polytechnique (2006).
http://www.imprimerie.polytechnique.fr/Theses/Files/Trinite.pdf

Exchange and correlation in the Electronic Structure of Solids, from Silicon to Cuprous oxide: GW approximation and beyond, F. Bruneval, Ecole Polytechnique (2005).

Semiempirical and ab initio calculations of optical properties in semiconductor superlattices, S. Botti, Università di Pavia, Italie (2002).

Publications :
32 papiers dans des journaux à referee(s), dont **8 articles** dans **Physical Review Letters** et **8 articles** dans **Physical Review B**.
21 articles depuis mon à arrivée à **CEA-DSM**.

Brevets : néant
Les programmes informatiques que je développe sont sous licence GNU.

Invitations :
Keynote lecture au Satellite Meeting du 15ème International Symposium on Intercalation Compounds, ISIC 15, à Beijing, Chine, 10-15 Mai 2009.

Papier invité à "16th International Symposium on Boron, Borides and Related Materials", à Matsue, Japon, 7-12 Septembre 2008.

Revue de projet à la Commission européenne sur la 3ème année du réseau d'excellence Nanoquanta, Aussois, 22 Septembre 2007, exposés délégués à J. Sjakste (LSI) et A. Castro (Berlin).

Rencontre annuelle du Groupement de Recherche "Micro et Nanothermique" Lyon, 6 Juin 2007, oral invité sur "*Excitation et relaxation électronique : études ab initio*".

Congrès annuel du groupement français pour les céramiques: Caen, France, 13-15 Mars 2007, oral invité sur "*Excitation et relaxation électronique : études ab initio*".

"*Marie Curie Training Course Molecular Simulations*", Tutorial "*Simulating matter at the nano-scale using density functional theory, pseudopotentials and plane waves*", CECAM Lyon, France, 13-17 Novembre 2006, invitation à donner deux cours.

Suite invitations :

Revue de projet à la Commission Européenne, 2ème année du réseau d'excellence Nanoquanta, Bruxelles, 23 Septembre 2006, un exposé scientifique de synthèse sur l'equipe d'intégration que j'ai co-coordonnée.

Workshop "Advances in the atomic-scale understanding of nano-structures", Lille, 26-27 Avril 2006, oral invité sur *Electronic excitations: ab initio calculations of electronic spectra*".

Revue de projet à la Commission européenne sur la 1ère année du réseau d'excellence Nanoquanta, Bruxelles, 30-31 Août 2005, un exposé scientifique de synthèse sur l'équipe d'intégration que je co-coordonne et un exposé sur la politique sociale au sein du réseau d'excellence.

ICCMSE 2004: "*International Conference of Computational Methods in Sciences and Engineering 2004*, Vouligmeni-Kavouri, Grèce, 19-23 Novembre 2004, Symposium sur "multiscale modeling of irradiation effects in solids and associated out-of-equilibrium processes", exposé invité sur la spectroscopie de perte d'énergie électronique.

Rencontre annuelle de Réseau de formation européen Research Training Network NANOAM, Paris, 5-7 Octobre 2004, exposé invité sur la spectroscopie de perte d'énergie électronique.

DIPC Workshop "*Modifications following different processes at surfaces*", San Sebastian, Espagne, Septembre 2003, exposé invité sur "*Anisotropy of the microscopic fluctuations of the polarization, confinement effects, and the dielectric function of crystals*".

ICTP-Psik workshop "*Ab-initio many-body theory for correlated electron systems*", Trieste, Italie, Août 2003,exposé invité sur "*Anisotropy of the microscopic fluctuations of the polarization, confinement effects, and the dielectric function of crystal*".

Project INTAS, Moscou, Octobre 2002, exposé invité sur "*Ab initio methods to calculate the electronic structure and the vibrational properties of solids*".

Séminaire invité à l'Ecole Centrale de Paris, Châtenay-Malabry, Juin 2002, sur les *Méthodes ab initio pour le calcul des propriétés spectroscopiques des matériaux*".

Congrès général de la Société Française de Physique, Strasbourg, Juillet 2001. Colloque "*Matériaux aux conditions extrmês*", exposé invité sur "*Etude ab initio des matériaux sous haute pression : transitions de phases de l'étain, spectre d'absorption infrarouge du bore alpha*".

Workshop "*Advances in first-principles computational condensed matter physics*", Miraflores de la Siera, Espagne, Janvier 2000, exposé invité sur "*The atomic structure and vibrational properties of icosahedral B_4C boron carbide*".

IX. Expertise scientifique

Rapporteur des journaux professionnels :

Nature Materials, Applied Physics Letters, Physical Review Letters, Physical Review B, European Physical Letters, European Physical Journal B, Journal of Physical Chemistry, International Journal of Nanotechnology, Computational Materials Science (Elsevier), Philosophical magazine, Chemical Physics Letters, Physica B, Superlattices and Microstructures, Physica Status Solidi Rapid Research , High Pressure Research (Taylor&Francis), Journal of physics : conference series.

Rapporteur des thèses de doctorat :

- M. Zemzemi "*Nano-indentation et Matière Ultra-Dure*" (Laboratoire Matériaux et Phénomènes Quantiques, Université Paris 7, 2006).

- S. Galamic-Mulaoerovic "*Electron-hole excitations and optical spectra of rare gas solids*", (Trinity college, Dublin, 2004).

Jurys de thèse et de master :

- Examinatrice dans le jury de thèse d'A. Nassour "*Etude vibrationnelle des alliages semiconducteurs II-VI et III-V*", (Université Paul Verlaine, Metz, 2008).

- Examinatrice dans le jury de thèse d'E. Gaudry "*Structure locale au-tour des impuretés dans les gemmes étudiée par spectroscopies et calculs ab initio*" (Université Paris VI, 2004).

- En 2007, membre du jury présidé par Prof. Michèle Gupta, du master INSNT "Matériaux pour les Structures et l'Energie" sur "*Réactivité de la surface de nickel vis-à-vis de son interaction avec l'ion uranyle : une approche théorique*", et sur "*Contribution à l'etude des propriétés de transport atomique dans les oxydes d'uranium par la modélisation ab initio*".

Co-organisation de conférences :

Juillet 2009: "*Thermoelectric transport: progress in first principles and, other approaches, and the interplay with experiment*", CECAM, Lausanne, Suisse.

Août 2008: Journées de la Matière Condensée JMC11, Strasbourg
Minicolloque "*Méthodes numériques pour le transport électronique et thermique dans les semiconducteurs*".

2002-2005: chaque année, conférence internationale NANOQUANTA en particulier en 2005 : "*40 years of the GW approximation for the electronic self-energy*"
http://www.fz-juelich.de/iff/GW2005

2004 : "*Progress in ab initio computational methods for condensed matter*", Janvier 2004, Gif-sur-Yvette (France).

Evaluation de projets :

Rapporteuse de l'US Army Research Office sur les matériaux riches en bore (2006).

Depuis 2003, évaluation des dossier de demandes au GENCI de temps de calcul sur les ordinateurs du CNRS (IDRIS) et/ou de l'Enseignement supérieur (CINES), pour le comité thématique Physique, Chimie et Propriétés des Matériaux (CT9).

X. Enseignement et formation professionnelle

European Union "*Marie Curie Training Course Molecular Simulations*", Tutorial "*Simulating matter at the nano-scale using density functional theory, pseudopotentials and plane waves*", CECAM Lyon, France, 13-27 Novembre 2006, invitation à donner deux cours (quatre heures).

En 1995-1997, Université de Marne La Vallée
Travaux dirigés de physique numérique (40 heures/an)

Stagiaires reçus au Laboratoire des Solides Irradiés :

- Neismon Fahé, "*Etude théorique du carbure de silicium*", stage de master de l'Université P. et M.Curie "Modélisation Statistique et Algorithmique des systèmes hors d'équilibre", Mars-Juillet 2007 (co-encadrement J. Sjakste et N. Vast).

- Xabier Zubizaretta, "*Etude de l'effet des états de semicoeur dans la structure de bandes et étude sous pression*", stage de master de l'Ecole Centrale "Matériaux et structures pour l'energie", Février-Juillet 2006 (co-encadrement J. Sjakste et N. Vast).

- Tiphaine TESSON, "*Etude et modélisation du métal de zirconium et de l'oxyde* ZrO_2", stage de maîtrise de l'Université Pierre et Marie Curie, Mai-Juin 2004 (co-encadrement L. Dash et N. Vast).

- José TORRES, "*Etude théorique de l'oxyde de titane* Ti_2O_3", stage de Maîtrise de physique fondamentale de l'Univ. Paris Sud, Mai-Juin 2004.

- Virginie Quéquet, "*Développements théoriques pour l'oxyde de titane* TiO_2", stage du DEA Sciences des Matériaux (Paris 6) et stage d'ingénieur de l'Ecole Centrale Paris, Mai-Septembre 2003.

- Rémi Braive, "*Etude théorique de l'oxyde de titane* Ti_2O_3", licence du magistère de Physique fondamental d'Orsay, 1er mai-15 Juillet 2003.

- Fabien Bruneval, "*Etude ab initio de la limite classique du tenseur diélectrique dans les hétérostructures GaAs/AlAs*", stage du DEA Sciences des Matériaux (Paris 6) et stage d'ingénieur de l'Ecole Centrale Paris, Mai-Septembre 2002.

XI. Divers

Langues
Anglais, allemand, italien, apprentissage du japonais depuis Sept. 2007

Membre
- de l'American Physical Society depuis 2008,
- de la Société Française de Physique depuis 1997,
- (élue) du conseil du Laboratoire des Solides Irradiés,
- de l'association "Femmes et Sciences" fondée par Claudine Hermann, première professeure de physique à l'Ecole Polytechnique, pour lutter contre les préjugés sur les carrières scientifiques au féminin.

Compétences techniques
Programmation et calcul sur des Centres de calculs nationaux IDRIS et CEA, utilisant des ressources de calcul vectorielles (NEC) et/ou parallèles (cluster de processeurs Opteron); poste de travail sous UNIX.

Appendix D

Liste de publications de N. Vast (Fr)

Entre crochets est indiqué le nombre de citations du papier dans ISI web of science, au 8 Avril 2009.
Indice H: 12.
13 papiers sont cités 12 fois et plus, 12 papiers le sont 14 fois et plus
En couleur verte: nombre de citation au 25 Nov. 2007. L'indice était H = 9.

D.1 Papiers résultant de mes travaux de recherche au Laboratoire des Solides Irradiés

34) E. Betranhandy, N. Vast, and J. Sjakste (2009). Boron carbide at high pressure. En préparation.

33) N. Vast (2008). Etude *ab initio* des propriétés physiques des matériaux. Document d'habilitation à diriger des recherches (2009).

32) N. Vast, J. Sjakste, and E. Betranhandy. Boron carbides from first principles. *Journal of Physics: Conference proceedings*, 2009. Article de revue avec 3 rapporteurs. Sous presse.

31) J. Sjakste, N. Vast, and E. Betranhandy (2009). Thermal and vibrational properties of boron carbide at 20% carbon concentration: an *ab initio* study. En préparation.

30) [0] J. Sjakste, N. Vast, and V. Tyuterev. *Ab initio* study of electron-phonon coupling and excitonic linewidth in GaAs under pressure and GaP. *Journal of Luminescence*, 128:1004, 2008. URL http://dx.doi.org/10.1016/j.jlumin.2007.10.037

29) [1] J. Sjakste, N. Vast, and V. Tyuterev. *Ab initio* method for the electron-phonon scattering times in semiconductors: application to

GaAs and GaP. *Physical Review Letters*, 99:236405, 2007. Selected by the American Physical Society for the January 2008 issue of Virtual Journal of Ultrafast Science. http://www.vjultrafast.org. URL http://link.aps.org/doi/10.1103/PhysRevLett.99.236405

28) [0] Virginie Trinité, Nathalie Vast, and Marc Hayoun. Effect of the localization of the semicore density on the physical properties of transition metals. *J. Phys. Cond. Matter*, 20:235239, 2008. URL http://dx.doi.org/10.1088/0953-8984/20/23/235239

27) J. Sjakste, V. Tyuterev, and N. Vast. In *Proceedings of Ninth Conference Gallium Arsenide and III-V Group Related Compounds GaAs (3-5 October, 2006, Tomsk, Russia)*, volume I.V., pages 74–77. Ed. Ivonin, 2006.

26) [9] Fabien Bruneval, Nathalie Vast, Lucia Reining, M. Izquierdo, F. Sirotti, and N. Barrett. Exchange and correlation effects in electronic excitation of Cu_2O. *Phys. Rev. Lett.*, 97:267601, 2006. URL http://link.aps.org/doi/10.1103/PhysRevLett.97.267601

25) [5] J. Sjakste, V. Tyuterev, and N. Vast. Intervalley scattering in GaAs: *ab initio* calculation of the effective parameters for Monte Carlo simulations. *Applied Physics A*, 86:301, 2007. URL http://dx.doi.org/10.1007/s00339-006-3786-7

24) [3] J. Sjakste, V. Tyuterev, and N. Vast. *Ab initio* study of $\Gamma - X$ intervalley scattering in GaAs under pressure. *Phys. Rev. B*, 74:235216, 2006. URL http://link.aps.org/doi/10.1103/PhysRevB.74.235216

23) [15] Fabien Bruneval, Nathalie Vast, and Lucia Reining. Effect of self-consistency on quasiparticles in solids. *Phys. Rev. B*, 74:045102, 2006. URL http://link.aps.org/doi/10.1103/PhysRevB.74.045102

22) [3] L.K. Dash, Fabien Bruneval, Virginie Trinité, Nathalie Vast, and Lucia Reining. Electronic excitations: *ab initio* calculations of electronic spectra and application to zirconia ZrO_2, titania TiO_2 and cuprous oxide Cu_2O. *Comp. Mat. Sci.*, 38:482, 2006. URL http://dx.doi.org/10.1016/j.commatsci.2005.09.010

21) [1] V.G. Tyuterev and N. Vast. Murnaghan's equation of state for the electronic ground state energy. *Comp. Mat. Sci.*, 38:350, 2006. URL http://dx.doi.org/10.1016/j.commatsci.2005.08.01

20) [16] F. Sottile, F. Bruneval, A.G Marinopoulos, L. Dash, S. Botti, V. Olevano, N. Vast, A. Rubio, and L. Reining. TDDFT from molecules to solids: the role of long-range interactions. *Int. J. Quant. Chem.*, 102:684, 2005. URL http://dx.doi.org/10.1002/qua.20486

19) [15] L.K. Dash, Nathalie Vast, Philippe Baranek, Marie-Claude Cheynet, and Lucia Reining. Electronic structure and electron energy-loss spectroscopy of ZrO_2 zirconia. *Physical Review B*, 70:245116, 2004.
URL http://link.aps.org/doi/10.1103/PhysRevB.70.245116

18) [7] S. Botti, N. Vast, L. Reining, V. Olevano, and L. C. Andreani. *Ab initio* and semi-empirical dielectric response of superlattices. *Phys. Rev. B*, 70:045301, 2004.
URL http://link.aps.org/doi/10.1103/PhysRevB.70.045301

17) [15] Matteo Calandra, Nathalie Vast, and Francesco Mauri. Superconductivity from doping boron icosahedra. *Phys. Rev. B*, 69:224505, 2004.
URL http://link.aps.org/doi/10.1103/PhysRevB.69.224505

16) [24] Silvana Botti, Francesco Sottile, Nathalie Vast, Valerio Olevano, Lucia Reining, Hans-Christian Weissker, Angel Rubio, Giovanni Onida, Rodolfo Del Sole, and R. W. Godby. Long-range contribution to the exchange-correlation kernel of time-dependent density functional theory. *Phys. Rev. B*, 69:155112, 2004.
URL http://link.aps.org/doi/10.1103/PhysRevB.69.155112

15) [71] A.G. Marinopoulos, L. Reining, A. Rubio, and N. Vast. Optical and loss spectra of carbon nanotubes: depolarization effects and intertube interactions. *Phys. Rev. Lett.*, 91:046402, 2003.
URL http://link.aps.org/doi/10.1103/PhysRevLett.91.046402

14) [14] S. Botti, N. Vast, L. Reining, V. Olevano, and L. C. Andreani. *Ab initio* calculation of the dielectric tensor of GaAs/AlAs superlattices. *Phys. Rev. Lett.*, 89:216803, 2002.
URL http://link.aps.org/doi/10.1103/PhsRevLett.89.216803

13) [24-26] N. Vast, L. Reining, V. Olevano, P. Schattschneider, and B. Jouffrey. Local field effects and the anisotropy of the electron energy loss spectrum of titanium dioxide TiO_2. *Phys. Rev. Lett.*, 88:37601, 2002.
URL http://link.aps.org/doi/10.1103/PhysRevLett.88.037601

12) [22] F. Mauri, N. Vast, and C. J. Pickard. Atomic structure of icosahedral B_4C boron carbide from a *first-principles* analysis of NMR spectra. *Phys. Rev. Lett.*, 87:085506, 2001.
URL http://link.aps.org/doi/10.1103/PhysRevLett.87.085506

D.2 Papiers résultant de mes travaux de recherche au CEA-DAM

11) [8-9] N. Vast and S. Baroni. Effects of isotopic disorder on the Raman spectrum of crystals : theory and *ab initio* calculation on diamond and germanium. *Phys. Rev. B*, 61:9387, 2000.
URL http://link.aps.org/doi/10.1103/PhysRevB.61.9387

10) [6] N. Vast and S. Baroni. Effects of isotopic disorder on the Raman spectrum of crystals : theory and *ab initio* calculation on diamond and germanium. *Comp. Mat. Sci.*, 17:395, 2000.
URL http://dx.doi.org/10.1016/S0927-0256(00)00059-8

9) [76] R. Lazzari, N. Vast, J.M. Besson, S. Baroni, and Andrea Dal Corso. Structural and vibrational properties of icosahedral B_4C boron carbide. *Phys. Rev. Lett.*, 83:3230, 1999.
Ibid, [3] R. Lazzari, N. Vast, J.M. Besson, S. Baroni, and Andrea Dal Corso. Erratum: structural and vibrational properties of icosahedral B_4 boron carbide. *Phys. Rev. Lett.*, 85:4194, 2000.
URL http://link.aps.org/doi/10.1103/PhysRevLett.85.4194
URL http://link.aps.org/doi/10.1103/PhysRevLett.83.3230

8) [17] N.Vast, J.M. Besson, S.Baroni, and A. Dal Corso. Atomic structure and vibrational properties of icosahedral α-boron and B_4C boron carbide. *Comp. Mat. Sci.*, 17:127, 2000.
URL http://dx.doi.org/10.1016/S0927-0256(00)00009-4

7) [2] Nathalie Vast. Propriétés vibrationnelles du bore α et du carbure de bore B_4C. *Thèse de doctorat. Université Paris VI, France et rapport CEA-R-5842*, 1999.
URL http://tel.archives-ouvertes.fr/tel-00297278/fr/

6) [44] N. Vast, S. Baroni, G. Zérah, J. M. Besson, A. Polian, M. Grimsditch, and J. C. Chervin. Lattice dynamics of icosahedral α-boron under pressure. *Phys. Rev. Lett.*, 78:693, 1997. URL http://link.aps.org/doi/10.1103/PhysRevLett.78.693
Confirmation expérimentale : M. Fujimori, T. Nakata, T. Nakayama, E. Nishibori, K. Kimura, M. Takata, and M. Sakata, Peculiar covalent bonds in α rhombohedral boron. *Phys. Rev. Lett.*, 82:4452, 1999.
URL http://link.aps.org/doi/10.1103/PhysRevLett.82.4452

5) [6] N. Vast, S. Baroni, G. Zérah, J. M. Besson, A. Polian, J.C. Chervin, and M. Grimsditch. Lattice-dynamics of α-boron from *ab initio* calculation and Raman scattering under high pressure. *Phys. Stat. Sol. (b)*, 198:115, 1996.
URL http://dx.doi.org/10.1002/pssb.2221980116

4) [N'apparaît plus dans ISI 6] T. Charpentier, G. Zérah, and N. Vast. Pseudopotentials including semicore states with an application to barium, α-cerium and thorium. *Phys. Rev. B*, 54:1427, 1996.
URL http://link.aps.org/doi/10.1103/PhysRevB.54.1427

3) [12] N. Vast, S. Bernard, and G. Zérah. Structural and electronic properties of liquid boron from a molecular-dynamics simulation. *Phys. Rev. B II*, 52:4123, 1995.
URL http://link.aps.org/doi/10.1103/PhysRevB.52.4123
Confirmation expérimentale : S. Krishnan, S. Ansell, J.J. Felten, K.J. Volin, and D.L. Price. Structure of liquid boron. *Phys. Rev. Lett.*, 81:586, 1998.
URL http://link.aps.org/doi/10.1103/PhysRevLett.81.586

2) [2] B. Siberchicot, N. Vast, and S. Matar. Band-structure calculation of the magnetocrystalline anisotropy energy Fe_3N. *International Journal of Modern Physics B*, 7:741, 1993.
URL http://dx.doi.org/10.1142/S0217979293001566

1) [2-3] N. Vast, B. Siberchicot, and G. Zérah. First-principles calculations of the magnetocrystalline anisotropy energy of the pnictide MnSb. *J. Phys. Condens. Matter*, 4:741, 1992.
URL http://dx.doi.org/10.1088/0953-8984/4/50/035

Appendix E

General bibliography

E.1

[1] W. Kohn. *Nobel Lectures, Chemistry 1996-2000.* World Scientific Publishing Co., Singapore, 2003.

[2] R. O. Jones and O. Gunnarsson. The density functional formalism, its applications and prospects. *Reviews of Modern Physics*, 61:689, 1989.

[3] P. Giannozzi, S. de Gironcoli, P. Pavone, and S. Baroni. *Ab initio* calculation of phonon dispersions in semiconductors. *Phys. Rev. B*, 43:7231, 1991.

[4] F. Mauri, O. Zakharov, S. de Gironcoli, S.G. Louie, and M.L. Cohen. Phonon softening and superconductivity in tellurium under pressure. *Phys. Rev. Lett.*, 77:1151, 1996.

[5] J. Sjakste, N. Vast, and V. Tyuterev. *Ab initio* method for the electron-phonon scattering times in semiconductors: application to GaAs and GaP. *Phys. Rev. Lett.*, 99:236405, 2007.

[6] Matteo Calandra, Nathalie Vast, and Francesco Mauri. Superconductivity from doping boron icosahedra. *Phys. Rev. B*, 69:224505, 2004.

[7] E. Runge and E.K.U. Gross. Density-functional theory for time-dependent systems. *Phys. Rev. Lett.*, 52:997, 1984.

[8] E. K. U. Gross and W. Kohn. Local density-functional theory of frequency-dependent linear response. *Phys. Rev. Lett.*, 55:2850, 1985.

[9] Silvana Botti, Francesco Sottile, Nathalie Vast, Valerio Olevano, Lucia Reining, Hans-Christian Weissker, Angel Rubio, Giovanni Onida, Rodolfo Del Sole, and R. W. Godby. Long-range contribution to the exchange-correlation kernel of time-dependent density functional theory. *Phys. Rev. B*, 69:155112, 2004.

[10] G. Onida, L. Reining, and A. Rubio. Electronic excitations: Density functional versus many body green's functions approaches. *Rev. Mod. Phys.*, 74:601, 2002.

[11] R. W. Godby, M. Schlüter, and L. J. Sham. Self-energy operators and exchange-correlation potentials in semiconductors. *Phys. Rev. B*, 37:10159, 1988.

[12] M. Lannoo, M. Schlüter, and L. J. Sham. Calculation of the kohn-sham potential and its discontinuity for a model-semiconductor. *Phys. Rev. B*, 32:3890, 1985.

[13] L. Hedin and B.I. Lundqvist. Solid state physics. volume 23, page 1. Academic Press, New York, 1969.

[14] L. Hedin. *Phys. Rev.*, 139:A796, 1965.

[15] S. Albretch, L. Reining, R. Del Sole, and G. Onida. *Phys. Rev. Lett.*, 80:4510, 1998.

[16] L. Benedict, E. Shirley, and R.B. Bohn. Theory of optical absorption in diamond, Si, Ge, and GaAs. *Phys. Rev. B*, 57:R9385, 1998.

[17] L. Benedict, E. Shirley, and R.B. Bohn. Optical absorption of insulators and the electron-hole interaction: An ab initio calculation. *Physical Review Letters*, 80:4514, 1998.

[18] M. Rohlfing and S. Louie. Electron-hole excitations in semiconductors and insulators. *Phys. Rev. Lett.*, 82:1959, 1998.

[19] N. Vast, L. Reining, V. Olevano, P. Schattschneider, and B. Jouffrey. Local field effects and the anisotropy of the electron energy loss spectrum of titanium dioxide TiO_2. *Phys. Rev. Lett.*, 88:37601, 2002.

[20] A.G. Marinopoulos, L. Reining, A. Rubio, and N. Vast. Optical and loss spectra of carbon nanotubes: depolarization effects and intertube interactions. *Phys. Rev. Lett.*, 91:046402, 2003.

[21] S. Botti, N. Vast, L. Reining, V. Olevano, and L. C. Andreani. *Ab initio* calculation of the dielectric tensor of GaAs/AlAs superlattices. *Phys. Rev. Lett.*, 89:216803, 2002.

[22] S. Botti. *Semiempirical and* ab initio *calculations of optical properties in semiconductor superlattices.* PhD thesis, Università di Pavia, Italie, 2002.

[23] S. Botti, N. Vast, L. Reining, V. Olevano, and L. C. Andreani. *Ab initio* and semi-empirical dielectric response of superlattices. *Phys. Rev. B*, 70:045301, 2004.

[24] L.K. Dash, Nathalie Vast, Philippe Baranek, Marie-Claude Cheynet, and Lucia Reining. Electronic structure and electron energy-loss spectroscopy of ZrO_2 zirconia. *Physical Review B*, 70:245116, 2004.

[25] F. Sottile, F. Bruneval, A.G Marinopoulos, L. Dash, S. Botti, V. Olevano, N. Vast, A. Rubio, and L. Reining. TDDFT from molecules to solids: the role of long-range interactions. *Int. J. Quant. Chem.*, 102:684, 2005.

[26] L.K. Dash, Fabien Bruneval, Virginie Trinité, Nathalie Vast, and Lucia Reining. Electronic excitations: *ab initio* calculations of electronic spectra and application to zirconia ZrO_2, titania TiO_2 and cuprous oxide Cu_2O. *Comp. Mat. Sci.*, 38:482, 2006.

[27] S. Faleev, M. van Schilfgaarde, and T. Kotani. All-electron self-consistent GW approximation: Application to Si, MnO, and NiO. *Phys. Rev. Lett.*, 93:126406, 2004.

[28] F. Bruneval. *Echange et Corrélation dans la Structure Electronique des Solides, du Silicium à l'Oxyde Cuivreux: Approximation GW et au-delà.* PhD thesis, Ecole Polytechnique, Palaiseau, France, 2005.

[29] Fabien Bruneval, Nathalie Vast, Lucia Reining, M. Izquierdo, F. Sirotti, and N. Barrett. Exchange and correlation effects in electronic excitation of Cu_2O. *Phys. Rev. Lett.*, 97:267601, 2006. and refererences herein.

[30] Fabien Bruneval, Nathalie Vast, and Lucia Reining. Effect of self-consistency on quasiparticles in solids. *Phys. Rev. B*, 74:045102, 2006.

[31] J. Sjakste, V. Tyuterev, and N. Vast. Intervalley scattering in GaAs: *ab initio* calculation of the effective parameters for Monte Carlo simulations. *Applied Physics A*, 86:301, 2007.

[32] J. Sjakste, V. Tyuterev, and N. Vast. emphAb initio study of $\Gamma - X$ intervalley scattering in GaAs under pressure. *Phys. Rev. B*, 74:235216, 2006.

[33] N. Vast. *Propriétés vibrationnelles du bore α et du carbure de bore B_4C.* PhD thesis, Université Paris VI, France, 1998.

[34] Nathalie Vast. Propriétés vibrationnelles du bore α et du carbure de bore B_4C. *Thèse de doctorat. Université Paris VI, France et rapport CEA-R-5842*, 1999.

[35] R.B. Kaner, J.J. Gilman, and S.H. Tolbert. Designing superhard materials. *Sciences*, 308:1268, 2005.

[36] N. Vast, S. Baroni, G. Zérah, J. M. Besson, A. Polian, J.C. Chervin, and M. Grimsditch. Lattice-dynamics of α-boron from *ab initio* calculation and Raman scattering under high pressure. *Phys. Stat. Sol. (b)*, 198:115, 1996.

[37] N. Vast, S. Baroni, G. Zérah, J. M. Besson, A. Polian, M. Grimsditch, and J. C. Chervin. Lattice dynamics of icosahedral α-boron under pressure. *Phys. Rev. Lett.*, 78:693, 1997.

[38] R. Lazzari, N. Vast, J.M. Besson, S. Baroni, and Andrea Dal Corso. Structural and vibrational properties of icosahedral B_4C boron carbide. *Phys. Rev. Lett.*, 83:3230, 1999.

[39] R. Lazzari, N. Vast, J.M. Besson, S. Baroni, and Andrea Dal Corso. Erratum: structural and vibrational properties of icosahedral B_4 boron carbide. *Phys. Rev. Lett.*, 85:4194, 2000.

[40] N.Vast, J.M. Besson, S.Baroni, and A. Dal Corso. Atomic structure and vibrational properties of icosahedral α-boron and B_4C boron carbide. *Comp. Mat. Sci.*, 17:127, 2000.

[41] G. Fanchini, J.W. McCauley, and M. Chhowalla. *Phys. Rev. Lett*, 97:035502, 2006. Les résultats de ce papier sont erronés. La forme du carbure de bore B_{12}-C-C-C est quasi inexistante selon nos calculs.

[42] F. Mauri, N. Vast, and C. J. Pickard. Atomic structure of icosahedral B_4C boron carbide from a *first-principles* analysis of NMR spectra. *Phys. Rev. Lett.*, 87:085506, 2001.

[43] M. I. Eremets, V. V. Struzhkin, H. Mao, and R. J. Hemley. *Science*, 293:272, 2001.

[44] A. R. Oganov, J. Chen, d Y. Ma C. Gatti a, C. W. Glass, Z. Liu, T. Yu, O. O. Kurakevych, and V. L. Solozhenko. *Nature*, 457:863, 2009.

[45] J.E. Saal, S. Shang, and Z.-K. Liu. The structural evolution of boron carbide via *ab initio* calculations. *Appl. Phys. Lett.*, 91:231915, 2007.

[46] A. Masago, K. Shirai, and H. Katayama-Yoshida. *Phys. Rev. B*, 73:104102, 2006.

[47] N. G. Szwacki, A. Sadrzadeh, and B. I. Yakobson. *Phys. Rev. Lett.*, 98:166804, 2007.

[48] N. Vast, J. Sjakste, and E. Betranhandy. Boron carbides from first principles. *J. Phys.: Conf. Ser.*, 176:012002, 2009.

[49] T.J. Vogler, W.D. Reinhart, and L.C. Chhabildas. Dynamic behavior of boron carbide. *J. Appl. Phys.*, 95:4173, 2004.

[50] M. Chen, J.W. McCauley, and K.J. Hemker. Shock-induced localized amorphization in boron carbide. *Science*, 299:1563, 2003.

[51] D. Ghosh, G. Subhash, C.H. Lee, and Y.K. Yap. Strain-induced formation of carbon and boron clusters in boron icarbide during dynamic indentation. *Applied Physics Letters*, 91:061910, 2007.

[52] X.Q. Yan, Z. Tangi, L. Zhang, J.J. Guo, C.Q. Jin, Y. Zhang, T. Goto, J.M. McCaulay, and M.W. Chen. Depressurization amorphization of single-crystal boron carbide. *Phys. Rev. Lett.*, 102:075505, 2009.

[53] X.Q. Yan, W.J. Li, and M.W. Chen. Raman spectroscopy of pressure-induced amorphous boron carbide. *Appl. Phys. Lett.*, 88:131905, 2006.

[54] V. Trinité. *Etude théorique des phases du titane.* PhD thesis, Ecole Polytechnique, Palaiseau, France, 2006.

[55] H. Dekura, K. Shirai, and H. Katayama-Yoshidai. Valence control of α-rhombohedral boron by electronic doping. *J. Phys. Cond. Matter*, 19:365, 2007.

[56] P. Umari, G. Stenuit, and S. Baronu. Bridging the size gap between density-functional and many-body perturbation theory. cond-mat/0811.1453.

[57] D.R. Hamann and D. Vanderbilt. *Phys. Rev. B*, 79:045109, 2009.

[58] B. Walker, A. M. Saitta, R. Gebauer, and S. Baroni. Efficient approach to time-dependent density-functional perturbation theory for optical spectroscopy. *Phys. Rev. Lett.*, 96:11300, 2006.

[59] K. Burke, R. Car, and R. Gebauer. Density functional theory of the electrical conductivity of molecular devices. *Phys. Rev. Lett.*, 97:146803, 2005.

[60] N. Wiser. *Phys. Rev.*, 129:62, 1963.

[61] H. Ehrenreich and M.H. Cohen. *Phys. Rev.*, 115:786, 1959.

[62] S.L. Adler. *Physical Review*, 126:413, 1962.

[63] P. Hohenberg and W. Kohn. *Phys. Rev.*, 136:B864, 1964.

[64] W. Kohn and L.J. Sham. *Phys. Rev.*, 140:A1133, 1965.

[65] W.E. Pickett. Pseudopotential methods in condensed matter applications. *Comp. Phys. Rep.*, 9:115, 1989.

[66] L. Landau and E. Lifchitz. *Mécanique Quantique.* Editions Mir, Moscou, 3rd edition, 1975.

[67] J.D. Jackson. *Classical electrodynamics.* John Wiley and Sons Inc, New York, 2nd edition edition, 1999.

[68] J. P. Perdew and Y. Wang. *Phys. Rev. B*, 45:13244, 1992.

[69] G.F. Giuliani and G. Vignale. *Quantum Theory of the Electron Liquid.* Cambridge University Press, Cambridge, 2005.

[70] E. N. Economou. *Green's functions in quantum physics.* Solid-state sciences. Springer Verlag, Berlin, 1979.

[71] J. Fink. In J.C. Fuggle and J.E. Inglesfield, editors, *Unoccupied electronic states*, page 204. Springer-Verlag, Berlin, 1992.

[72] W. Macke. *Z. Naturf.*, 5a:192, 1950.

[73] J. Hubbard. The dielectric theory of electronic interaction in solids. *Proc. Phys. Soc.*, 68:976, 1955.

[74] M. S. Hybertsen abd S. G. Louie. *Phy. Rev. B*, 35:5585, 1987.

[75] A. Georges, G. Kotliar, W. Krauth, and M. J. Rozenberg. *Rev. Mod. Phys.*, 73:515, 2001.

[76] J.T. Houghton and S.D. Smith, editors. *Infra-red physics.* Clarendon Press, Oxford, 1966.

[77] J. Schwitalla and H. Ebert. *Phys. Rev. Lett.*, 80:4586, 1998.

[78] C. Colliex and P. Trebbia. *Physica Fennica*, 9:S1, 80, 1975.

[79] S. Albrecht. *Optical Absorption spectra of semiconductors and insulators:* ab initio *calculations of many-body effects.* PhD thesis, Ecole Polytechnique, France, 1999.

[80] R.F. Egerton, editor. *Electron energy-loss spectroscopy in the microscope.* Plenum Press, New York, 1986.

[81] V. Olevano and L. Reining. *Phys. Rev. Lett.*, 86:5962, 2001.

[82] S. Ostanin, A.J. Craven, D.W. McComb, D. Vlachos, A. Alavi, A.T. Paxton, and M.W. Finnis. *Phys. Rev. B*, 65:224109, 2002.

[83] I.M. Ross, W.M. Rainforth, A.J. Scott, A.P. Brown, R. Brydson, and D.W. McComb. *Inst. Phys. Conf. Ser.*, 168:303, 2001.

[84] R.H. French, S.J. Glass, F.S. Ohuchi, Y.N. Xu, and W.Y. Ching. *Phys. Rev. B*, 49:5133, 1994.

[85] C. D. Spataru, S. Ismail-Beigi, L. X. Benedict, and S. G. Louie. *Phys. Rev. Lett.*, 92:077402, 2004.

[86] B. Kralik, E.K. Chang, and S.G. Louie. *Phys. Rev. B*, 57:7027, 1998.

[87] S. Brahms, S. Nikitine, and J.P. Dahl. On the band structure and the absorption spectrum of Cu_2O. *Physics Letters*, 22:31, 1966.

[88] S. Baroni (2009). Private communication.

[89] L. Reining, V. Olevano, A. Rubio, and G. Onida. *Phys. Rev. Lett.*, 88:066404, 2002.

[90] S. Baroni, S. de Gironcoli, A. Dal Corso, and P. Giannozzi. Phonons and related crystal properties from density-functional perturbation theory. *Rev. Mod. Phys.*, 73:515, 2001.

[91] F. Mauri and S.G. Louie. *Phys. Rev. Lett.*, 76:4246, 1996.

[92] J.R. Cheeseman, G.W. Trucks, T.A. Keith, and M.J. Frisch. *J. Chem. Phys.*, 104:14, 1996.

[93] C.J. Pickard and F. Mauri. *Phys. Rev. B*, 63:245101, 2001.

[94] J. P. Perdew, J.A. Chevary, S.H. Vosko, K.A. Jackson, M.R. Pederson, D.J. Singh, and C. Fiolhais. *Phys. Rev. B*, 46:6671, 1992. PW91 functional.

[95] J. P. Perdew, J.A. Chevary, S.H. Vosko, K.A. Jackson Pederson, D.J. Singh, and C. Fiolhais. *Phys. Rev. B*, 48:4978, 1993. PW91 functional.

[96] M. Gatti, F. Bruneval, V. Olevano, and L. Reining. Understanding correlations in vanadium dioxide from first principles. *Phys. Rev. Lett.*, 99:266402, 2007.

[97] S. Biermann, A. Poteryaev, A.I. Lichenstein, and A. Georges. Dynamical singlets and correlation-assisted peierls transition in vo2. *Phys. Rev. Lett.*, 94:026404, 2005.

[98] D. W. Bullett. Structure and bonding in crystalline boron and b12c33. *Journal of Physics C: Solid State Physics*, 15(3):415–426, 1982.

[99] E. D. Jemmis, D. Eluvathingal, M. M. Balakrishnarajan, and P. D. Pancharatna. A unifying electron-counting rule for macropolyhedral boranes, metallaboranes, and metallocenes. *Journal of the American Chemical Society*, 123(18):4313–4323, 2001.

[100] E. D. Jemmis, D. Eluvathingal, and M. M. Balakrishnarajan. Polyhedral boranes and elemental boron: direct structural relations and diverse electronic requirements. *Journal of the American Chemical Society*, 123(18):4324–4330, 2001.

[101] D. Emin. *Phys. Today*, 320(1):55, 1987.

[102] R. J. Nelmes, J. S. Loveday, R. M. Wilson, W. G. Marshall, J. M. Besson, S. Klotz, G. Hamel, T. L. Aselage, and S. Hull. *Phys. Rev. Lett*, 74:2268, 1995.

[103] B. Morosin, G.H. Kwei, A.C. Lawson, T.L. Aselage, and D. Emin. *Journal of Alloys and Compounds*, 226:121, 1995.

[104] G.H. Kwei and B. Morosin. *J. Phys. Chem.*, 100:8031, 1996.

[105] B. Morosin, T.L. Aselage, and R.S. Feigelson. *Mater. Res. Symp. Proc.*, 97:145, 1987.

[106] A.C. Larson. *Boron Rich Solids Conf. Proc.*, volume 140. AIP, New York, 1986.

[107] B. Morosin, T.L. Aselage, and D. Emin. *Boron Rich Solids Conf. Proc.*, volume 231. AIP, New York, 1991.

[108] F.A. Fernandez-Lima, C. Ribeiro Ponciano, E. Frota da Silveira, and M.A. Chaer Nascimento. *Chemical Physics Letters*, 445:147, 2007.

[109] A. Marini, P. García-Gonzáles, and A. Rubio. *Phys. Rev. Lett.*, 96:136404, 2006.

[110] M. Lazzeri, A. Vittadini, and A. Selloni. *Phys. Rev. B*, 63:155409, 2001.

[111] A. Janotti, S.-H. Wei, and D.J. Singh. *First-principles* study of the stability of BN and C. *Phys. Rev. B*, 64:174107, 2001.

[112] M.T. Yin and M.L. Cohen. *Phys. Rev. B*, 29:6996, 1984.

[113] H. Rydberg, M. Dion, N. Jacobson, E. Schröder, P. Hyldgaard, S.I. Simak, D.C. Langreth, and B.I. Lundqvist. Vand der waals density functional for layered structures. *Phys. Rev. Lett.*, 91:126402, 2003.

[114] M. Fuchs and X. Gonze. Accurate density functionals: Approaches using the adiabatic-connection fluctuation-dissipation theorem. *Phys. Rev. B: Condens. Matter Mater. Phys.*, 65(23):235109, Jun 2002.

[115] F. Furche and T. Van Voorhis. Fluctuation-dissipation theorem density-functional theory. *The Journal of Chemical Physics*, 122(16):164106, 2005.

[116] P. García-Gonzáles, J. J. Fernandez, A. Marini, and A. Rubio. Advanced correlation functionals: application to bulk materials and localized systems. *The Journal of Physical Chemistry A*, 111(49):12458–12465, 2007.

[117] Judith Harl and Georg Kresse. Cohesive energy curves for noble gas solids calculated by adiabatic connection fluctuation-dissipation theory. *Phys. Rev. B: Condens. Matter Mater. Phys.*, 77(4):045136, 2008.

[118] H. Dekura and K. Shirai. (2008) Private communication.

[119] M. Widom and M. Mihalkovič. Symmetry-broken crystal structure of elemental boron at low temperature. *Phys. Rev. B*, 77:064113, 2008.

[120] M. Widom and M. Mihalkovič. this proceedings http://euler.phys.cmu.edu/widom/pubs/PDF/vib.pdf.

[121] Shunli Shang, Yi Wang, Raymundo Arroyave, and Zi-Kui Liu. Phase stability in α- and β-rhombohedral boron. *Phys Rev B: Condens Matter Mater Phys*, 75(9):092101, 2007.

[122] M.J. van Setten, M.A. Uijttewaaland G.A. de Wijs, and A. Robert. Thermodynamic stability of boron: the role of defects and zero point motion. *J. Am. Chem. Soc.*, 129(9):2458–2465, 2007.

[123] T. Ogitsu, F. Gygi, J. Reed, Y. Motome, E. Schwegler, and G. Galli. Imperfect crystal and unusuak semiconductor: Boron, a frustated element. *Journal of the American Chemical Society*, 131:1903, 2009.

[124] U. Kuhlmann, H. Werheit, and K.A. Schwetz. *Journal of Alloys and Compounds*, 189:249, 1992.

[125] D. R. Tallant, T. L. Aselage, A.N. Campbell, and D. Emin. *Phys. Rev. B*, 40:5649, 1989.

[126] U. Kuhlmann and H. Werheit. *Phys. Stat. Sol.*, 175:85, 1993.

[127] H. Werheit, R. Schmechel, U. Kuhlmann, T.U. Kampen, W. Mönch, and A. Rau. On the reliability of the raman spectra of boron-rich solids. *Journal of Alloys and Compounds*, 291:28, 1999.

[128] R.J. Kirkpatrick, T. Aselage, B.L. Phillips, and B. Montez. *Boron Rich Solids Conf. Proc.*, volume 231. AIP, New York, 1991.

[129] T.M. Duncan. *J. Am. Ceram. Soc.*, 106:2270, 1984.

[130] T. Harazono, Y. Hiroyama, and T. Watanabe. *Bull. Chem. Soc. Jpn*, 69:2419, 1996.

[131] D. Simeone, C. Mallet, P. Dubuisson, G. Baldinozzi, C. Gervais, and J. Maquet. *J. Nucl. Mater.*, 277:1, 2000.

[132] D.M. Bylander and L. Kleinman. Struture of $B_{13}C_2$. *Phys. Rev. B*, 43:1487, 1991.

[133] N. Troullier and J. L. Martins. *Phys. Rev. B*, 43:1993, 1991.

[134] We call stable at 0 K a structural model whose formation energy is negative with respect to a decomposition into diamond plus α-boron, and is the lowest one among structures with the same carbon concentration.

[135] W. Hayami. *Phys. Rev. B*, 60:1523, 1999.

[136] H. Werheit. In O. Madelung, editor, *Landolt-Börnstein, Boron compounds*, volume 41D, page 2. Springer-Verlag, Berlin, 2000.

[137] H. Werheit. This conference, 2008.

[138] M.W. Chase. *NIST-JANAF Thermochemical Tables, Part I, Al-Co*, volume 9. National Institute of Standards and Technology, 4th edition, 1998.

[139] D. Smith, A.S. Dworking, and E.R. Van Artsdalen. The heat of combustion and formation of boron carbide. *Journal of the American Chemical Society*, 77:2654, 1955.

[140] M. Lüders, M.A. Marques, N.N. Lathiotakis, A. Floris, G. Profeta, L. Fast, A. Continenza, S. Massida, and E.K. Gross. *Phys. Rev. B*, 72:024545, 2005.

[141] M.A. Marques, M. Lüders, N.N. Lathiotakis, G. Profeta, A. Floris, G. Profeta, L. Fast, A. Continenza, E.K. Gross, and S. Massida. *Phys. Rev. B*, 72:024546, 2005.

[142] B. Zhou N. Stojić, A. Dal Corso and S. Baroni. Ab initio simulation of photoemission spectroscopy in solids: plane-wave pseudopotential approach with application to normal-emission spectra of cu(001) and cu(111). *Phys. Rev. B*, 77:195116, 2008.

[143] J. Sjakste, N. Vast, and V. Tyuterev. *Ab initio* study of electron-phonon coupling and excitonic linewidth in GaAs under pressure and GaP. *Journal of Luminescence*, 128:1004, 2008.

[144] S.P. Garg R.J. Ackermann and E.G. Rauh. *J. Am. Ceram. Soc.*, 60:341, 1977.

[145] A.E. McHale and R.S.Roth, editors. *Phase Equilibria Diagrams.* Ceramics Division, National Institute of Standards and Technology, Gaithersburg, Maryland, 1996.

[146] X. Zhao and D. Vanderbilt. *Phys. Rev. B*, 65:075105, 2002.

[147] T. Ishikawa, H. Yamaoka, Y. Harada, T. Fujii, and T. Nagasawa. *Nature*, 416:64, 2002.

[148] S. Meriani, editor. *Zirconia'88. Advances in Zirconia Science and Technology.* Elsevier, New York, 1989.

[149] E.J. Walter, S.P. Lewis, and A.M. Rappe. *Surface Science*, page 44, 2001.

[150] V. Fiorentini and G. Gulleri. *Phys. Rev. Lett.*, 89:266101, 2002.

[151] R.Puthenkovilakam, E.A. Carter, and J. P. Chang. *Phys. Rev. B*, 69:155329, 2004.

[152] A. Meldrum, L.A. Boatner, and R.C. Ewing. *Phys. Rev. Lett.*, 88:025503, 2002.

[153] C. Morant, J.M. Sanz, and L. Galï¿½. *Phys. Rev. B*, 45:1391, 1992.

[154] E.G. Rauh R.J. Ackermann and C.A. Alexander. *High. Temp. Sci.*, 7:305, 1975.

[155] G. Teufer. *Acta Crystallogr.*, 15:1187, 1962.

[156] P. Aldebert and J.P. Traverse. *J. Am. Ceram. Soc.*, 68:34, 1985.

[157] G. Fadda, L. Colombo, and G. Zanzotto. First-principles stufy of the structural and elastic properties of zirconia. Submitted (2009). Private communication.